Limitations of the Microtremor Method: A Case Study in the Los Angeles Basin, California

by

Deblina Bose

A thesis submitted to the Graduate Faculty of
Auburn University
in partial fulfillment of the
requirements for the Degree of
Master of Science

Auburn, Alabama
December 13, 2010

Approved by

Lorraine W. Wolf, Chair, Professor of Geology and Geography
Ashraf Uddin, Associate Professor of Geology and Geography
Ming-Kuo Lee, Professor of Geology and Geography

Abstract

Microtremor data from 16 broadband seismic stations across the Los Angeles basin are used to explore limitations of Nakamura's (1989) method for estimating resonant frequencies, amplification, and ground vulnerability to determine the sources of peaks in horizontal-to-vertical spectra ratios (HVSR) of microtremor data. Spectral peaks observed were analyzed in the context of stratigraphic boundaries inferred from well logs, geologic cross-sections and velocity-depth profiles generated from 3D California velocity model. The temporal stability of observed spectra from each station was tested by comparing time segments from different years. Spectral peaks and amplification values from HVSRs were compared with those from the 2008 Diamond Bar earthquake. The study suggests that microtremor data might be useful for determining resonant periods in sedimentary basins where strata are flat lying; however, a more thorough understanding of the method's limitations is necessary before it can be used to map amplification factors and ground vulnerability.

Acknowledgments

I would like to thank the Geological Society of America for funding this project through a student research grant. Appreciation is extended to the Southern California Earthquake Data Center and Incorporated Research Institutions for Seismology for access to data archives that were essential for completing this research. Thanks to my committee members Dr. Ming-Kuo Lee and Dr. Ashraf Uddin for their support and contribution. My deepest gratitude goes to the head of my committee Dr. Lorraine W. Wolf, whose constant guidance made this research possible. Her encouragement and support provided the motivation and inspiration. Thanks to rest of the faculty and staff of the Geology Department, Auburn University, for their support and assistance.

I would like to thank God for giving me the strength and knowledge to complete this project. I am obliged to my husband Nilanjan Roy and my parents for giving me their invaluable support.

Table of Contents

List of Figures

List of Tables

CHAPTER I

INTRODUCTION

The Los Angeles basin is located on the eastern part of the Pacific plate; within the transform boundary zone of the Pacific plate and the North American plate (Fig. 1). The basin is a northwest-plunging syncline with maximum depth of 9 km comprising Miocene to Pleistocene sediments and sedimentary rocks overlying the Cretaceous schist and granitic basement (Yerkes et al., 1965; Wright, 1991; Suss and Shaw, 2003). The Los Angeles basin is considered a region of moderate seismic activity, where earthquakes with magnitudes ranging from M = 0.8 to M = 7.0 affect the daily life of Los Angeles residents (Bilodeau et al., 2007). Studies of historic earthquakes have revealed more damage to life and property in areas of loose, unconsolidated sediments than in areas of basement rock. Hence, understanding the reaction of basin sediments to earthquake-induced ground motions is important for assessing seismic hazards. Borehole explorations of an area provide reliable data about subsurface conditions, although they are expensive, slow, and localized. To meet with these limitations, Nakamura (1989) proposed the use of ambient ground motions, known as "microseisms" or "microtremors," to assess site characteristics, such as resonant frequency and amplification of earthquake waves, in sedimentary basins.

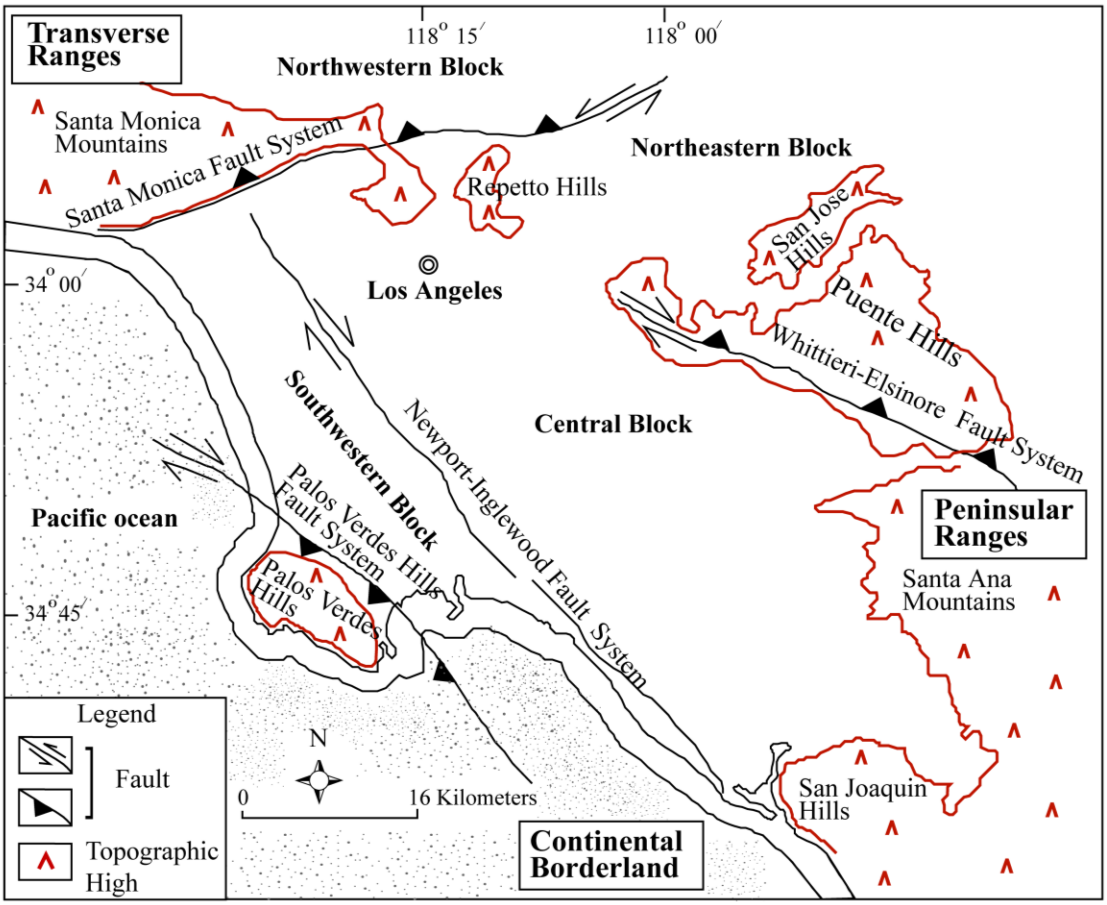

Figure 1. Map showing location of Los Angeles basin with major structural blocks, fault systems, and topographic highs (modified from Blake, 1991).

Microtremors are ground vibrations with very small amplitudes caused by both human activities, such as traffic or industrial work, and natural phenomena, such as sea waves, storms, and winds. The method is based on the assumption that deformational strains experienced at the ground surface in a sediment-filled basin can be related to strains experienced in the basement beneath the basin by a transfer function. One method of deriving the transfer function is based on the computation of horizontal-to-vertical spectral ratios (HVSRs). This study uses broadband microtremor data to analyze

subsurface geology, predominant periods or resonance frequencies, amplification factors, and vulnerability indices of sites within the Los Angeles basin. The study also compares characteristics derived from microtremors with those derived from the 2008 Diamond Bar earthquake. Lastly, the study explores conditions under which the microtremor method provides reliable estimates of site effects during earthquake-generated ground motions and circumstances that limit its applicability.

CHAPTER II

BACKGROUND STUDY OF LOS ANGELES BASIN

2.1. Tectonic Setting

The Los Angeles basin is located within the transform boundary zone of the Pacific plate and the North American plate (Suss and Shaw, 2003) (Fig. 1). It is surrounded by the Continental Borderland and Peninsular ranges in the south and Transverse Ranges in the north. The Los Angeles region was subjected to multiple stages of tectonic deformation from Oligocene to early Pliocene (Yerkes et al., 1965; Campbell and Yerkes, 1976; Wright, 1991). The area was characterized by simultaneous occurrence of extension or normal faulting and strike-slip faulting with periodic volcanism around 22 to 16 Ma (Yerkes et al., 1965). This stage was followed by further rifting and crustal-block rotation, which led to the opening of the Continental Borderland and building of Transverse Ranges during late Miocene (Yerkes et al., 1965; Wright, 1991). During early Pliocene, eroded sediments formed a thick sedimentary sequence within the central trough and extension changed to contraction, further deforming the Los Angeles basin (Yerkes et al., 1965; Wright, 1991). The pre-existing normal faults were rejuvenated as reverse faults. The Transverse Ranges were characterized by west-trending left-lateral reverse faults, whereas the Continental Borderland and Peninsular Ranges were

dominated by the northwest-trending right-lateral strike-slip faults (Fig. 1) (Yerkes et al., 1965; Wright, 1991; Schneider et al., 1996).

2.2. Geologic Setting

The present-day Los Angeles basin is an alluvium-rich northwest-trending syncline situated on the coast of southern California between latitude 33° 30′ N and 34° 00′ N and longitude 117°45′ W and 118°30′ W (Yerkes et al., 1965). The Los Angeles basin is distinguished for its great structural relief and complexity. The basin is bounded by the Santa Monica Mountains in the north, Repetto Hills, Puente Hills and San Jose Hills in the east, and Santa Ana Mountains and San Joaquin Hills in the southeast (Fig. 1) (Yerkes et al., 1965; Blake, 1991). Buried Quaternary alluvial deposits of Pleistocene age, with a maximum depth of 9 km, unconformably overlie the Mesozoic Catalina schist and granitic basement rocks bounded by distinct fault systems (Yerkes et al., 1965; Fuis and Ryberg, 2001; Suss and Shaw, 2003). Yerkes et al. (1965) divided the basin into four fault-bounded structural blocks based on different lithologies: the Northwestern Block, Northeastern Block, Central Block, and the Southwestern Block, which are discussed below.

Northwestern Block

The northwestern block is separated from the other blocks by the west-trending left-lateral reverse Santa Monica Fault system (Fig. 1). The major structural features in this block include the Santa Monica Mountains and the San Fernando Valley. The

basement rock of this block consists of the Santa Monica slate, which is overlain by late Cretaceous to Pleistocene marine clastic sediments with locally interbedded Miocene volcanic rocks (Yerkes et al., 1965; Blake, 1991).

Northeastern Block

The northeastern block is separated from the Central block by the northwest-trending right-lateral reverse Whittier-Elsinore Fault system. The major topographic highs in this area include the Repetto Hills, San Jose Hills, and the Puente Hills (Fig 1). The granitic basement rock in this region is overlained by thick sequence of late Cretaceous to Pleistocene marine clastic sedimentary rocks, Miocene volcanic and non-marine sedimentary rocks (Yerkes et al., 1965; Blake, 1991).

Southwestern Block

The southwestern block is separated from the Central block by the northwest-trending right-lateral Newport-Inglewood Fault system. The main topographic feature in this area is represented by the Palos Verdes Hills (Fig. 1). The Mesozoic Catalina schist constitutes the basement, with the superjacent rocks comprising Miocene to Holocene marine clastics with local Miocene igneous intrusions (Yerkes et al., 1965; Blake, 1991).

Central Block

The central block forms the fault-bounded central northwest plunging syncline with a depth of 4.3 km in the southwestern part to a maximum of 9 km in the central part of the block. Prominent topographic highs in this area include the Santa Ana Mountains and the San Joaquin Hills in the southeastern and southern parts of the block respectively (Fig 1). The basement rock towards the eastern side of the block is granitic and is assumed to be formed during northern extension of the Peninsular Ranges. The granitic rocks coincide stratigraphically with the Catalina schist, which forms the basement rock at the western side of the central block (Yerkes et al., 1965; Blake, 1991).

2.3. Stratigraphy

The subsurface formations of the Los Angeles basin are divided into two groups by a mid-Cretaceous unconformity (Yerkes et al., 1965). Below the unconformity are the basement rocks, consisting of an early Cretaceous granitic batholith and the Catalina schist. Above the unconformity is a thick sequence of sedimentary and volcanic superjacent rocks of middle Miocene to Pleistocene age (Yerkes et al., 1965; Blake, 1991). Figure 2 shows the superjacent rocks from the southwestern to the central block, which are discussed below from oldest to youngest.

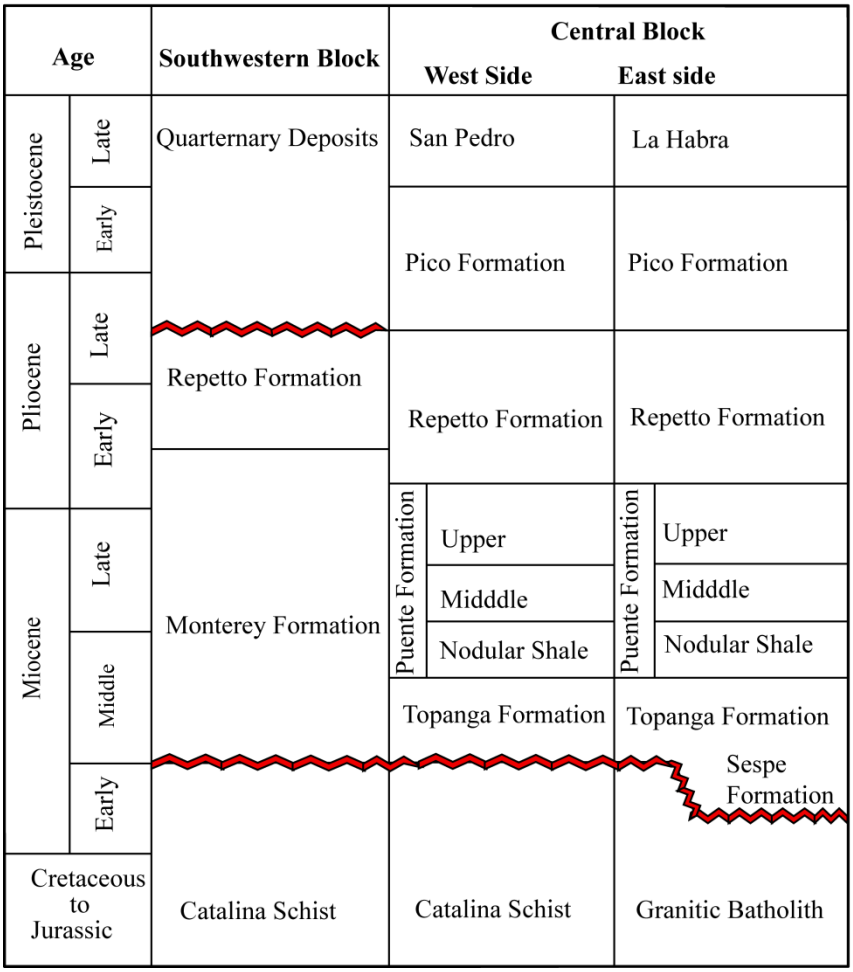

Figure 2. Generalized stratigraphic column from southwestern block (Puente Hills) to the central block (Fig. 1) of Los Angeles basin. Lithologies of the formations are described in text. Wavy lines are unconformities (modified from Blake, 1991).

Monterey Formation

The Monterey Formation, ranging in age from middle Miocene to early Pliocene, rests unconformably on the Catalina schist. It represents a middle to upper bathyal depositional environment and has an approximate thickness of 700 m (Blake, 1991). Dominant rock types that comprise the Monterey Formation are the phosphatic and organic-rich shale, limestone, calcareous sandstone, and volcanic tuff (Yerkes et al., 1965; Blake, 1991).

Sespe Formation

The early Miocene Sespe Formation is a 1000-m-thick non-marine, fluvial sequence of variegated sandstones (Blake, 1991). It is mostly present in the southern part of the Los Angeles basin. The Sespe Formation comprises sandstones, conglomeratic sandstones, and sandy siltstones (Blake, 1991).

Topanga Formation

The middle Miocene Topanga Group rests unconformably on the granitic basement towards the east side of the central block. This group has an approximate thickness of about 640 m and represents an inner-neritic to middle-bathyal depositional environment (Blake, 1991). Lithology of the Topanga Group is represented by coarse-grained sandstone interbedded with sandy shale, dark siltstone, tuff, and local basalt intrusions (Blake, 1991; Schneider et al., 1996).

Puente Formation

Overlying the Topanga Group is the 2.4-km-thick sequence of middle to late Miocene Puente Formation (Blake, 1991). The Puente formation represents a middle to upper bathyal depositional environment. The formation is further divided into lower, middle, and upper members. The lower member, known as the "Nodular" shale, comprises glauconitic and phosphatic nodular shale interbedded with massive sandstones (Blake, 1991; Schneider et al., 1996). Thick feldspathic sandstone beds interbedded with siltstone and shale characterize the middle member of the Puente formation (Blake, 1991). Interbedded diatomaceous siltstone and shale form the upper member of the Puente Formation (Schneider et al., 1996).

Repetto Formation

The Pliocene Repetto Formation represents a lower-bathyal depositional environment (Blake, 1991). It has a considerable thickness of 5 km, comprising interbedded fine-to-coarse-grained pebbly sandstone, sandy shale, siltstone, and claystone (Yerkes et al., 1965; Blake, 1991).

Pico Formation

The late Pliocene to early Pleistocene Pico Formation represents a neritic to middle-bathyal depositional environment (Blake, 1991). It has a thickness varying

between 300 and 900 m and is dominated by massive siltstones and mudstones locally interbedded with silty sandstones (Blake, 1991; Schneider et al., 1996).

Recent Deposit

The Lomita Marl and Timms silt in the southwestern block and the San Pedro and La Habra Formation in the central block are the upper Pleistocene to Holocene units of the study area. They signify a transition from an inner-neritic to a non-marine depositional environment (Blake, 1991). The deposits are rich in sandy silt, unconsolidated calcareous sand, and marl in the southwestern area, whereas unconsolidated silt, sand, clay and gravel cover the central trough (Blake, 1991).

2.4. Regional Seismicity

The geologic history of California is complicated because the state consists mostly of terranes accreted to the western edge of North America over the last few hundred million years. Movement of the Pacific plate with respect to the North American plate resulted in major episodes of folding, faulting, and mountain building. Current motions of these plates generate frequent, but moderate earthquakes along major strike-slip and dip-slip thrust fault systems (Hauksson, 1990). In addition to the San Andreas Fault system, there are numerous shallow-dipping reverse faults and blind-thrust faults capable of producing large earthquakes (Somerville et al., 2006). Figure 3 shows the magnitude and location of recent earthquakes since 1965 and highlights some significant

earthquakes in California that were responsible for widespread damage in the respective regions. The most active fault system is the San Jacinto Fault Zone in Southern California, which has produced large events in 1899, 1918, and 1923, with magnitudes M = 6.0, M = 6.8, and M = 6.3, respectively (Fig. 3). The largest recorded earthquake in California was the 1857 Fort Tejon earthquake (M_w = 7.9) (Fig. 3). This earthquake ruptured the San Andreas Fault over a distance of 475 km. The most destructive earthquake to date was the 1906 San Francisco earthquake (M_w = 7.9). More recently, the 1989 Loma Prieta earthquake (M_w = 6.9) and the 1994 Northridge earthquake (M_w = 6.7) (Fig. 3), which affected the San Francisco bay area and the Greater Los Angeles area, respectively, caused widespread damage (http: //earthquake.usgs.gov/earthquakes/states/; http://www.data.scec.org/).

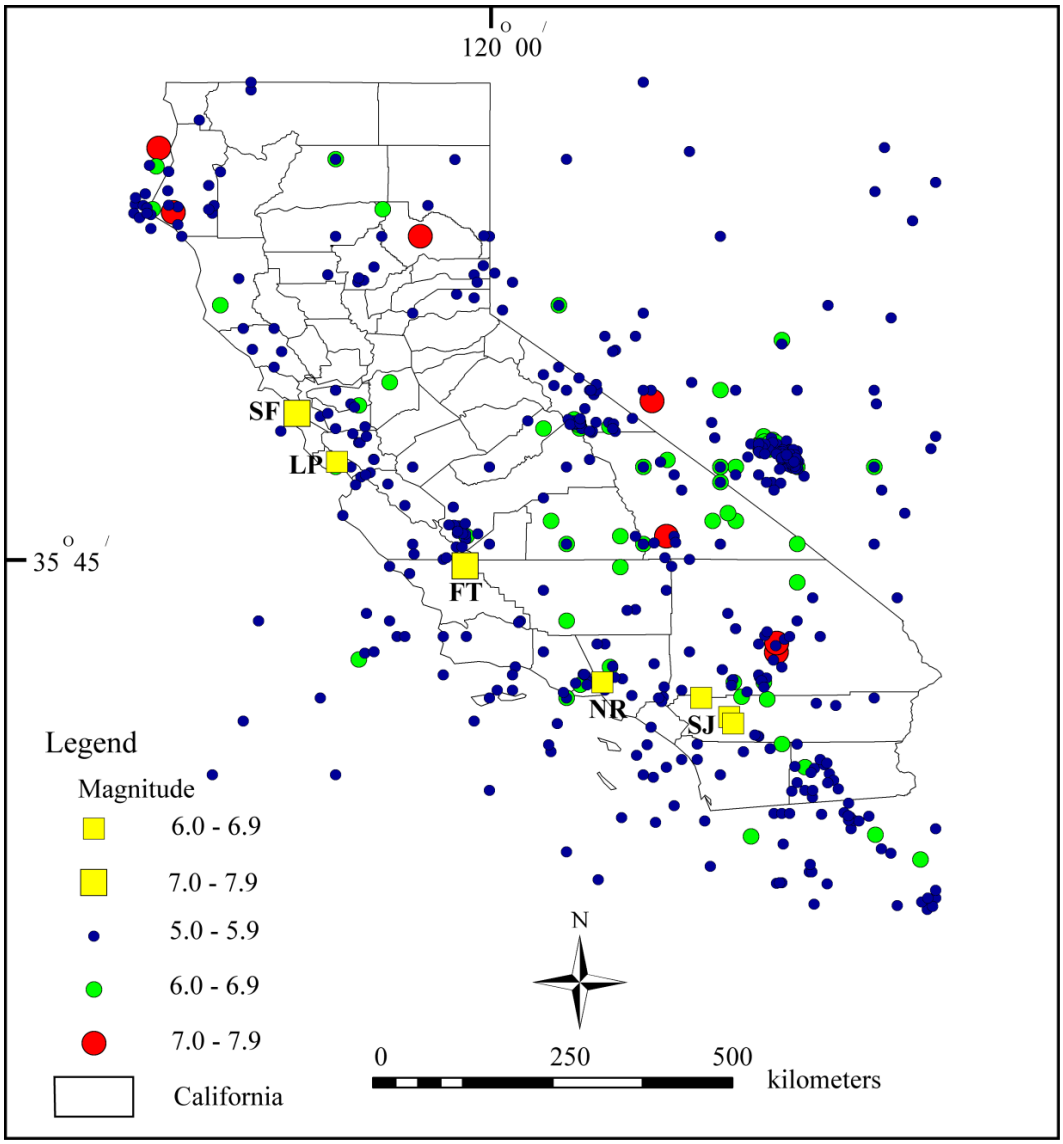

Figure 3. Recent earthquakes (M ≥ 5) in California since 1965. Squares refer to magnitude and location of significant earthquakes mentioned in text: SF (1906 San Francisco), LP (1989 Loma Prieta), FT (1857 Fort Tejon), NR (1994 Northridge), and SJ (1899, 1918, and 1923 San Jacinto) (modified from http://www.data.scec.org/).

2.5. Probabilistic Seismic Hazard Analysis

A probabilistic seismic hazard analysis map (Fig. 4) shows the hazard from anticipated earthquakes around Los Angeles area (http://www.consrv.ca.gov/cgs). The term "probabilistic" reflects the uncertainties in the size and location of earthquakes and the resulting ground motions affecting a particular site. Earthquake shaking hazards are calculated using historic earthquakes, fault-slip rates, and potential for amplification of seismic waves by near-surface geologic materials.

Seismic waves are amplified more by soft sediments than hard rocks. Hence, several researchers have concentrated their hazard analyses on mapping near-surface sediments. Surficial geologic units with distinct age, lithology, and grain size are classified based on the shear-wave velocities to a depth of 30 m (V_s 30) (Wills et al., 2000; Wills and Chalan, 2006). Wills et al. (2000) obtained average V_s 30 values from 556 profiles in the Los Angeles basin and used this information to establish characteristic velocity ranges for the different sedimentary layers. They observed that fine-grained alluvium and sedimentary rocks of Miocene age cover most of the upper part of the basin with typical V_s 30 values between 300 and 550 m/s.

Figure 4 shows the probable relative intensity of ground shaking and damage in a 50-year period in areas around the Los Angeles County from future earthquakes. The shaking potential is calculated as the level of ground motion that has a 2% chance of exceedance in 50 years (http://www.consrv.ca.gov/cgs). The areas more susceptible to high ground shaking and damage, such as the Los Angeles and Ventura County, are

shown on the map in shades of pink. This type of hazard analysis is used in developing building codes, prioritizing vulnerable areas, and estimating future earthquake losses.

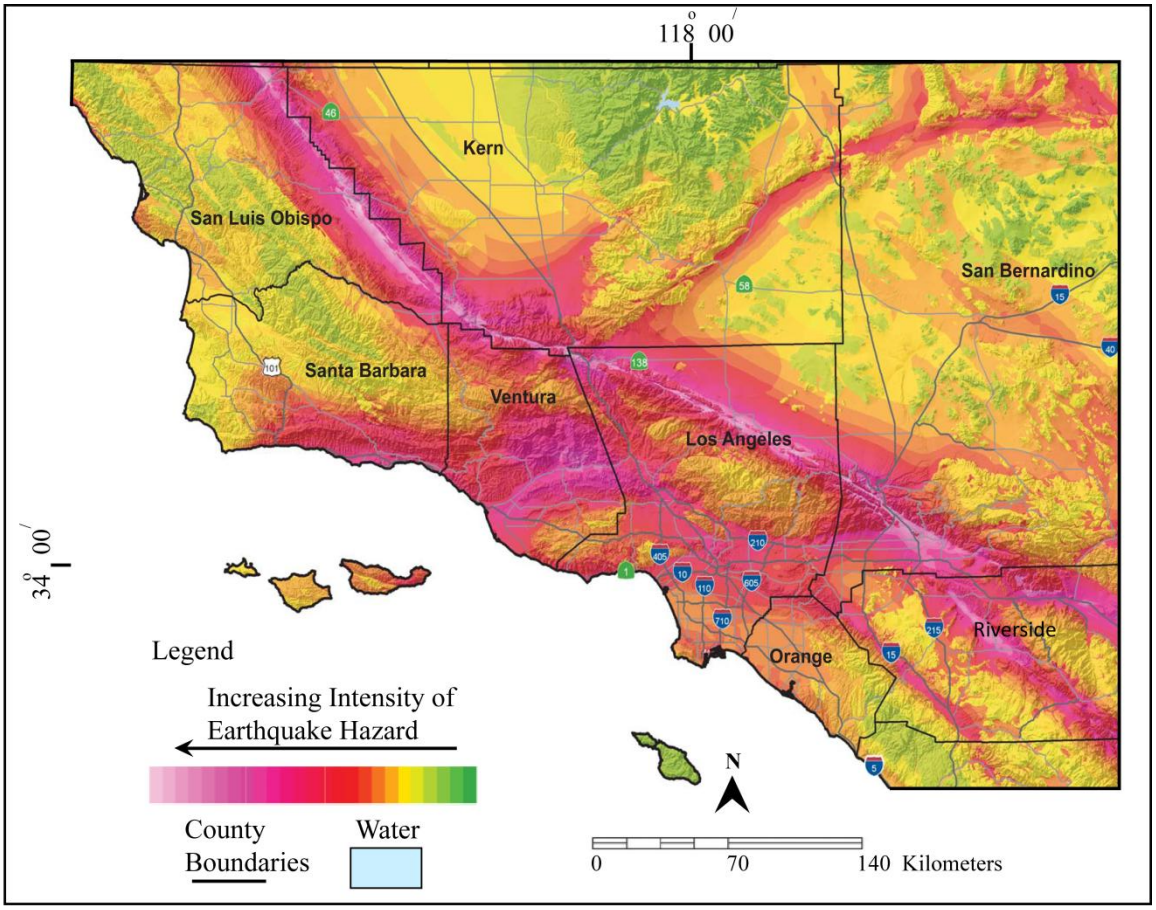

Figure 4. Earthquake shaking hazard map of Los Angeles and surrounding counties calculated using historic earthquakes, fault-slip rates, and amplification of seismic waves by near-surface geologic materials. The map shows expected level of ground motion with a 2% chance of exceedance over a period of 50 years. The areas more susceptible to high ground shaking and damage are shown in shades of pink (modified from http://www.conservation.ca.gov/cgs).

2.6. The Microtremor Method

Ground motions experienced at a site are a function of the earthquake source, wave path, and the characteristics of the site itself. Microtremors have been used to analyze site effects and characteristics of sediments due to earthquake-induced ground motion (Nakamura, 1989; Lermo and Chavez-Garcia, 1993; Huang and Tseng, 2002). The site effect is considered as an empirical transfer function that captures the influence of surficial units on earthquake ground motions. Site characteristics, such as fundamental period, wave amplification, and ground vulnerability are influenced by sediment type, location, and thickness of sedimentary units.

Two techniques are commonly used for determining site effects: the standard spectral ratio and the H/V ratio methods (Katz, 1976; Nakamura, 1989; Lermo and Chavez-Garcia, 1993; Huang and Teng, 1999; Delgado, 2000; Huang, 2002) (Fig. 5). The standard spectral ratio method is calculated by dividing the horizontal spectrum of ground motion measured at a sediment site (S_{HS}), by that measured at a rock or reference site (S_{HB}). In this method, shear-wave records from an earthquake are used for estimation of the spectral ratio, S_T, where

$$S_T = S_{HS} / S_{HB} \tag{1}$$

Nakamura (1989) and Lermo and Chavez-Garcia (1993) used a spectral ratio, E_S, to estimate the amplitude effect of the source given by

$$E_S = S_{VS} / S_{VB} \tag{2}$$

where S_{VS} and S_{VB} are the power spectra of vertical motions on the surface and those on the basement, respectively. Nakamura (1989) assumed that the low-velocity surface layers do not amplify the vertical component of the microtremor spectrum. To compensate for the source effect (E_S), Nakamura (1989) and Lermo and Chavez-Garcia (1993) proposed a modified site effect function, (S_{TT}), where

$$S_{TT} = S_T / E_S \tag{3}$$

and $$S_{HB} / S_{VB} \sim 1$$

Thus, the modified site effect becomes

$$S_{TT} = S_{HS} / S_{VS} \tag{4}$$

This suggests that the transfer function or the effect of sediment on wave propagation is solely based on ground motions at sediment sites and is given by H/V spectral ratio (*HVSR*),

$$HVSR = \frac{(Hn + He)/2}{Vz} \tag{5}$$

where *Hn*, *He*, and *Vz* are the horizontal and vertical components of ground motion in the north, east, and vertical directions, respectively. The resulting spectrum is independent of source and path and is used to determine fundamental periods or predominant frequencies, which appear as peaks in the spectra. The HVSR method eliminates the requirement of a reference or basement site to derive the transfer function for sedimentary basins.

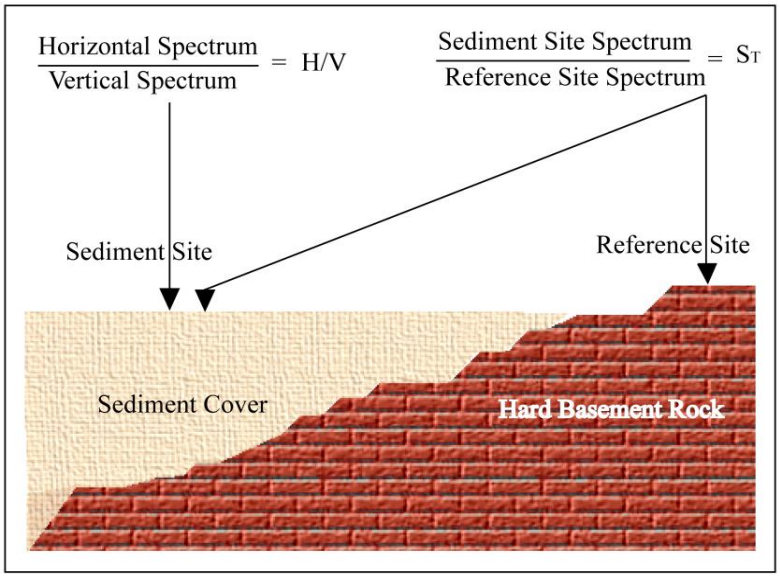

Figure 5. Assumptions of microtremor method to derive transfer function for sedimentary basins using H/V (Nakamura, 1989) and standard spectral ratios (modified from Ibs-von Seht and Wohlenberg, 1999). See text for discussion.

2.7. Application of the Microtremor Method

The spectral analysis of microtremors is an alternate way to characterize the site response. The relationship between local site response and microtremor characteristics, such as predominant period or resonant frequency, site amplification, and liquefaction vulnerability, was first studied many years ago (Gutenberg, 1957; Kanai and Tanaka, 1961). Since then, many researchers have used microtremor motions to understand the influence of basin geology on ground motions (Katz, 1976; Kagami et al., 1982; Field et al., 1990). An approach by Nakamura (1989) uses HVSR from ambient noise at a single sediment site (Fig. 5). This technique has been implemented by many researchers

(Ohmachi et al., 1991; Field and Jacob, 1993, 1995; Lermo and Chavez-Garcia, 1993, 1994; Yamanaka et al., 1993; Suzuki et al., 1995; Bonilla et al., 1997; Hartzell et al., 1998; Bodin and Horton, 1999; Huang and Teng, 1999, 2002; Horike et al., 2001; Huang, 2002; Hardesty et al., 2010).

Lermo and Chavez-Garcia (1993, 1994) applied the H/V method to access the empirical transfer function in three cities in Mexico, where site effects were responsible for significant destruction during the 1985 Michoacán earthquake. Their results indicated that the H/V ratio method was able to provide a robust estimate of frequency in the first resonant mode, and a rough assessment of wave amplification. Field and Jacob (1993) collected microtremor data and applied the HVSR method in their study at a site in Flushing Meadows, New York. The results suggested the H/V ratio is an effective and reliable tool to calculate the fundamental frequency of a layered sedimentary basin. In a latter study, Field and Jacob (1995) compared the three various site-response techniques that are independent of reference site to estimate the source and path effects using aftershock events of the 1989 Loma Prieta earthquake in California. The three techniques were the parameterized source and path effects inversion, H/V spectral ratios of the shear-wave aftershock data, and the H/V spectral ratios using ambient seismic noise. Their examination revealed that the techniques were successful in identifying the fundamental resonant frequency of the study area.

Suzuki et al. (1995) collected microtremor and strong-motion data in Hokkaido, Japan. Their results illustrated that the peak frequency of the H/V ratio corresponded well to the predominant frequency estimated from the thickness of a sedimentary unit. Bonilla et al. (1997) performed a detail study of 38 aftershocks of the 1994 Northridge

earthquake. They concluded that predominant frequency peaks from the H/V method matched with those of the earthquake, but not the amplification values. Huang and Tseng (2002) utilized Nakamura's method in the Yuan-Lin area, Taiwan. Beside fundamental frequency and amplification values, they proposed the application of microtremor method to identify sites susceptible to strong ground shaking. The Yuan-Lin area experienced intense liquefaction during the 1999 Chi Chi earthquake. Their study found higher values of ground vulnerability for areas of severe liquefaction. Ibs-von Seht and Wohlenberg (1999) collected microtremor measurements from 102 sites in the Lower Rhine embayment, Germany. Combining Nakamura's (1989) technique with standard spectral ratio, they calculated sediment thickness from the predominant peak in the microtremor spectra.

Smith (2000) conducted microtremor study in the southern part of the New Madrid Seismic Zone (NMSZ). He collected data from 113 sites in the metropolitan Memphis area. Smith (2000) applied the HVSR technique and correlated the resonant periods with the distinct lithologic units within the study area. In his results, he concluded that the longer periods corresponded to the interface between sediment and Paleozoic basement rocks and the shorter period with a shallow subsurface loess unit. His results were supported in a latter study done by Hardesty et al. (2010) in the Mississippi embayment.

The standard spectral ratio method has been applied for the microtremor study in Los Angeles basin byYamanaka et al. (1993).Two sites were chosen for this study: the University of Southern California (USC), a sediment site characterized by thick sediment cover, and the La Canada site, a rock site about 30 km northeast of USC with very thin

sediment cover. Microtremor measurements taken at both sites obtained predominant periods ranging between 6 to 7 s, which is in agreement with the predominant periods obtained from local earthquake ground motions (Yamanaka et al., 1993).

CHAPTER III

METHODOLOGY

3.1. Data Acquisition

3.1.1. Site Selection

Seismic stations used in this study are located in the southwestern, central, and northeastern blocks of the Los Angeles basin. Most are located in areas underlain by a thick sedimentary sequence with little nearby bedrock exposure. Sixteen broadband, 3-component, high-gain (sampling rate = 40 Hz) permanent seismic stations within the Southern California Earthquake Center database (SCEC) were chosen for the study (Fig. 6). Some of these stations are located in areas of relatively flat-lying basement, whereas others are located in regions of high structural complexity, such as on the steeply dipping flanks of folds or near fault zones (Fig. 6). These broadband stations were chosen because they continuously record seismic data. The station codes, names, and depths to basement are displayed in Table 1.

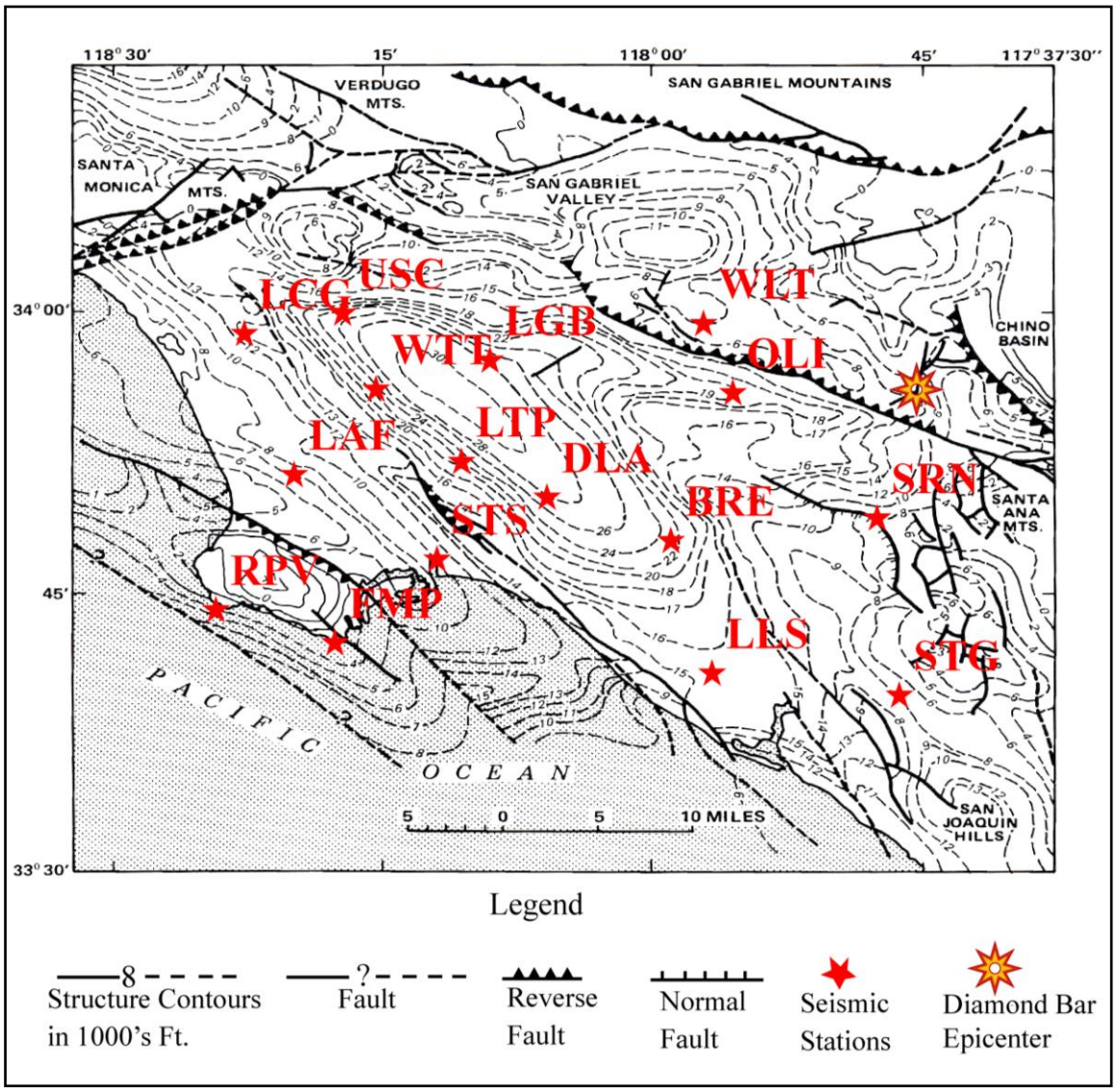

Figure 6. Major structural features and contours on basement surface showing basement depths for sixteen seismic stations located in the Los Angeles basin. The map also shows location of 2008 Diamond Bar earthquake (modified from Yerkes et al., 1965). See Table 1 for station information.

Table 1. Station codes, names, and depth to basement as used in the study.

Station Code	Station Name (http://www.data.scec.org/)	Depth of Basement (m) (Fig. 6)
BRE	Barre Substation	7010
DLA	Del Amo	8534
FMP	Fort Macarthur Park	610
LAF	La Fresa	2134
LCG	La Cienega	3962
LGB	Laguna Bell	8230
LLS	Ellis	4572
LTP	Lighthipe	7315
OLI	Olinda	5791
RPV	Ranchos Palos Verdes	1219
SRN	Serrano	3048
STG	Santiago	2438
STS	State Street	3048
USC	University of Southern California	7300
WLT	Watts	2438
WTT	Walnut	7315

3.1.2. Microtremor Data Acquisition

Microtremor data from the 16 selected stations were acquired from SCEC database (http://www.data.scec.org/index.html). SCEC has approximately 350 seismic stations in the Southern California region. Sensors at the stations have a flat instrument response from 0.03 to 50 Hz. They are capable of measuring wide range of ground motion frequencies, from local background noise to large earthquake ground motions. The recorded signals are digitized and transmitted in real-time to the California Institute of Technology, where they are added to the SCEC database.

To obtain the fundamental characteristics (for example, resonant frequencies and relative amplitudes) of the microtremors and to test their stability over time, seismic data from the selected stations were extracted from the SCEC database in one-hour time segments for five consecutive years (from 2004 through 2008) using the following approach. First, the SCEC catalogs were searched to identify time periods during which no earthquakes occurred to ensure that the microtremor data recorded during these times were free from any strong ground motion effects and consisted solely of background noise. The identified time segments were then extracted from the SCEC database using the "Seismogram Transfer Program" (STP) (http://www.data.scec.org/STP/stp.html), a graphical interface program for retrieving waveform data. Broadband data from these time segments were downloaded in a format compatible with the Seismic Analysis Code (SAC format) for analysis. Gain-corrected data from each component (north, east, and vertical) were stored separately for each station.

3.1.3. Earthquake Data Acquisition

To compare the results from the weak motion analysis with strong-motions, earthquake data were extracted from SCEC as triggered events. For this study, data from 2008 Diamond Bar earthquake (M = 5.5) (Fig. 6) which occurred in the greater Los Angeles area was chosen. A unique identification number specifies each of the triggered events; the Diamond Bar is referenced in the SCEC database as event identification number "12340231". Similar to the procedure for obtaining the microtremor data, the

gain-corrected earthquake data were downloaded for all three components and stored separately.

3.1.4. Shear-Wave Velocity Data Acquisition

To test the hypothesis that spectral peaks are related to impedance contrasts within subsurface strata, shear-wave velocity data were obtained using the 3D Velocity Model of California (http://www.data.scec.org/3Dvelocity/). This FORTRAN based model integrates information on subsurface velocities derived from several sources, such as seismic refraction data, strong-motion data, and geotechnical data. Using the 3D velocity model, one can extract V_P, V_S, and density at any user-specified latitude-longitude and depth position within the area covered by the model. Shear-wave velocities from the surface to the sediment-basement interface at 100-m depth intervals were compiled from the model for each station location.

3.1.5. Other Supporting Data

Supporting data such as stratigraphic sections and well logs were collected to assist in interpreting the results of the microtremor study. These additional data were compiled from published papers (for example, United States Department of the Interior Geological Survey, Professional Paper 420-A Plate 1, Plate 2, and Plate 4). The stratigraphic data and well logs provided information regarding lithology, depth, and thickness of major stratigraphic units within the basin. Used in conjunction with the

shear-wave velocity model, knowledge of the stratigraphy allowed for estimates of acoustic impedance contrasts at subsurface boundaries that could be related to peaks in the microtremor spectrum.

3.2. Data Processing

3.2.1. Microtremor Data Analysis

Data acquired for each station were investigated for signal transients and artifacts. Data artifacts or transients include noise sources originating from an identifiable event close to the seismometer, such as a car door slamming or construction work. Since fundamental resonant periods are generated by long-period waves traveling through the basin, these short-period noise sources are undesirable. Time segments free from data transients were selected for the HVSR calculation using the Matlab™ power spectral density function (PSD). A three-step procedure was followed for creating HVSR from the recorded time series (Fig. 7). First, clean data segments from recorded time series were extracted to produce power spectra for each component, horizontal east (*He*), horizontal north (*Hn*), and vertical (*Vz*). Secondly, spectra from the two horizontal velocity components (*He* and *Hn*) of the microtremors were averaged and divided by the vertical component (*Vz*) to get the HVSR (Equation 5). Thirdly, data were processed using Hanning windows of 8192 or 4096 samples, overlapping by half of the window length. Spectra were plotted as relative power (amplitude squared) versus period, where predominant periods appeared as the peaks in the spectra. Errors for peaks were determined by taking the width of the peak at half its height.

3.2.2. Shear-Wave Velocity Analysis

Velocity-depth functions calculated for each station using 3D Velocity Model of California were examined to determine velocity discontinuities (Fig. 8). These abrupt changes in shear-wave velocity usually correspond to high impedance contrasts in sub-surface strata. Nakamura (2000) proposed that peaks observed in the HVSR spectra were related to the impedance contrast between sediments and underlying basement rocks by a quarter-wavelength relationship:

$$T = 4Z / V_S \qquad (6)$$

where, T is period (s), Z is depth (m), and V_S is shear-wave velocity (m/s) at that depth. Predicted periods for each station location were calculated using the above equation and estimates of shear-wave velocity and depth to discontinuities as observed from the velocity-depth curve. These predicted peak periods were compared with the observed peaks from the power spectra to investigate whether the observed spectral peaks were likely to be related to impedance contrasts.

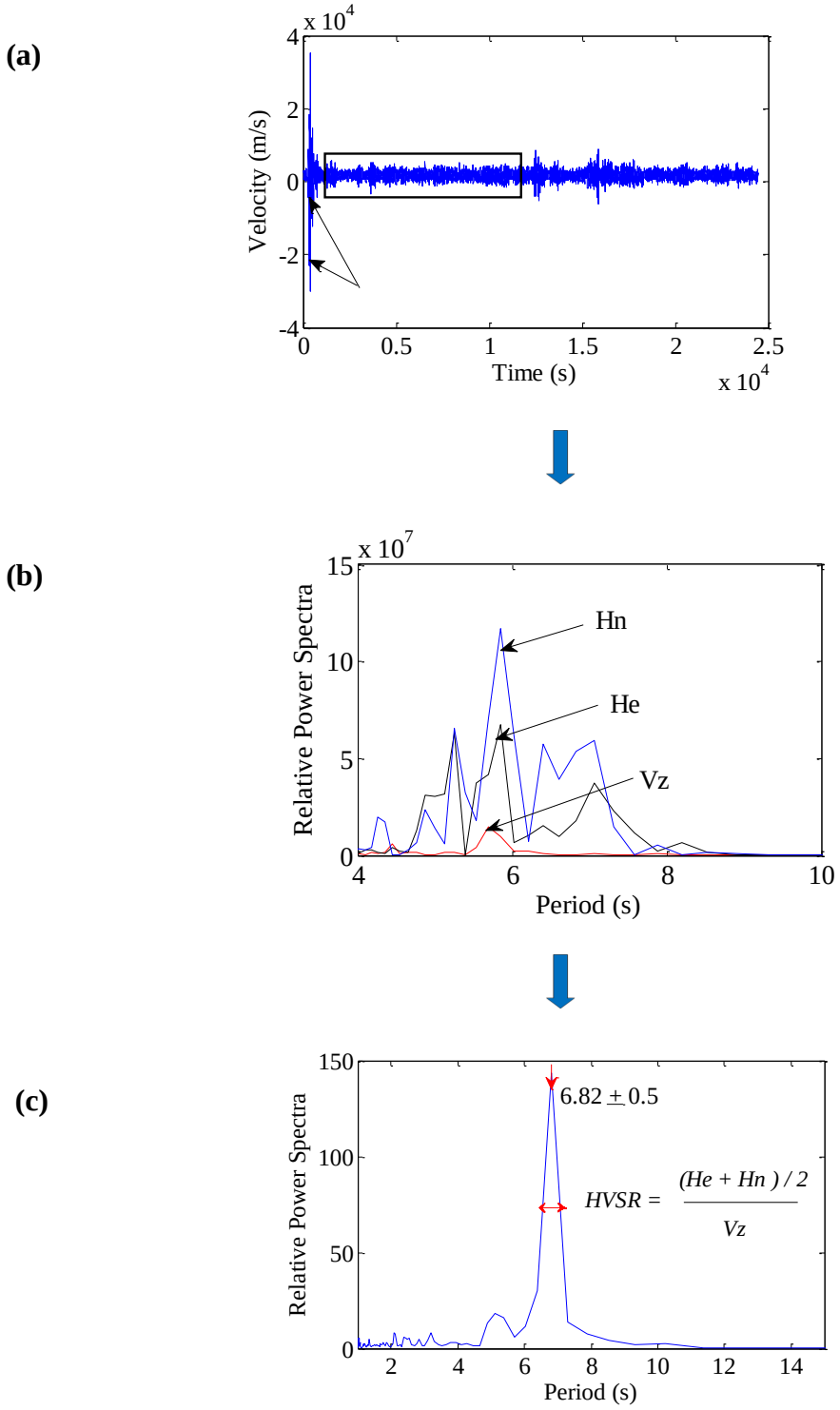

Figure 7. (a) Example of continuous seismic data recording for duration of 1 hour for station STS. Thin arrows point out data transients. Clean time segment (rectangular box) represents data selected for analysis. (b) Computed power spectra for horizontal (*He* and *Hn*) and vertical (*Vz*) components. (c) HVSR calculated showing predominant period (vertical red arrow) with possible error (horizontal red arrows).

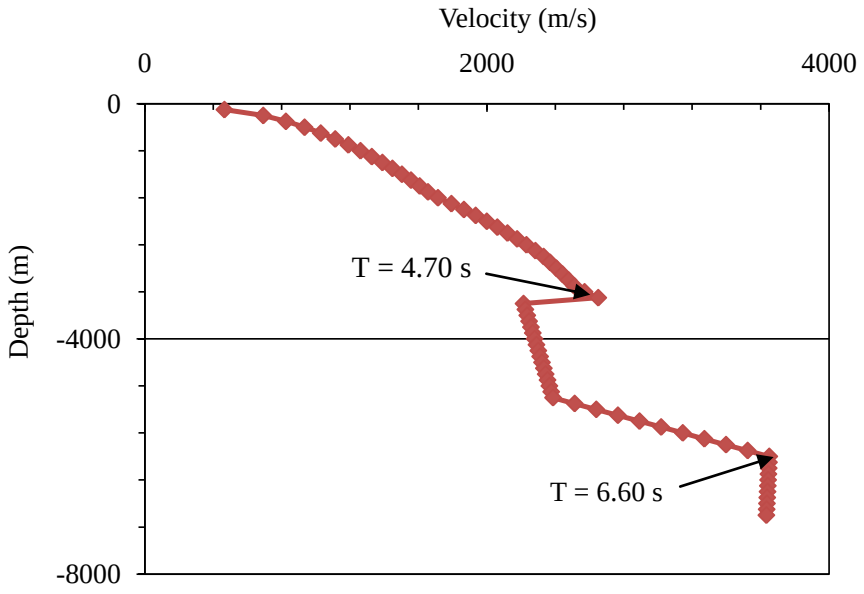

Figure 8. Example of velocity-depth curve for station STS produced from 3D Velocity Model of California (http://www.data.scec.org/3Dvelocity/). Velocity discontinuities and predicted periods indicated by arrows are calculated using equation 6.

3.2.3. Earthquake Ground Motion Analysis

Seismic data from the 2008 Diamond Bar earthquake (event ID #12340231) were analyzed using Matlab™ PSD for each station. A typical 3-component seismogram from this event is shown in Figure 9. For the study, samples focused around the shear-wave portion of the seismogram were analyzed using Hanning window lengths of 8192, 4096 or 2048 samples. The horizontal components (*He* and *Hn*) from a sediment site (for example, station STS) were averaged and divided by the horizontal components from a rock or reference site which has little sediment cover (for example, station FMP) to produce the power spectra. The spectral peaks generated from the earthquake data using

the standard spectral ratio method (Equation 1) were then compared with those generated from microtremor data (Equation 5) (Fig. 10).

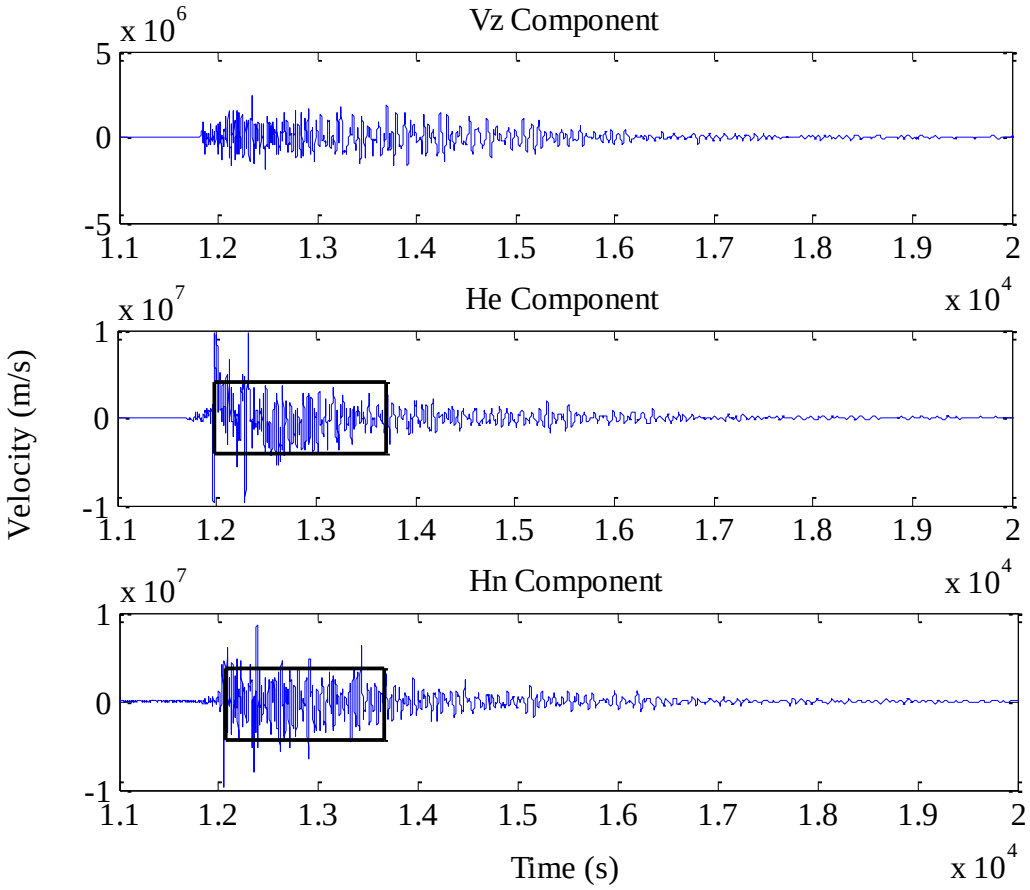

Figure 9. Example of a 3-component seismogram for Diamond Bar earthquake obtained from SCEC for station STS (http://www.data.scec.org/index.html). Horizontal components sample focused around shear-wave and longer period portions (rectangular boxes) are used in the standard spectral ratio analysis.

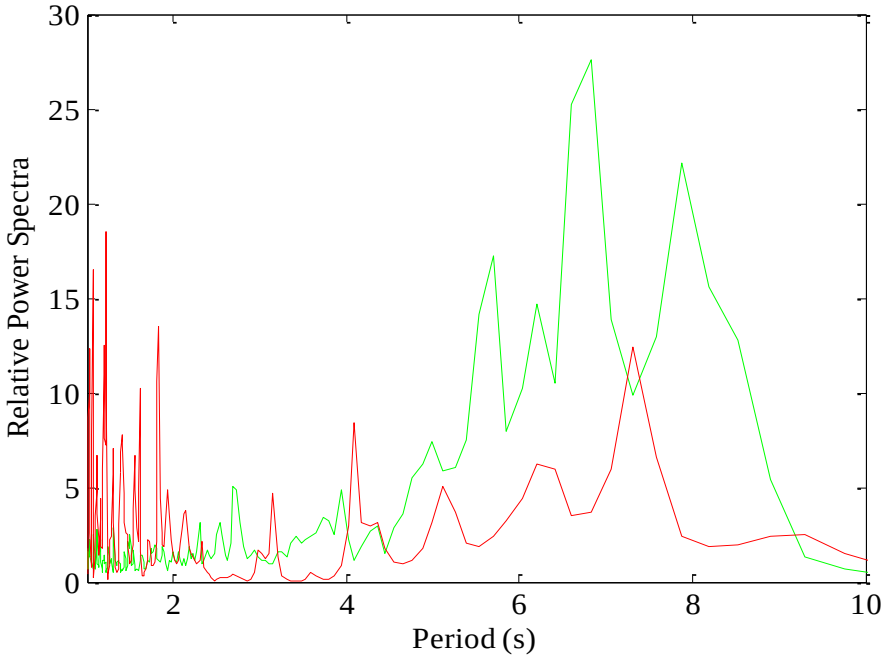

Figure 10. Power spectra showing peaks obtained from earthquake data (red) and microtremor data (green) for STS station. Predominant periods from two sources are comparable from 5.0 to 9.0 s (microtremor) and 4.0 to 7.50 s (earthquake).

CHAPTER IV

RESULTS

Microtremor waveforms and earthquake seismograms used in the analysis are shown in Appendix A and Appendix B, respectively. Table 2 and Table 3 display the time and duration of each seismic recording and the length of data segments extracted for frequency analysis at each of the 16 stations. The length is listed as the number of samples in the data segment, given the sampling rate of 40 samples per second. The length of the Hanning window used in frequency analysis of data from each station varied and was determined by trial and error based on consistency of spectral peaks.

Table 2. Data segments used in microtremor analysis for each station for 2004-10-13-07:00:00 to 2004-10-13-08:00:00. All stations had a sampling rate of 40 Hz.

Station Code	Starting Sample	End Sample	Length (samples)	Length (sec)	Length (min)	Hanning Window
BRE	634	23430	22796	569.9	9.50	8192
DLA	14050	22730	8680	217	3.62	4096
FMP	49070	106300	57230	1430.75	23.85	8192
LAF	39720	68260	28540	713.5	12.0	4096
LCG	8279	36750	28471	711.77	11.86	4096
LGB	4562	31190	26628	665.70	11.09	8192
LLS	22260	48080	25820	645.50	10.76	4096
LTP	1002	71750	70748	1768.70	29.50	8192
OLI	340	34690	34350	858.75	14.31	8192
RPV	365	27210	26845	671.13	11.18	8192
SRN	7686	39440	31754	793.85	13.23	8192
STG	15460	31590	16130	403.25	6.720	8192
STS	9344	35670	26326	658.15	10.97	4096
USC	1431	28350	26919	672.97	11.21	4096
WLT	4745	19380	14635	365.87	6.09	4096
WTT	4251	18060	13809	345.255	5.75	4096

Table 3. Data segments used in analysis of 2008 Diamond Bar earthquake (event ID #12340231).

Station Code	Starting Sample	End Sample	Length (samples)	Length (sec)	Length (min)	Hanning Window
BRE	12000	12960	960	24.00	0.40	8192
DLA	11980	13360	1380	34.50	0.58	4096
FMP	12120	13500	1380	34.50	0.58	8192
LAF	12120	13500	1380	34.50	0.58	4096
LCG	12000	13380	1380	34.50	0.58	4096
LLS	12000	13380	1380	34.50	0.58	4096
LTP	11970	13350	1380	34.50	0.58	8192
OLI	11690	12650	960	24.00	0.40	8192
SRN	11850	13000	1150	28.75	0.48	8192
STG	12000	13000	1000	25.00	0.42	8192
STS	12000	13380	1380	34.50	0.58	4096
USC	12000	12960	960	24.00	0.40	4096
WLT	11880	13260	1380	34.50	0.58	4096
WTT	12000	13380	1380	34.50	0.58	4096

Table 4. Data segment used to test the temporal stability of microtremor peaks over time.

Station Code	Year	Start Sample	End Sample	Length (samples)	Hanning Window
LAF	2004	533	20030	19497	4096
	2005	31760	68500	36740	4096
	2006	55210	85580	30370	4096
	2007	80770	138800	58030	4096
	2008	830	21350	20520	4096
LGB	2004	4562	31190	26628	8192
	2005	40260	53880	13620	8192
	2006	1657	88240	86583	8192
	2007	1009	61490	60481	8192
	2008	83110	142900	59790	8192
LLS	2004	22260	48080	25820	4096
	2005	20350	37390	17040	4096
	2006	22130	77300	55170	4096
	2007	852	68270	67418	4096
	2008	87900	142600	54700	4096
STS	2004	9344	35670	26326	4096
	2005	38920	58280	19360	4096
	2006	17370	32710	15340	4096
	2007	107400	143200	35800	4096
	2008	1925	12130	10205	4096
USC	2004	1431	28350	26919	4096
	2005	6616	17280	10664	4096
	2006	4313	37880	33567	4096
	2007	33160	117000	83840	4096
	2008	6733	88700	81967	4096
WTT	2004	11250	32420	21170	8192
	2005	6275	37200	30925	8192
	2006	44690	99170	54480	8192
	2007	78680	143100	64420	8192
	2008	15770	61960	46190	8192

Figure 11 through 26 shows the HVSRs of observed microtremor peaks, peaks obtained from the Diamond Bar earthquake, and the predicted peaks from velocity-depth function (equation 6) for each station. The results for each station are discussed below.

Barre Substation (BRE)

BRE is located in the central part of the Los Angeles basin and on the flanks of a major northwest-trending Los Angeles syncline (Fig. 6). A thick sediment cover of 7000 m consists of Holocene sediments underlain by Miocene sandstones that overlie granitic batholith. Figure 11a shows the HVSR from microtremor data (green line) and spectral peaks from the Diamond Bar earthquake (red line). Spectra from the microtremors show observed peaks at 4.0, 6.5 to 7.5, 8.0 to 11.0, and 14.0 s, with most of the energy centering around 9.5 $\pm$ 0.5 s. The earthquake spectra show peaks at 2.4 and 6.5 $\pm$ 0.5 s, the latter being the dominant one. Here, very little similarity exists between microtremor and earthquake peaks. Figure 11b displays the result from the 3D California shear-wave velocity model. The velocity-depth curve shows a velocity discontinuity at 4000 m, giving predicted period of 6.11 s (Equation 6). Thereafter the velocity increases sharply to 3600 m/s at depth of 7000 m, giving predicted peak period of 8.0 s. The observed peaks from the microtremor data show a resemblance with the predicted peaks.

The microtremor peak around 7.0 $\pm$ 0.5 s and the earthquake peak at 6.5 $\pm$ 0.5 s are most likely due to the impedance contrasts between members of the Puente Formation (Fig. 2). The longer period around 9.5 $\pm$ 0.5 s from microtremors possibly corresponds to the sediment-basement interface between the Miocene Topanga Group or Miocene to upper Eocene Sespe Formation and the granitic batholith.

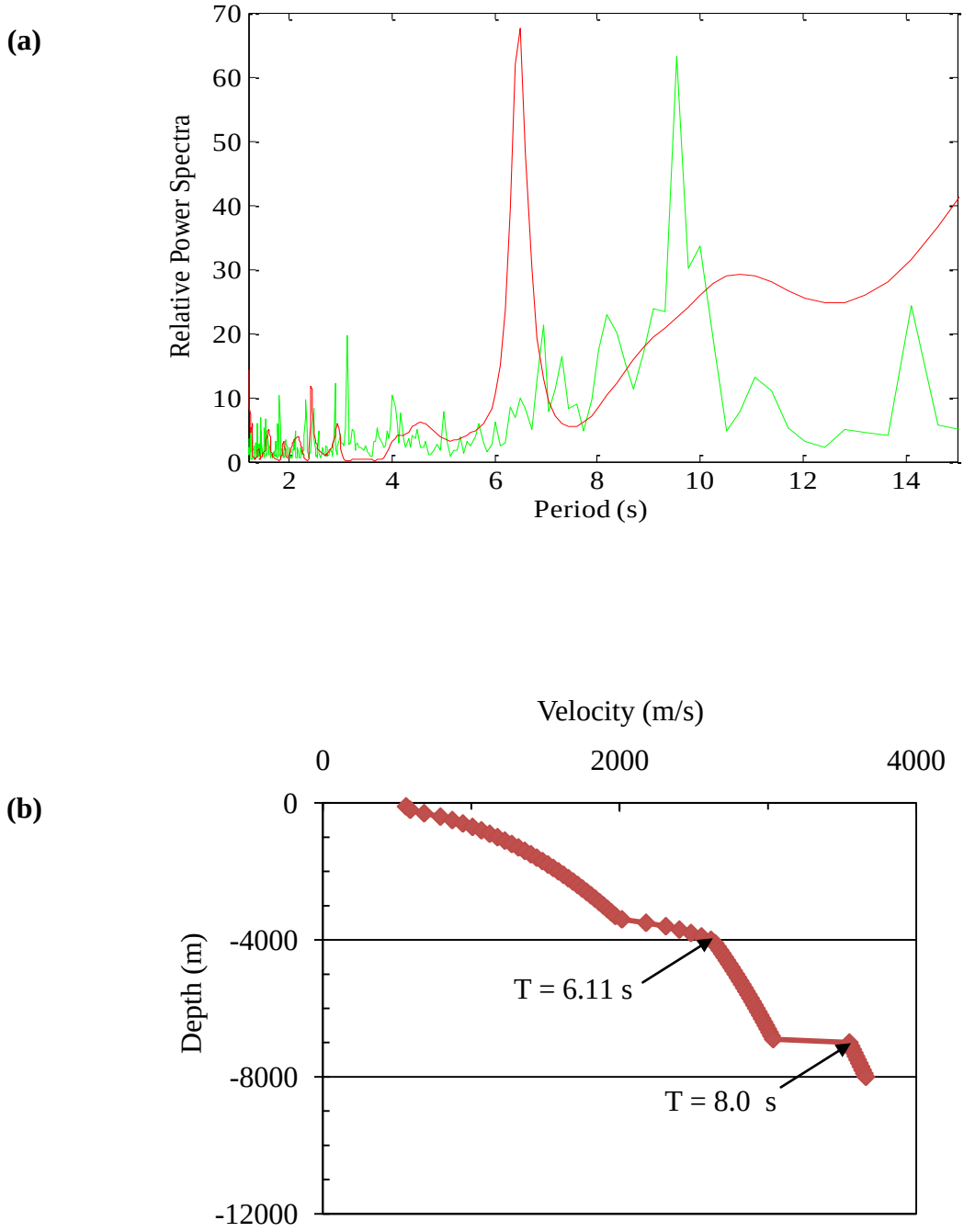

Figure 11. (a) Analysis of microtremor data (green) and earthquake data (red) from Diamond Bar earthquake for BRE. Microtremor data have length and Hanning window of 634:23430 and 8192, respectively. Earthquake data have length and Hanning window of 12000:12960 and 8192, respectively. Predominant periods from two sources show peaks at 9.5 ± 0.5 and 6.5 ± 0.5 s. (b) Velocity-depth curve from 3D velocity model of California (http://www.data.scec.org/3Dvelocity/). Velocity discontinuities and predicted periods indicated by arrows are calculated using equation 6.

Del Amo (DLA)

DLA is located in the central part of the Los Angeles basin and on the flank of the syncline (Fig. 6). Here, thick sediment cover of more than 8000 m overlies a granitic batholith. Figure 12a shows the HVSR from microtremor data and the spectral peaks from the Diamond Bar earthquake. Spectra from the microtremors show observed peaks at 5.25, 6.02, 8.20, and 10.24 s, with most of the energy concentrated around 10.24 $\pm$ 0.5 s. The earthquake spectra show peaks at 4.0, 5.0, 6.4, and 7.31 s. The peaks show some correlation in the intermediate ranges of 5.0 to 6.0 s from the two sources. Figure 12b displays the result from velocity model analysis. The velocity-depth curve shows a gradual increase of velocity to a depth of 5800 m, where a higher velocity gradient occurs to small velocity high is observed at 6000 m, giving a predicted period of 8.63 s (Equation 6). A sharp velocity step from 3000 m/s to 3600 m/s is observed at depth beyond 8500 m. This velocity discontinuity gave predicted period of 9.60 s.

The peaks in the microtremor and earthquake data in the range of 5.0 to 6.0 s could be due to an impedance contrast between members of the Puente Formation (Fig. 2). The longer peak in the microtremor spectra around 10.24 $\pm$ 0.5 s likely correspond to the sediment-basement interface between the Miocene Topanga Group or Miocene to upper Eocene Sespe Formation and the granitic batholith.

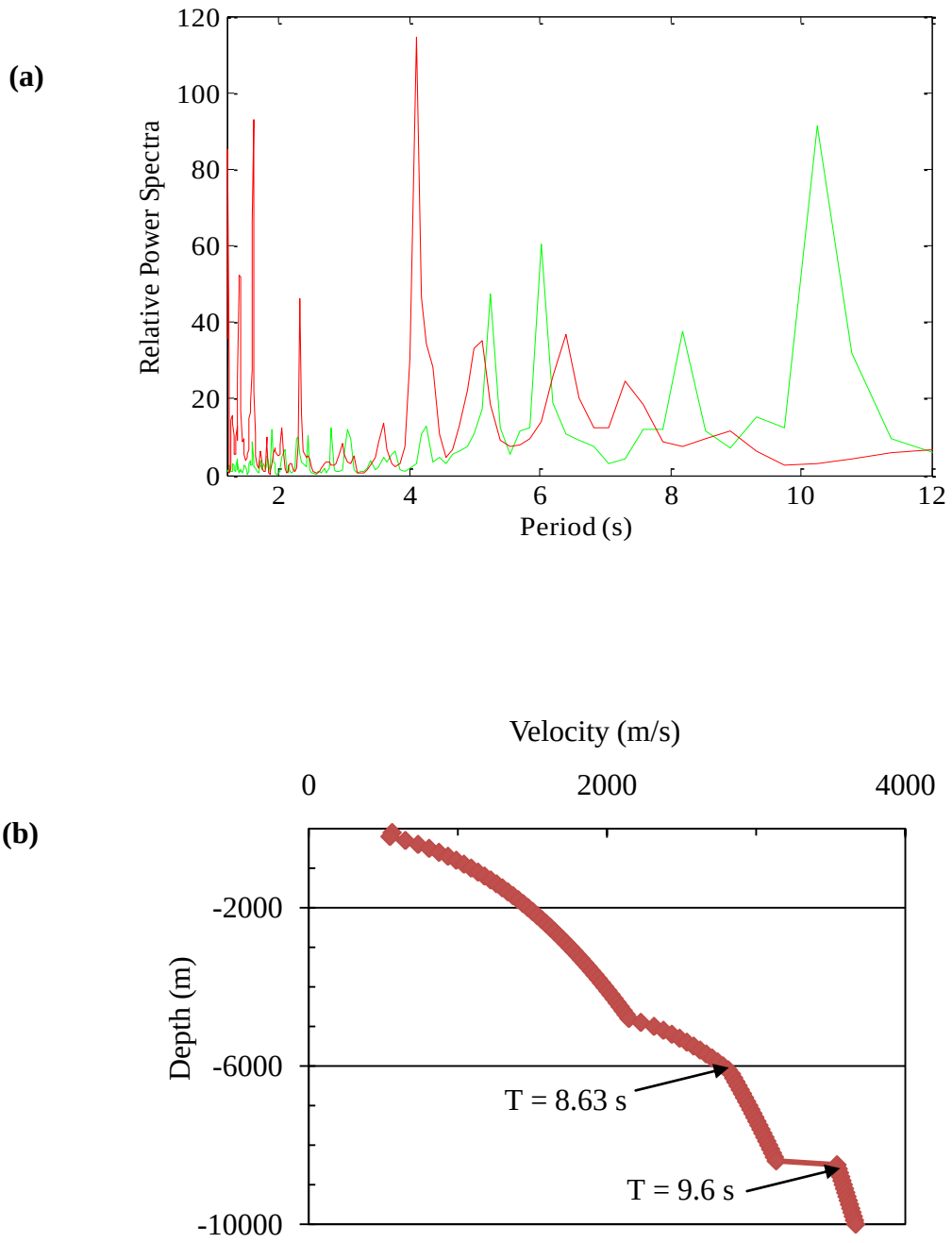

Figure 12. (a) Analysis of microtremor data (green) and earthquake data (red) from Diamond Bar earthquake for DLA. Length and Hanning window for microtremor data are 14050:22730 and 4096, respectively. Earthquake data have length and Hanning window of 11980:13360 and 4096, respectively. Intermediate peaks from two sources show agreement in the range 5.0 to 6.4 s. (b) Velocity-depth curve from 3D velocity model of California (http://www.data.scec.org/3Dvelocity/). Velocity discontinuities and predicted periods indicated by arrows are calculated using equation 6. Predicted period at 9.6 s matches with the observed long period at 10.24 ± 0.5 s from microtremor.

Fort Macarthur Park (FMP)

FMP is located in the southwestern part of the Los Angeles basin near the coast (Fig. 6). It rests on a thin cover (~ 610 m) of sediment and sedimentary rocks of recent deposits and Monterey shale, overlying the Mesozoic Catalina schist basement. Due to the relatively thin sediment cover, FMP is used as a reference or rock site for calculating the earthquake power spectra using standard spectral ratio method. Figure 13a shows the HVSR from microtremor data. Spectra from the microtremors show observed peaks around 3.0 to 4.0 s. The spectra are relatively flat out to ~ 10.0 s. The velocity-depth curve shows constant velocity of 2860 m/s to a depth of 1000 m (Fig. 13b). Subsequently, the velocity is observed to increase steadily with depth corresponding to a discontinuity at 5000 m. The discontinuities at 1000 and 5000 m generate predicted periods of 1.4 and 6.0 s, respectively.

The H/V spectra show small amplification corresponding to shallow sediment thickness. Peaks between 1.0 and 2.0 s most likely relate to the interface between the middle Miocene Monterey shale and the Mesozoic Catalina schist (Fig. 2). Intermediate and longer periods may be due to effects associated with the near-shore location of the FMP station.

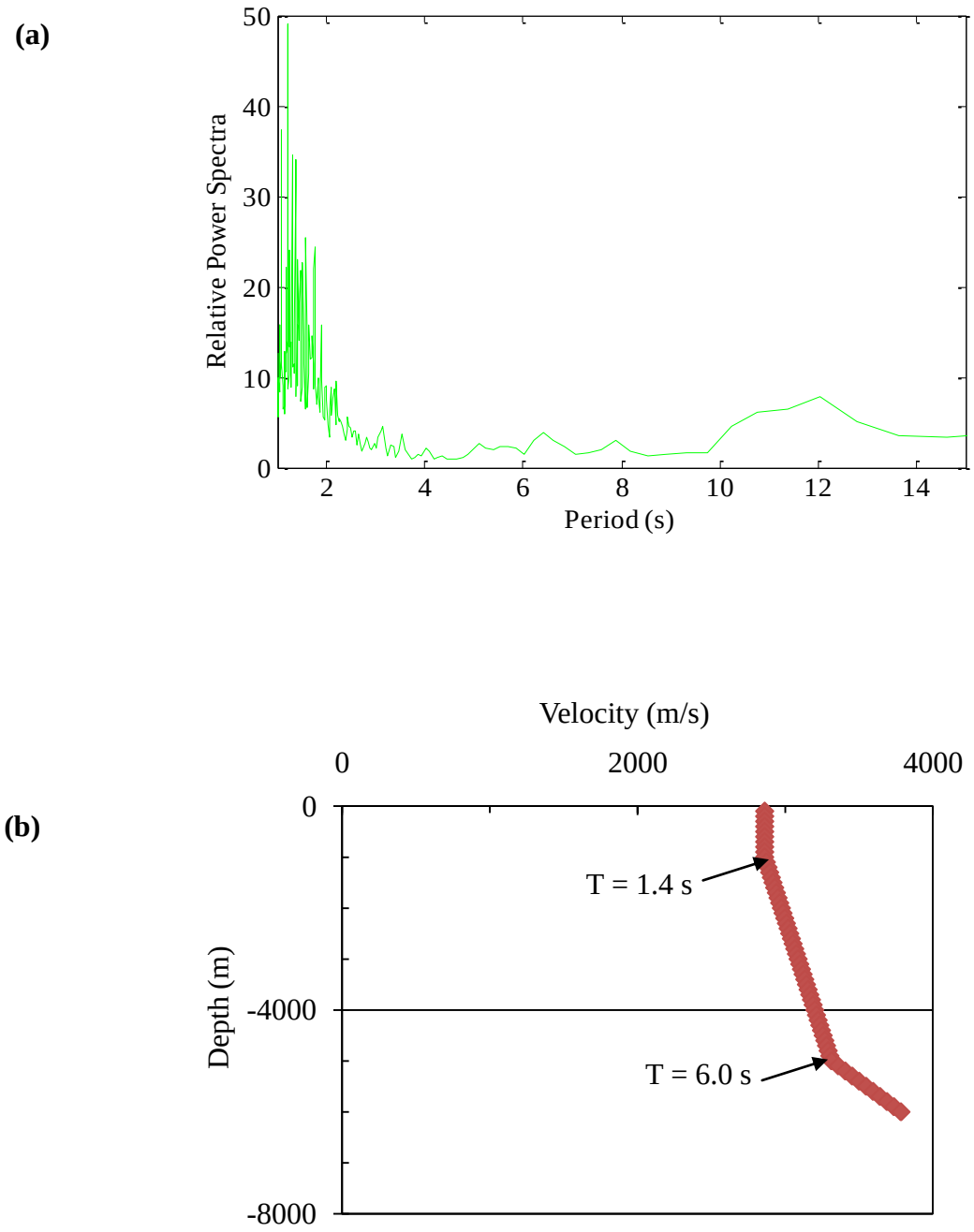

Figure 13. (a) Microtremor data analysis for FMP. Length of data segment and Hanning window used are 49070:106300 and 8192, respectively. Low amplification observed in H/V spectra indicates shallow basement depth. (b) Velocity-depth curve from 3D velocity model of California (http://www.data.scec.org/3Dvelocity/). Velocity discontinuities and predicted periods indicated by arrows are calculated using equation 6.

La Fresa (LAF)

LAF is located in the southwestern part of the Los Angeles basin and on relatively flat area (Fig. 6). Sediment cover of 2000 m over the Catalina schist basement characterizes the station. Figure 14a shows HVSR from the microtremor data and spectral peaks from the Diamond Bar earthquake. Spectra from microtremors show observed peaks at 5.50 to 6.02 and 7.06 to 8.20 s. The earthquake spectra show peaks at 4.09 and 7.31 s. As illustrated in Figure 14b, velocity discontinuities are observed at 2500 and 5100 m giving predicted periods at 4.02 and 7.50 s respectively.

Shallow basement depth from contour maps, stratigraphic sections, and velocity-depth profile reveals that the intermediate period around 5.70 $\pm$ 0.3 s correspond to impedance contrasts between the Miocene Monterey shale and the Mesozoic Catalina schist (Fig. 2). The prominent longer periods observed from microtremor and earthquake around 7.6 $\pm$ 0.6 and 7.31 $\pm$ 0.26 s, respectively could not be related to any stratigraphic interface, but may be due basement structure complexity.

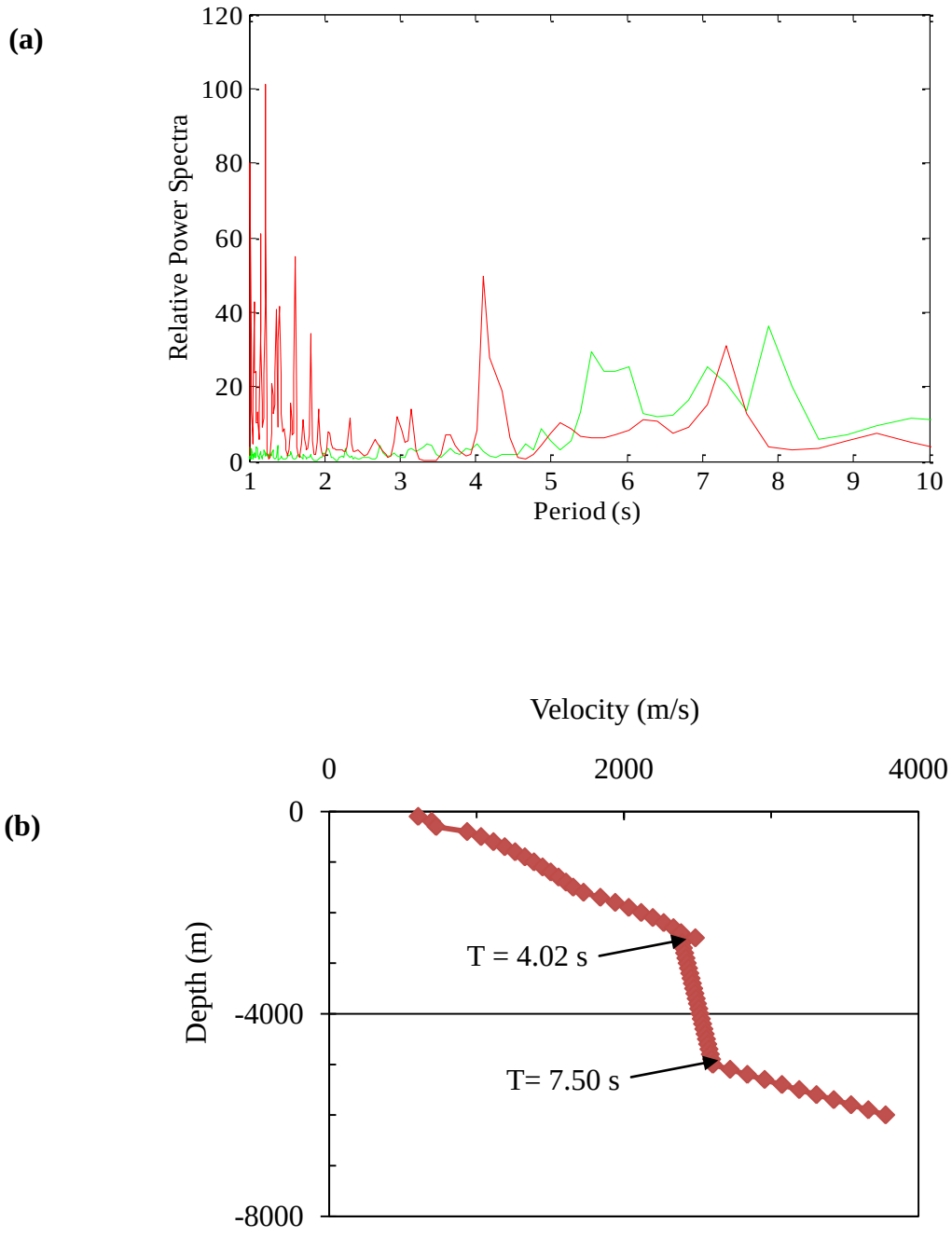

Figure 14. (a) Analysis of microtremor data (green) and earthquake data (red) from Diamond Bar earthquake for LAF. Microtremor data segment and Hanning window used are 39720:68260 and 4096, respectively. Earthquake analysis uses data length 12120:13500 and Hanning window 8192. Longer periods observed from microtremor and earthquake ~ 7.0 s shows good match. (b) Velocity-depth curve from 3D velocity model of California (http://www.data.scec.org/3Dvelocity/). Velocity discontinuities and predicted periods indicated by arrows are calculated using equation 6.

La Cienega (LCG)

LCG is located in the southwestern part of the Los Angeles basin on a relatively flat area (Fig. 6). Depth to basement from different sources, such as the basement contour map (Fig. 6), stratigraphic sections (United States Department of the Interior Geological Survey, Professional Paper 420-A Plate 1, Plate 2, and Plate 4), and the velocity-depth model, have different values, ranging from 4000 to 6000 m. Figure 15a shows the HVSR and standard spectral ratio for LCG. Microtremor spectra show observed peaks at 4.0, 5.12, 6.60, 7.58, and 9.30 s. The earthquake spectra show peaks at 4.0, 5.12, and 7.31 s. Velocity-depth curve in this area shows gradual increase of velocity to a depth of 2400 m (Fig. 15b). Thereafter, sharp velocity increase over a depth of 100 m is observed, giving a predicted period of 4.33 s. This is followed by a velocity reversal at depth between 4000 to 5000 m, beyond which velocity increases sharply. The predicted period of 6.40 s is estimated from the discontinuity at 6000 m.

Here, results from the three sources, such as microtremor, earthquake, and velocity-depth model are comparable. The intermediate period from microtremor and earthquake around 4.56 $\pm$ 0.56 s corresponds to lithologic contacts between members of the Puente Formation. The predominant longer periods at 6.60 $\pm$ 0.60 s (microtremor) and 7.30 $\pm$ 0.40 s (earthquake) can be related to the impedance contrast between the older Miocene Topanga sandstones and the granitic batholith (Fig. 2).

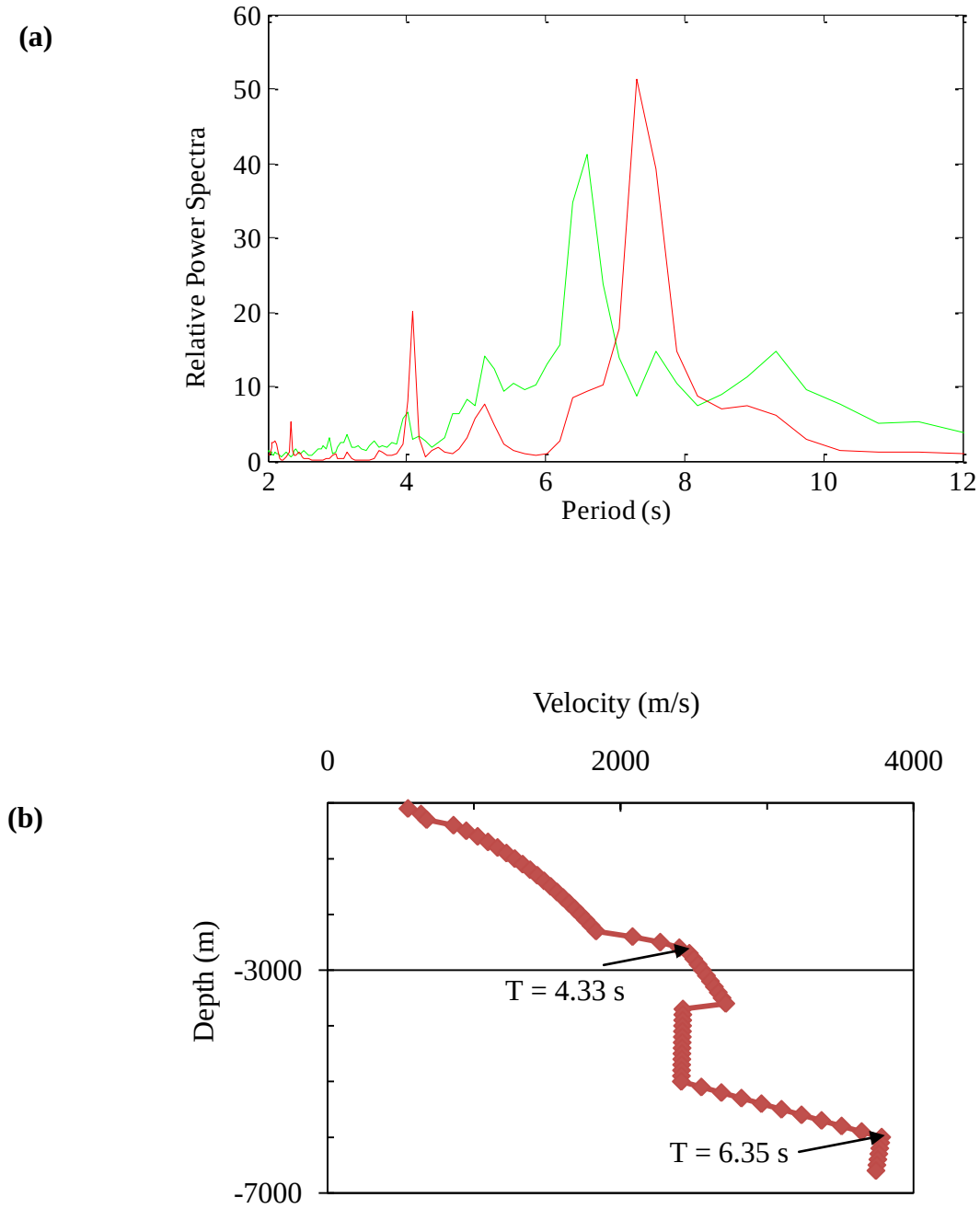

Figure 15. (a) Analysis of microtremor data (green) and earthquake data (red) from Diamond Bar earthquake for LCG. Length of data segment and Hanning window used for microtremor are 8279:36750 and 4096, respectively. Earthquake analysis uses data segment 12000:13380 and Hanning window 4096. Here predominant period from two sources ranging from 6.0 to 8.0 s are comparable. (b) Velocity-depth curve from 3D velocity model of California (http://www.data.scec.org/3Dvelocity/). Velocity discontinuities and predicted periods indicated by arrows are calculated using equation 6.

Laguna Bell (LGB)

LGB is located in the western flank of the central Los Angeles syncline (Fig. 6). A thick sediment cover of 7000 to 8000 m consisting of Holocene sediments and Miocene sandstones rests unconformably over the granitic basement. Earthquake data from the Diamond Bar event were not available for LGB from SCEC; hence, strong motion analysis could not be performed. As shown in Figure 16a, the microtremor spectra shows dominant peak at 7.06 and small peaks at 4.0 to 6.0, 8.40, 9.0 to 10.0, and ~ 14.0 s. Velocity-depth curve shows gradual increase of velocity with depth up to 7000 m, after which a velocity discontinuity is observed, giving a predicted period of 8.6 s (Fig. 16b).

The intermediate peaks from microtremor around 5 ± 1.0 s are due to the impedance contrast between members of Puente Formation. The predominant period from microtremor (~ 7.0 s) and the predicted period from velocity-depth curve (8.6 s) most likely relates to the sediment-basement impedance contrast between the older Miocene Topanga sandstone and the Cretaceous granitic batholith (Fig. 2).

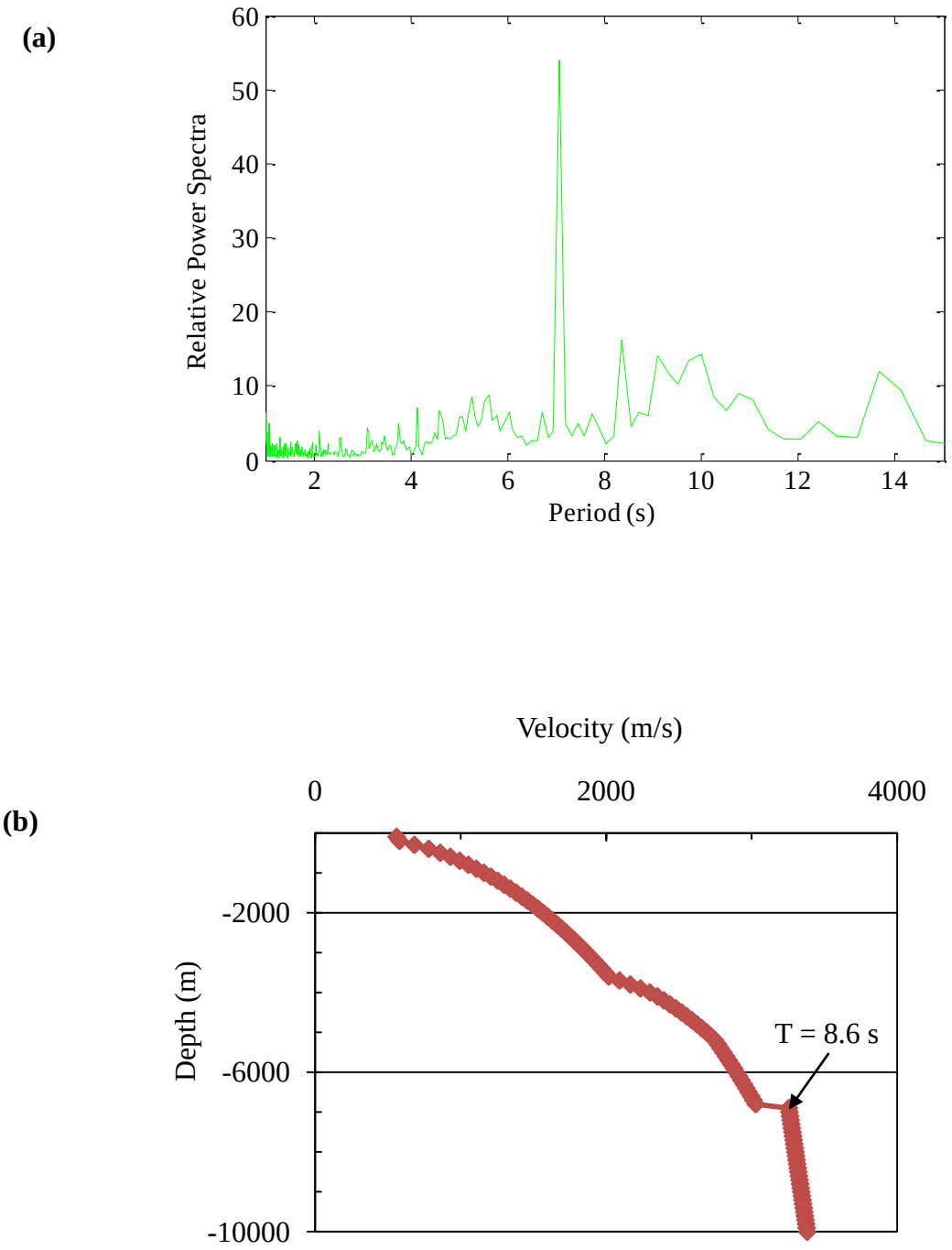

Figure 16. (a) H/V spectra showing microtremor data for LGB. Length of data segment and Hanning window used are 4562:31190 and 8192, respectively. Spectra shows prominent peak at 7.06 s. (b) Velocity-depth curve from 3D velocity model of California (http://www.data.scec.org/3Dvelocity/). Velocity discontinuity and predicted period indicated by arrow is calculated using equation 6. Here observed and predicted periods show similarity at ~ 8.0 s.

Ellis (LLS)

LLS is located in the southwestern part of the central Los Angeles basin on relatively flat area (Fig. 6). Sediment cover of 4500 m over the Catalina schist basement characterizes the site. Figure 17a shows the HVSR from microtremor data and spectral peaks from the Diamond Bar earthquake. Microtremor spectra show a broad observed peak at 6.60 to 7.31 s, with most energy concentrated around 7.31 $\pm$ 0.3 s. The earthquake spectra show peaks at 4.09, 6.40, and 7.31 s. Figure 17b illustrates the result from 3D velocity model, where gradual increase in velocity to a depth of 1700 m is observed. This is followed by sharp velocity discontinuities at 2000 and 5000 m corresponding to predicted periods of 3.50 and 6.80 s, respectively.

Comparable results are obtained from microtremor, earthquake, and velocity-depth profile studies. The shorter period in the microtremor spectra at 4.0 s most likely corresponds to impedance contrast between the Monterey Formation and the upper Topanga Formation. The longer period around 7.31 $\pm$ 0.3 s could be related to the stratigraphic contact between the Topanga Formation (interbedded with Sespe Formation) and the Catalina schist basement (Fig. 2).

(a)

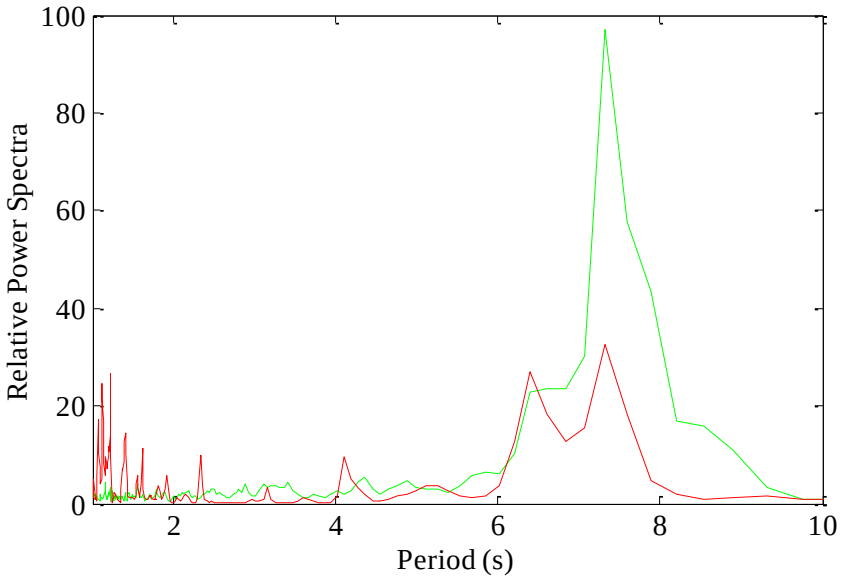

(b)

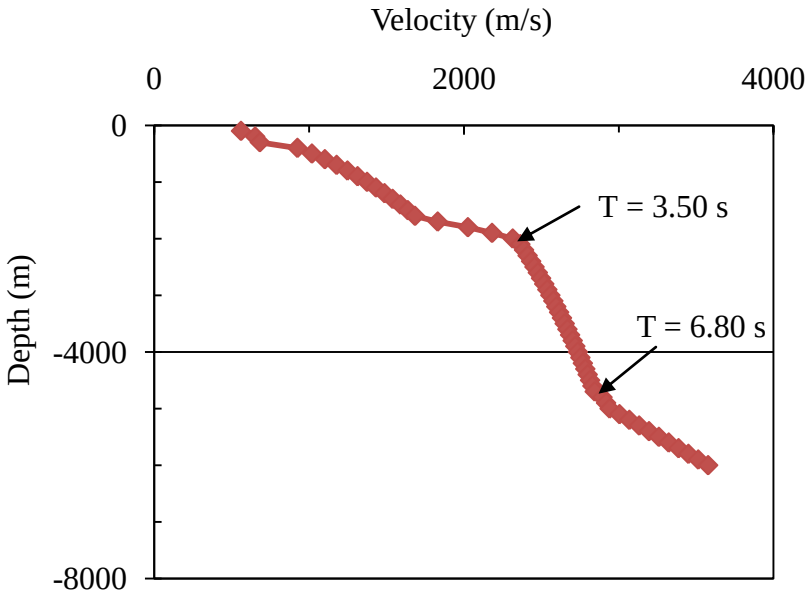

Figure 17. (a) Spectra showing microtremor data (green) and earthquake data (red) from Diamond Bar earthquake for LLS. Length of data segment and Hanning window used for microtremor analysis are 22260:48080 and 4096, respectively. Earthquake analysis uses data segment 12000:13380 and Hanning window 4096. Here predominant peaks from two sources are in good match. (b) Velocity-depth curve from 3D velocity model of California (http://www.data.scec.org/3Dvelocity/). Velocity discontinuities and predicted periods indicated by arrows are calculated using equation 6.

Lighthipe (LTP)

LTP is located on the steeply dipping western flank of the central Los Angeles syncline (Fig. 6). The area is characterized by thick sediment cover of 7300 m comprising of the Puente and the Topanga Formations, resting unconformably over the granitic basement rock. Analyses of microtremor and earthquake data for LTP show dominant peaks at 7.45 s, however, small peaks around ~ 6.4 and 9.0 s from microtremors are also observed (Fig. 18a). The velocity-depth model shows gradual increase in velocity up to a depth of 7700 m (Fig. 18b). Beyond this depth, a velocity discontinuity is observed, giving rise to the predicted period of 9.05 s.

The intermediate period around 6.4 ± 0.57 s from microtremors corresponds to the lithologic contacts between members of Puente Formation. The increase energy present in the spectra at ~ 9.0 s likely relates to the impedance contrast between the older Miocene Topanga sandstone and the Cretaceous granitic batholith basement (Fig. 2).

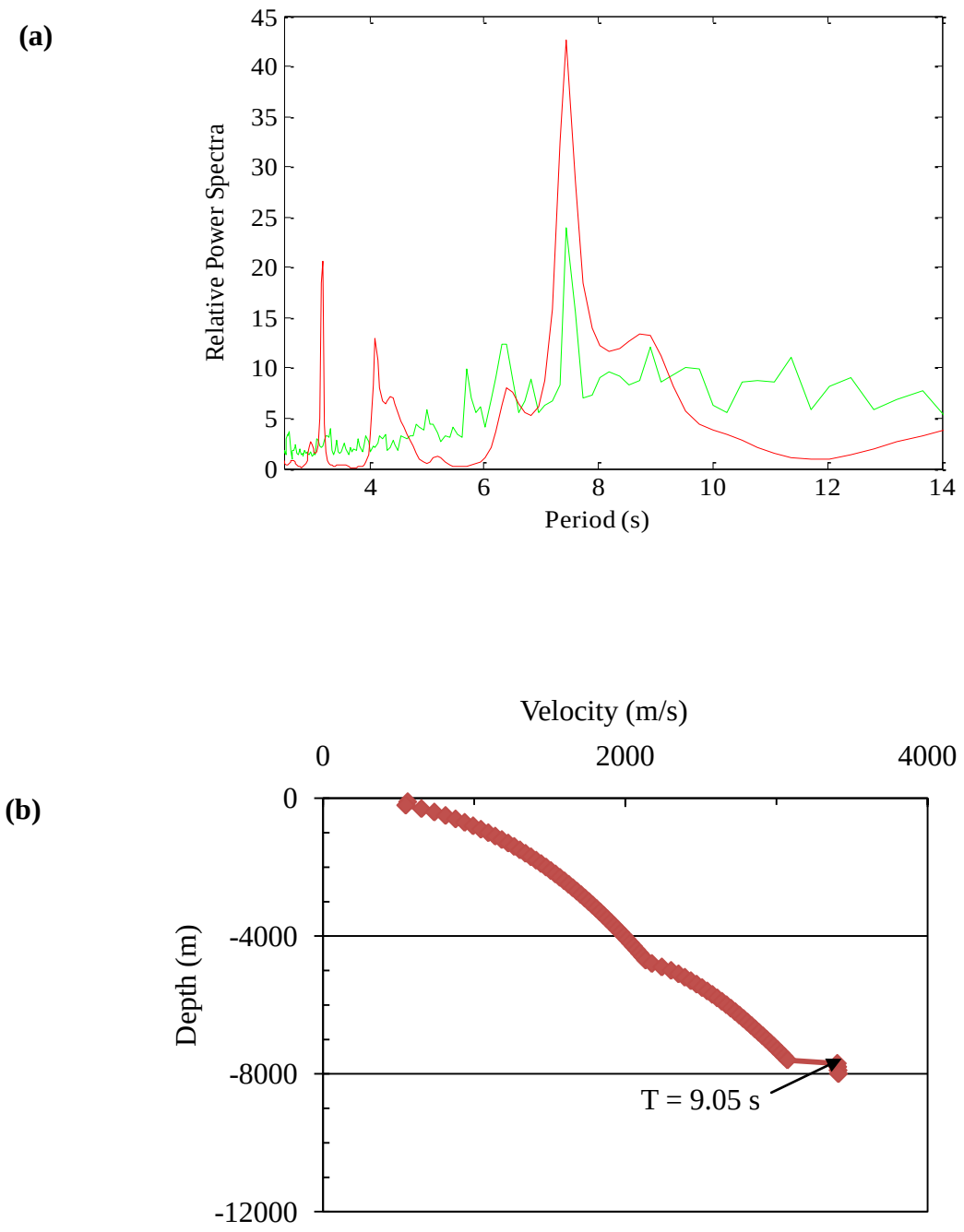

Figure 18. (a) Analysis of microtremor data (green) and earthquake data (red) from Diamond Bar earthquake for LTP. Length of data segment and Hanning window used for microtremor are 1002:71750 and 8192, respectively. Earthquake analysis uses data length 11970:13350 and Hanning window 8192. Here predominant peaks from two sources are in good match at 7.50 s. (b) Velocity-depth curve from 3D velocity model of California (http://www.data.scec.org/3Dvelocity/). Velocity discontinuity and predicted period indicated by arrow is calculated using equation 6.

Olinda (OLI)

OLI is located in a complex and steeply dipping western part of the central Los Angeles basin. It is represented by sediment cover of about 6000 m (Fig. 6), consisting of the Topanga and the Sespe Formations unconformably over the granitic basement. Microtremor spectra show many peaks, from short to long period (Fig. 19a). Short to intermediate peaks range from 1.5 to 5.0 s, whereas the long-periods are observed at 6.02 and ~ 8.2 s. The earthquake spectra show peaks at 3.2 and 4.0 s. The velocity-depth profile for OLI (Fig. 19b) shows gradual increase in velocity to a depth of 5000 m, after which velocity increases sharply. The velocity discontinuity at 6000 m gives an estimate of predicted period of 7.10 s.

The small periods obtained at 2.0 to 3.0 s may be due to lithologic contacts between the Pico and Repetto Formations or structural complexities. Intermediate peaks at 3.4 to 5.0 s could be due the stratigraphic contacts between members of the Puente Formation. The longer period around 7.0 ± 1 s can be correlated to the impedance contrasts between the interbedded Topanga and Sespe Formations and the underlying granitic batholith (Fig. 2).

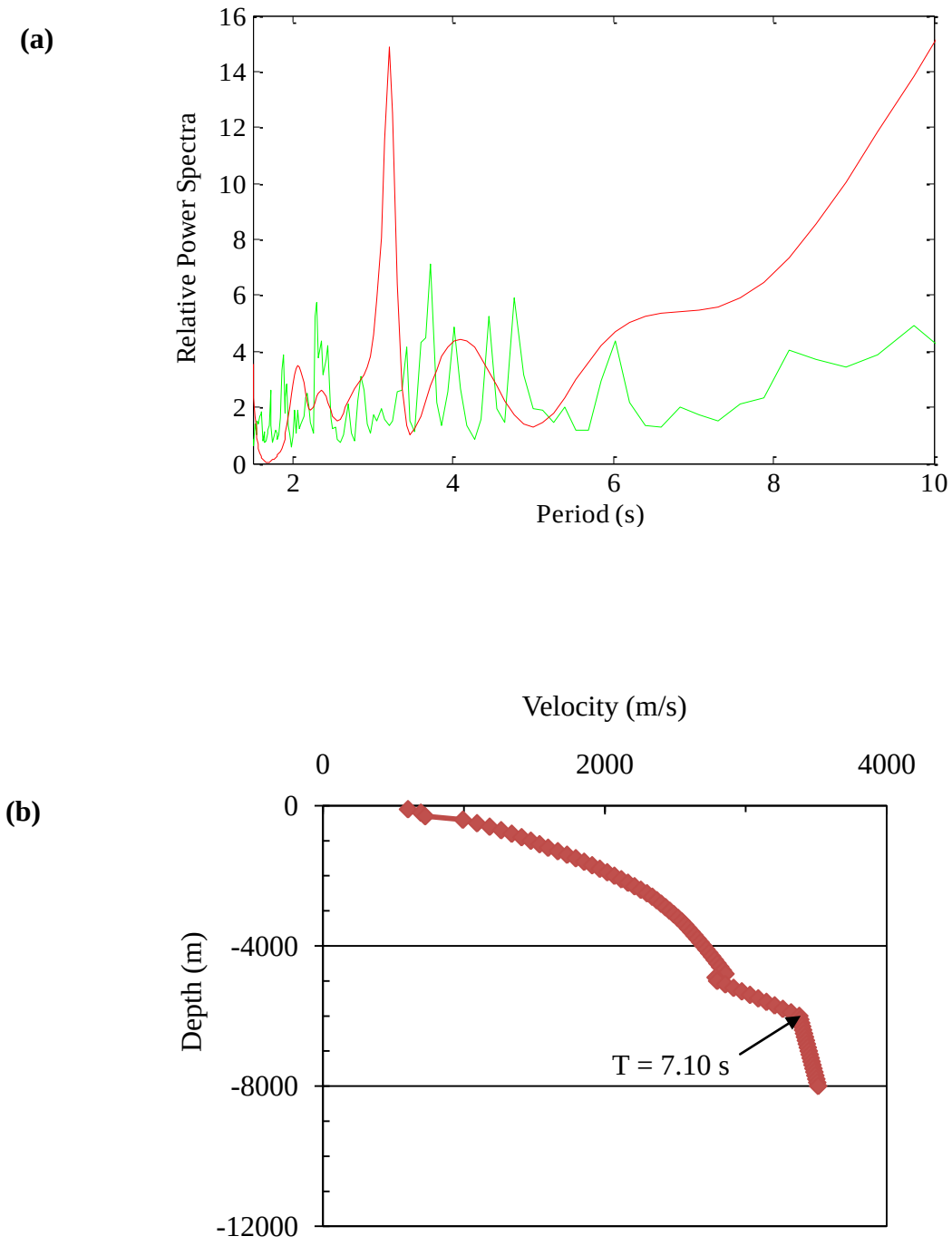

Figure 19. (a) Analysis of microtremor data (green) and earthquake data (red) from Diamond Bar earthquake for OLI. Microtremor spectra use data segment and Hanning window of 340:34690 and 8192, respectively. The respective numbers for earthquake analysis are 11970:13350 and 8192. (b) Velocity-depth curve from 3D velocity model of California (http://www.data.scec.org/3Dvelocity/). Velocity discontinuity and predicted period indicated by arrow is calculated using equation 6. Here, observed and predicted periods at ~ 7.0 s are in good match.

Ranchos Palos Verdes (RPV)

RPV is located in the southwestern part of the Los Angeles basin, close to the coast (Fig. 6). It rests on a thin cover (~1000 m) of sediment and sedimentary rocks of recent deposits and the Monterey shale, overlying the Mesozoic Catalina schist basement. Due to the thin sediment cover, RPV can also be considered as a reference or rock site. Figure 20a shows the HVSR from microtremor data. Spectra from the microtremors are relatively flat out to 10.78 s, where a large peak is present. The RPV velocity model is displayed in figure 20b. The velocity-depth curve shows constant velocity of 2950 m/s corresponding to a depth of 1000 m, after which it increases slightly until 5000 m. is observed. The discontinuities at 1000 and 5000 m produce predicted periods of 1.4 and 6.2 s, respectively.

The microtremor spectra show little amplification that concurs with shallow basement depth of RPV site. The peak around 3.0 to 4.0 s most likely relates to the basement interface depth between the middle Miocene Monterey shale and the Mesozoic Catalina schist (Fig. 2). The longer period observed at 10.78 s may be due to effects associated with the near-shore location of the RPV station.

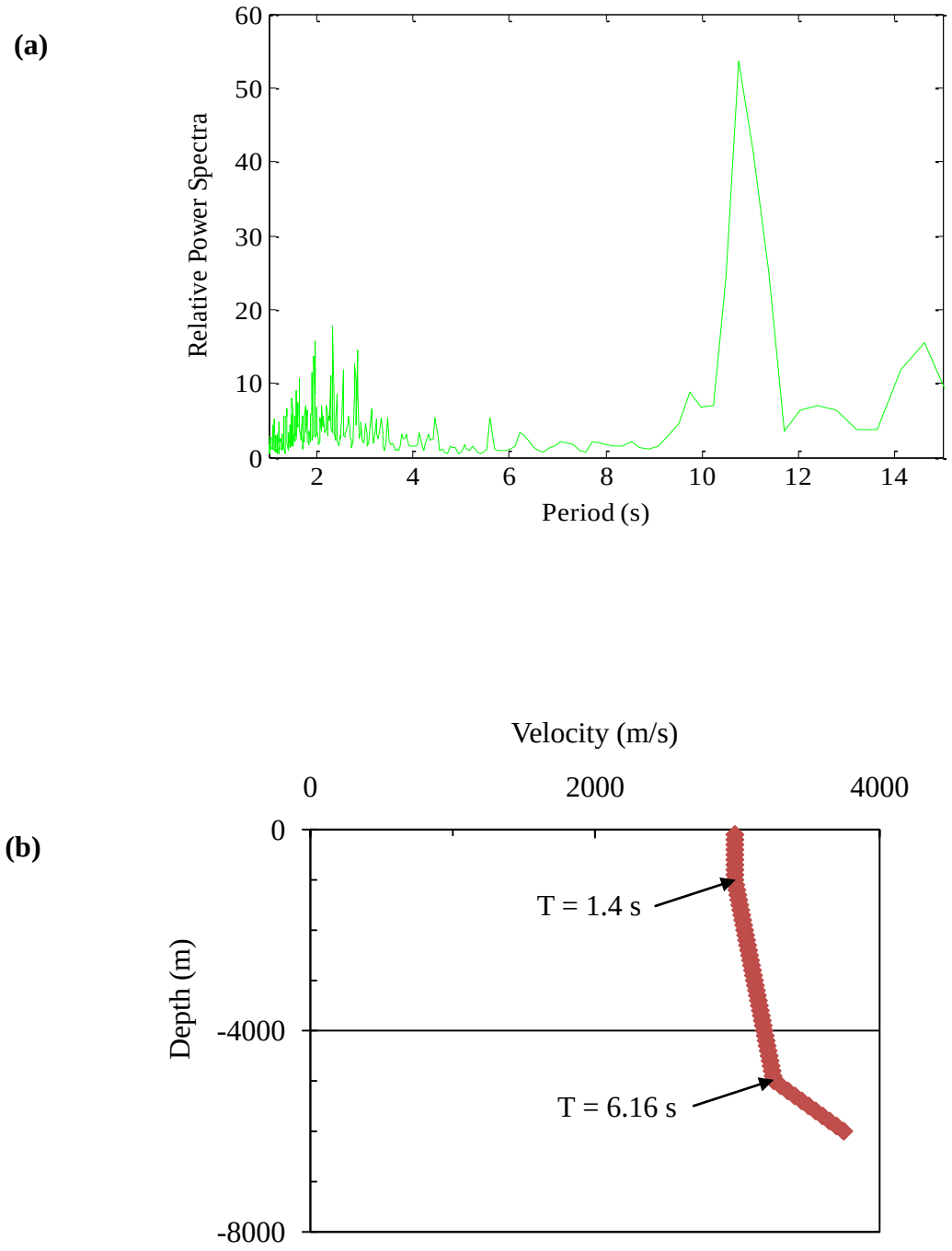

Figure 20. (a) Microtremor data analysis for RPV. Length of data segment and Hanning window used are 365:27210 and 8192, respectively. Low amplification observed in H/V spectra indicates shallow basement depth. Longer period ~ 10.78 s is associated with effects due to near-shore location of RPV (b) Velocity-depth curve from 3D velocity model of California (http://www.data.scec.org/3Dvelocity/). Velocity discontinuities and predicted periods indicated by arrows are calculated using equation 6.

Santiago (STG)

STG is located in the southern part of the central Los Angeles basin. It is situated in a relatively flat area between the Santa Ana Mountains and the San Joaquin Hills (Fig. 6). Depth to basement from different sources, such as the basement contour map, stratigraphic sections, and the 3D velocity model, give different depth values, ranging from 2450 to 6000 m. Microtremor spectra show observed peaks at 4.87, 5.85, 6.60 to 7.06, and 7.87 s (Fig. 21a). The earthquake spectra show small peaks at 4.45 and 6.60 s. The 3D velocity analysis (Fig. 21b) yields a constant velocity of 2227 m/s to a depth of 1000 m, then increases between 1000 and 6000 m. The periods calculated from the velocity discontinuities at 1000 and 6000 m are 2.0 and 6.20 s, respectively.

The energy present at periods from 2 to 3 s and 4.87 to 5.85 s are possibly related to stratigraphic contacts between the Pico and Repetto Formations, and the Miocene Topanga or Miocene to upper Eocene Sespe Formation and the granitic batholith, respectively (Fig. 2). The longer period around 7.24 ± 0.64 s could not be related to any stratigraphic interface.

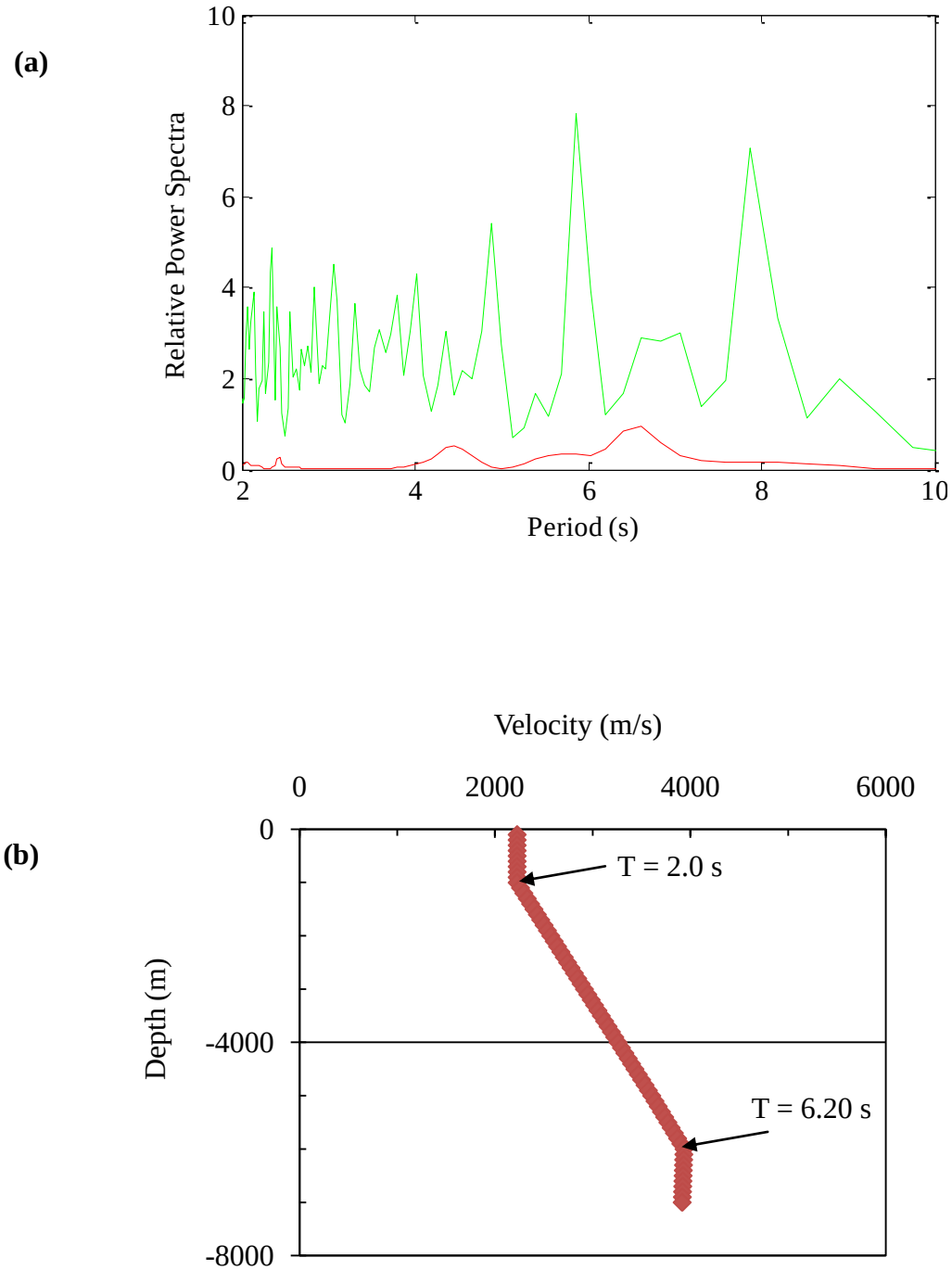

Figure 21. (a) Analysis of microtremor data (green) and earthquake data (red) from Diamond Bar earthquake for STG. Length of data segment and Hanning window used for microtremor are 15460:31590 and 8192, respectively. Earthquake analysis uses respective numbers 12000:13000 and 8192. (b) Velocity-depth curve from 3D velocity model of California (http://www.data.scec.org/3Dvelocity/). Velocity discontinuities and predicted periods indicated by arrows are calculated using equation 6.

Serrano (SRN)

SRN is located in the southeastern part of the central Los Angeles basin. It is situated in a structurally complex area, where the Santa Ana Mountains and normal faults are present in close proximity (Fig. 6). Depth to basement from different sources, such as the basement contour map and velocity-depth model, ranges from 3048 to 6000 m. The microtremor spectra show a relatively flat spectrum with small peaks at 4.20 and 6.40 s, whereas peaks of the earthquake spectra occur at 4.30 to 5.0 s, with a dominant peak at 6.60 s (Fig. 22a). The velocity-depth model maintains a constant value of 2150 m/s until a depth of 1000 m, and then it increases steadily to a depth of 6000 m (Fig. 22b). The corresponding predicted periods evaluated at 1000 and 6000 m are at 2.0 and 6.40 s, respectively.

The observed period in the earthquake spectra at 4.20 s most likely relates to the contact between the Miocene Topanga Group or Miocene to upper Eocene Sespe Formation, and the granitic batholith (Fig. 2). Source of the longer period is unknown, but the velocity reversal at 6000 m suggests structural complexity.

(a)

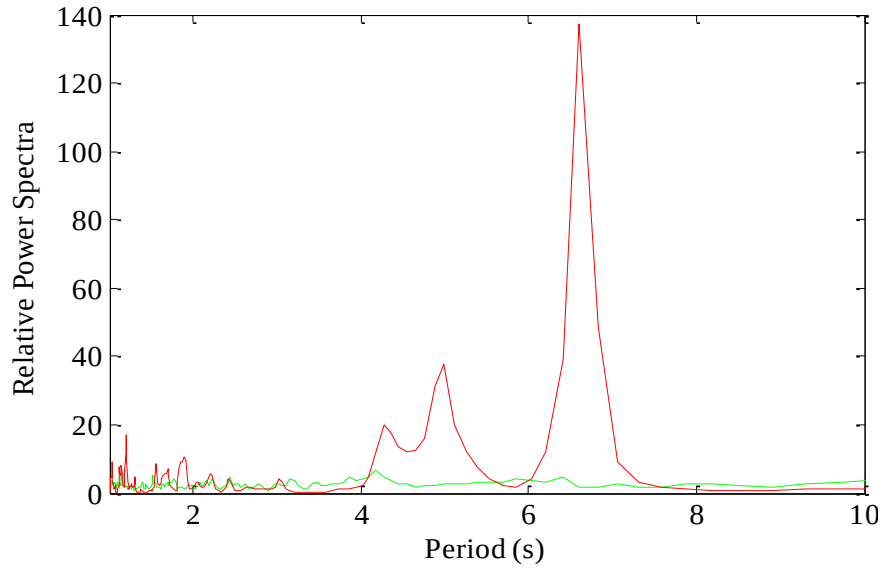

(b)

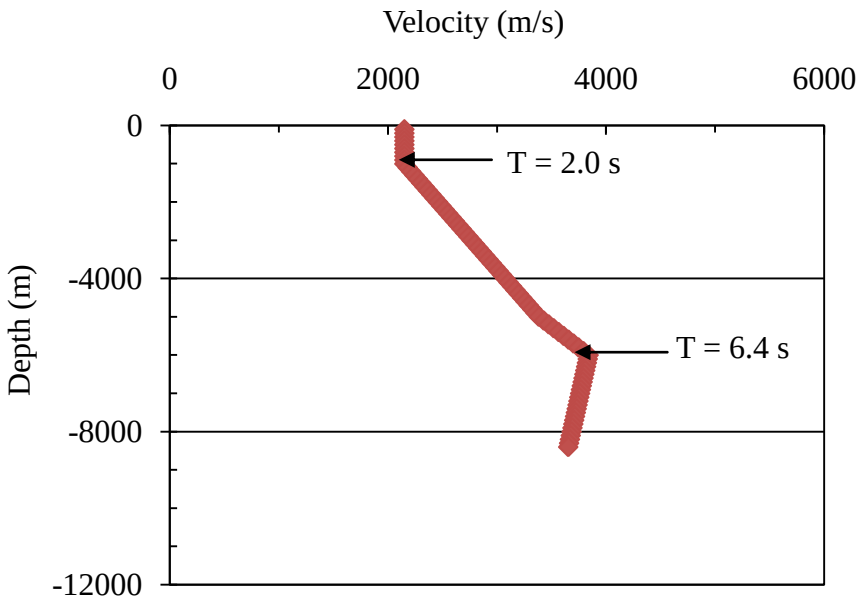

Figure 22. (a) Analysis of microtremor data (green) and earthquake data (red) from Diamond Bar earthquake for SRN. Length of data segment and Hanning window used for microtremor and earthquake analyses are 7686:39440, 8192, and 11850:13000, 8192, respectively. (b) Velocity-depth curve from 3D velocity model of California (http://www.data.scec.org/3Dvelocity/). Velocity discontinuities and predicted periods indicated by arrows are calculated using equation 6.

State Street (STS)

STS is located in the southwestern part of the Los Angeles basin on a relatively flat area and close to the coast (Fig. 6). Basement depth estimates for STS vary from 3000 to 6000 m. The microtremor spectra show observed peaks at 2.73 to 4.0, 5.0 to 5.68, and 6.82 to 7.87 s, while peaks of the earthquake spectra are located at 4.09, 5.12, 6.40, and 7.31 s (Fig. 23a). In general, the periods in which most energy is amplified agrees for the two spectra around 6.82 ± 1.0 s. The velocity-depth model shows a gradual increase in velocity to depth of 3300 m, after which a velocity reversal is observed (Fig. 23b). The discontinuity at this depth gave period of 4.7 s. However, velocity increases sharply between 5000 and 6000 m, giving predicted period of 6.60 s at 6000 m depth.

Impedance contrasts between the Monterey shale and the Catalina schist are the possible sources of peaks in the intermediate range periods (Fig. 2). The longer period peak, from 6.60 to 7.87 s, may be associated with the station's proximity to the shoreline or due to structural complexity within the basement as revealed from velocity reversal.

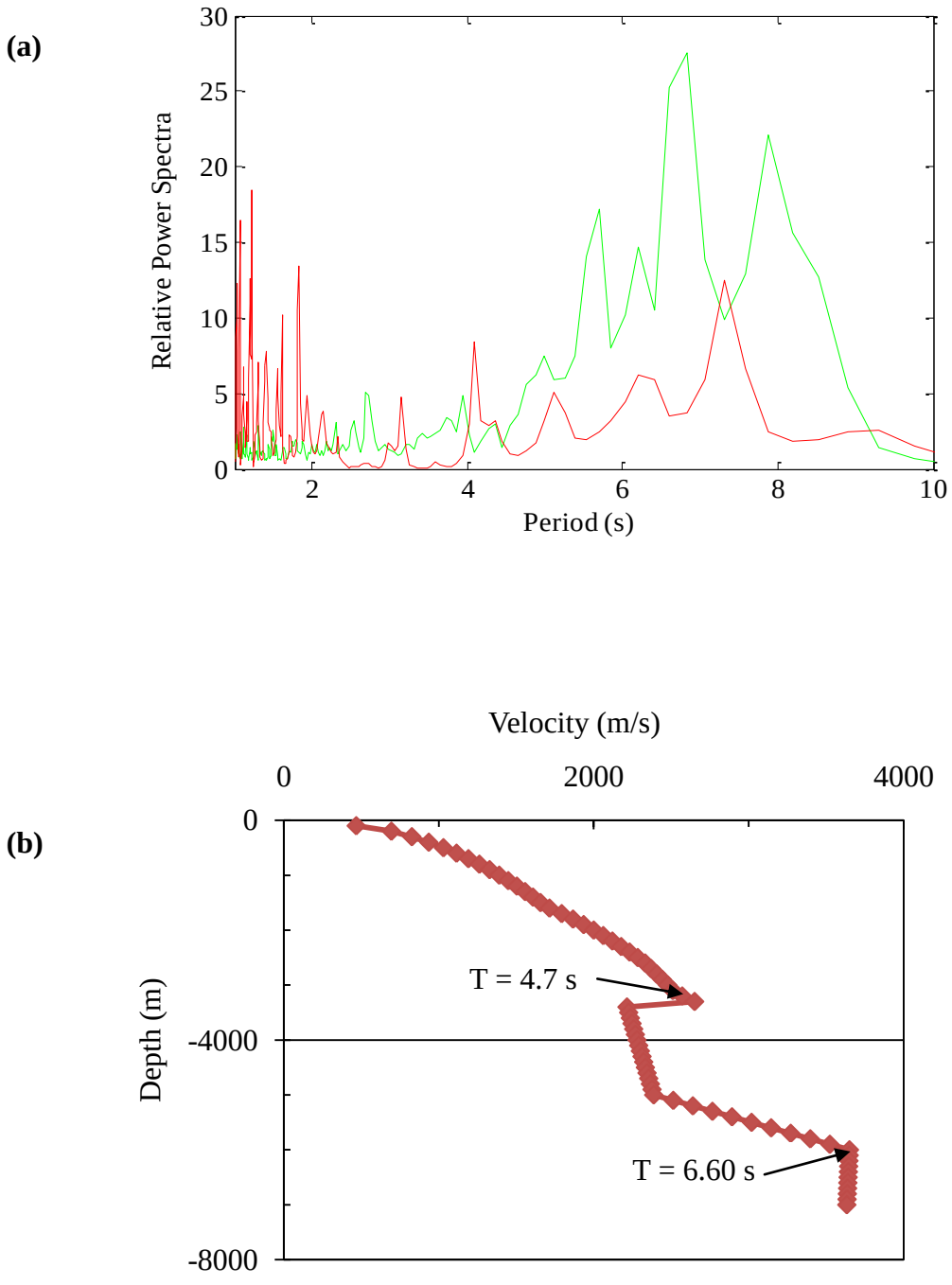

Figure 23. (a) Analysis of microtremor data (green) and earthquake data (red) from Diamond Bar earthquake for STS. Data segment and Hanning window used for microtremor analysis are 9344:35670 and 4096, respectively. Earthquake spectra use data segment and Hanning window of 12000:13380 and 4096, respectively. Most of energy is amplified around 6.82 ± 1.0 s for the two spectra. (b) Velocity-depth curve from 3D velocity model of California (http://www.data.scec.org/3Dvelocity/). Velocity discontinuities and predicted periods indicated by arrows are calculated using equation 6.

University of Southern California (USC)

USC is located in the northern part of the central Los Angeles basin. It is situated on the flanks of the syncline with thick sediment cover of 7000 m that overlies the granitic batholith basement (Fig. 6). The microtremor spectra show observed peaks at 4.0 to 4.45 and around 6.4 ± 1.0 s and the earthquake spectra show peaks at 4.45 and around 6.4 ± 0.4 s (Fig. 24a). The velocity model shows a steady increase of velocity up to 5000 m depth, beyond which it rises sharply (Fig. 24b). The velocity discontinuity at depth of 6000 m gives a predicted period of 6.12 s.

The microtremor, earthquake, and velocity-depth profile results for USC show very good correlation. The intermediate period peaks from 4.0 to 4.45 s correspond to the lithologic contacts between the members of Puente Formation. The longer period peaks at 6.12 to 6.40 s could be due to the impedance contrasts between the older Miocene Topanga sandstones and the Cretaceous granitic batholith basement (Fig. 2).

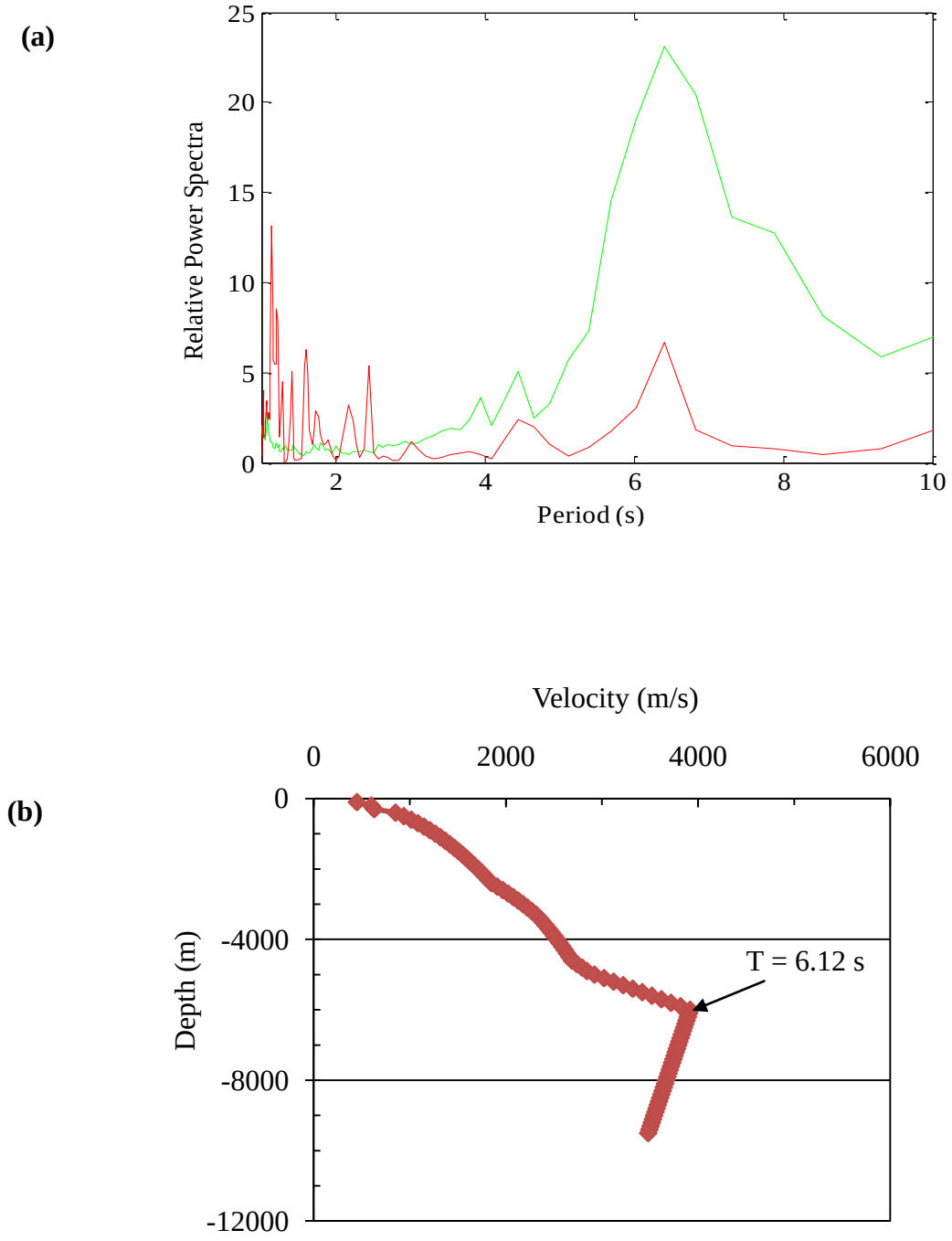

Figure 24. (a) Analysis of microtremor data (green) and earthquake data (red) from Diamond Bar earthquake for USC. Microtremor data segment and Hanning window used are 1431:28350 and 4096, respectively. The respective numbers for earthquake spectra are 12000:12960 and 4096. (b) Velocity-depth curve from 3D velocity model of California (http://www.data.scec.org/3Dvelocity/). Velocity discontinuities and predicted periods indicated by arrows are calculated using equation 6. Here observed and predicted periods show very good agreement around ~ 6.0 s.

Walnut (WLT)

Walnut or WLT is located in the northeastern part of the central Los Angeles basin. It is separated from the central part by the northwest-trending Whittier-Elsinore Fault System (Fig. 6). Depth to basement values from different sources for WLT varies from 2400 to 6000 m. The microtremor spectra show several peaks at 2.66, 4.0 to 7.58, and 9.75 s. The Diamond Bar earthquake spectra also show several peaks at 3.0 and 4.2 to 7.58 s (Fig. 25a). Three distinct velocity discontinuities are observed in the velocity profile at depths of 1000, 2500, and 6000 m (Fig. 25b). These give predicted periods at 2.02, 4.13, and 6.44 s, respectively.

The shorter period at 2.02 to 2.66 s could be related to the lithologic contact between the Pico and Repetto Formations. The intermediate periods from 4.01 to 5.25 s correspond to the impedance contrasts between members of the Puente Formation. The longer periods from 6.4 to 7.58 s could be related to the sediment-basement interface between the Topanga Formation and the granitic batholith basement (Fig. 2).

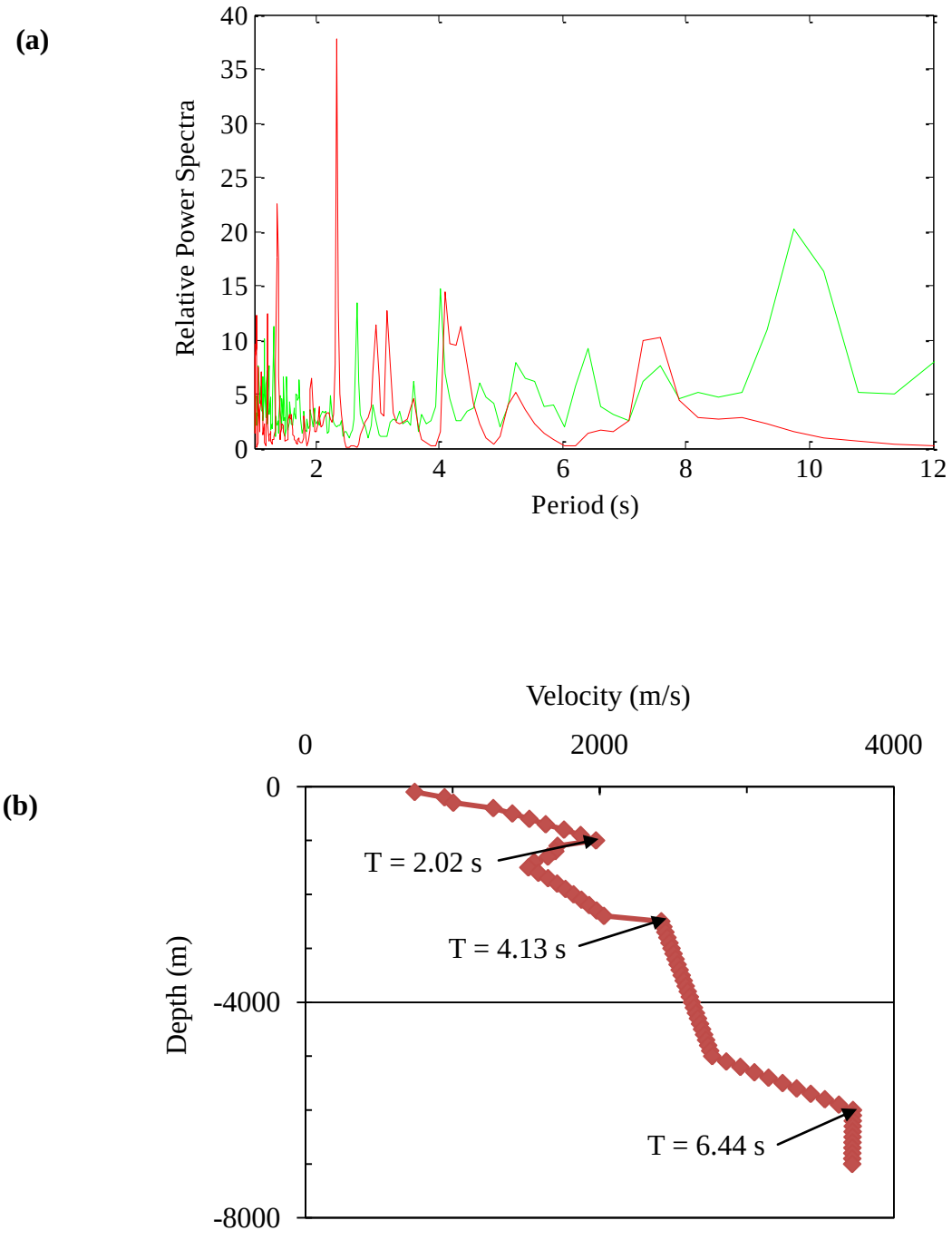

Figure 25. (a) Analysis of microtremor data (green) and earthquake data (red) from Diamond Bar earthquake for WLT. Microtremor data segment and Hanning window used are 4745:19380 and 4096, respectively. The respective numbers for earthquake spectra are 11880:13260 and 4096. (b) Velocity-depth curve from 3D velocity model of California (http://www.data.scec.org/3Dvelocity/). Velocity discontinuities and predicted periods indicated by arrows are calculated using equation 6. Here observed and predicted period ranges show good agreement.

Watts (WTT)

WTT is located in the western flank of the central Los Angeles syncline. It is separated from the southwestern part by the northwest-trending Newport-Inglewood Fault System (Fig. 6). Depth to basement for WTT ranges from 7300 to 8000 m. The observed peaks from microtremor spectra are positioned at 5.25, 6.20, 7.06, 8.53, and 10.24 s, while those for the earthquake spectra occur at 3.2, 4.09, and 7.31 s (Fig. 26a). The velocity model shows a steady increase of velocity up to 8000 m depth, beyond which it rises sharply (Fig. 26b). The discontinuity at this depth gives predicted period of 9.21 s.

The intermediate period around 5.25 to 6.20 s could be related to the impedance contrasts between the members of Puente Formation. The longer period ranging from 8.53 to 10.24 s is possibly due to the impedance contrasts between the older Miocene Topanga sandstones and the Cretaceous granitic batholith basement (Fig. 2).

(a)

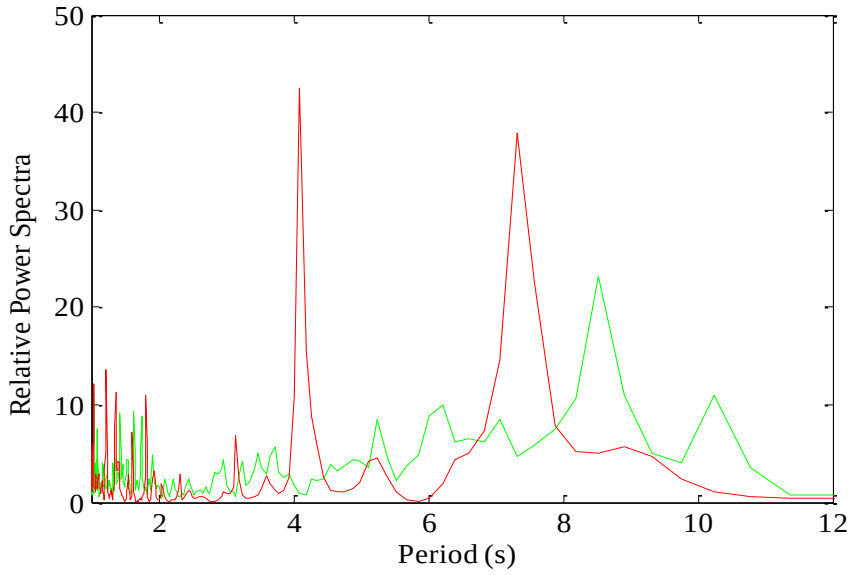

(b)

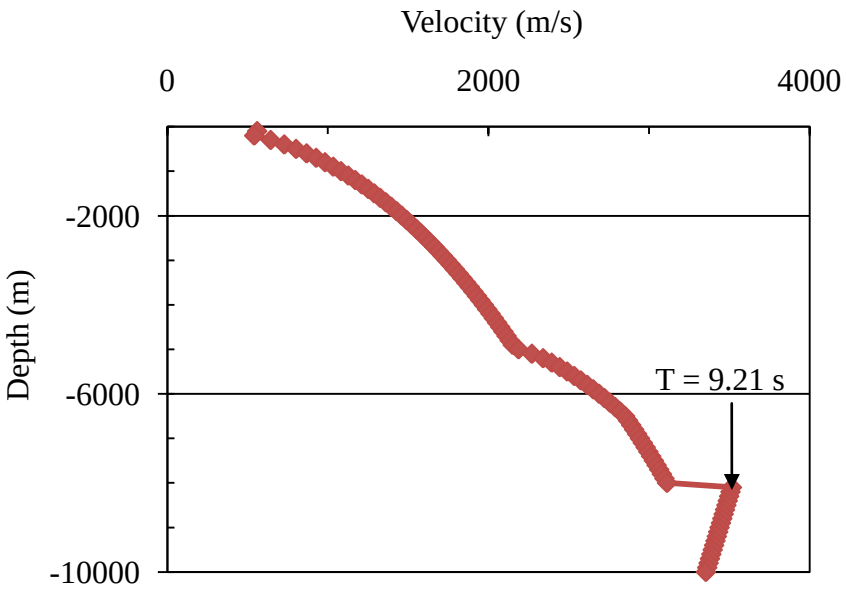

Figure 26. (a) Analysis of microtremor data (green) and earthquake data (red) from Diamond Bar earthquake for WTT. Microtremor data segment and Hanning window used are 4251:18060 and 4096, respectively. Earthquake analysis uses data length 12000:13380 and Hanning window 8192. (b) Velocity-depth curve from 3D velocity model of California (http://www.data.scec.org/3Dvelocity/). Velocity discontinuities and predicted periods indicated by arrows are calculated using equation 6. Here observed and predicted periods at ~ 9.0 s are in good agreement.

Temporal stability of microtremor peaks over time

Microtremor data from six stations, LAF, LGB, LLS, STS, USC, and WTT, from 2005 through 2008 were analyzed to test the consistency of spectral peaks over time. The choice of stations used depended upon their locations and depths to basement. The objective of this test was to detect whether the spectral peak positions are independent of subsurface structures and path effects. Table 4 shows the length of data and Hanning window used for the selected six stations. Stations such as LAF, LLS, and STS are located in areas with relatively subdued basement topography and moderate basin thickness (< 4.5 km). On the other hand, stations LGB, USC, and WTT lie on the flanks of a steeply dipping syncline and have basement depths more than 7 km.

Figure 27 through Figure 32 shows HVSRs for these six stations over the 5-year period. Spectra from LAF, LLS, STS, and USC show one or two dominant peaks that are consistent over time. This observation is specially striking for USC, which despite having a deep basement produces consistent results. The spectral peaks from LGB and WTT show much variability over with time.

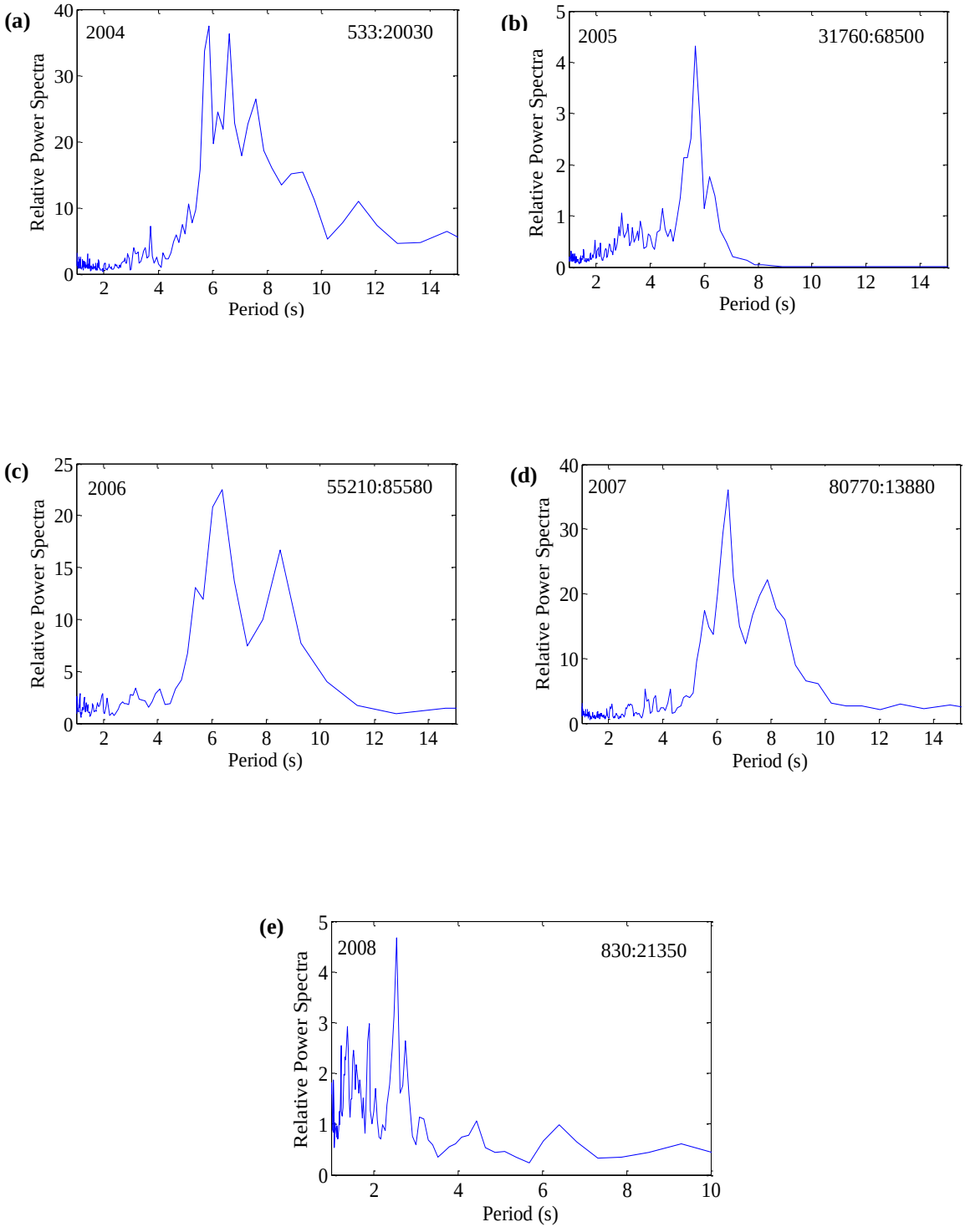

Figure 27 (a – e). HVSRs from year 2004 through 2008 for LAF station (depth < 2.5 km). Upper right corner of spectra shows length of extracted data segment in samples, analyzed using Hanning window 4096. Dominant peaks range from 5.70 to 6.60 s and are consistent over time. Energy in the 8 to 10 s range is present in some records.

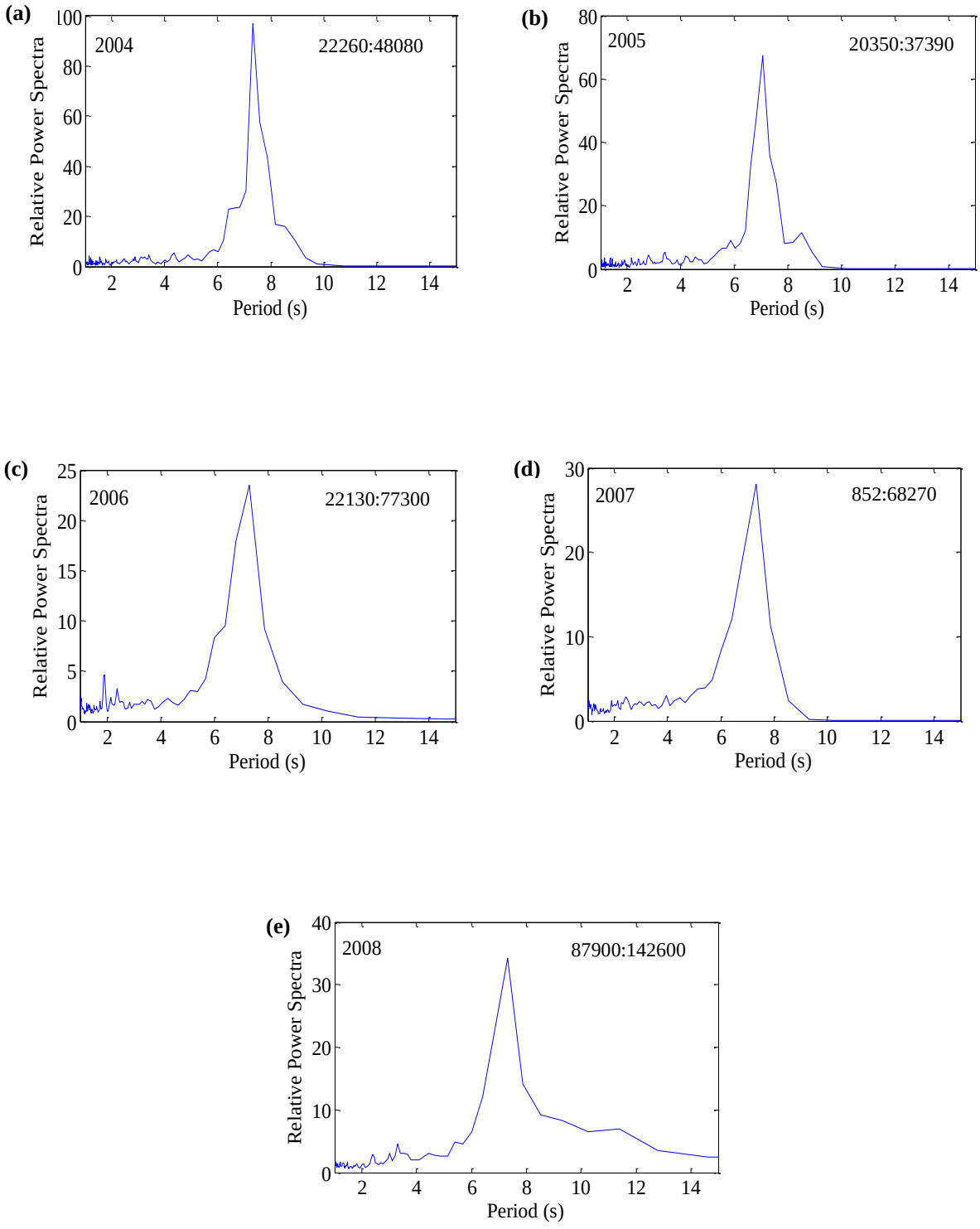

Figure 28 (a – e). HVSRs from year 2004 through 2008 for LLS station (depth ~ 4.5 km). Upper right corner of spectra shows length of extracted data segment in samples, analyzed using Hanning window 4096. Dominant peak ranges from 7.06 to 7.31 s and is stable over time.

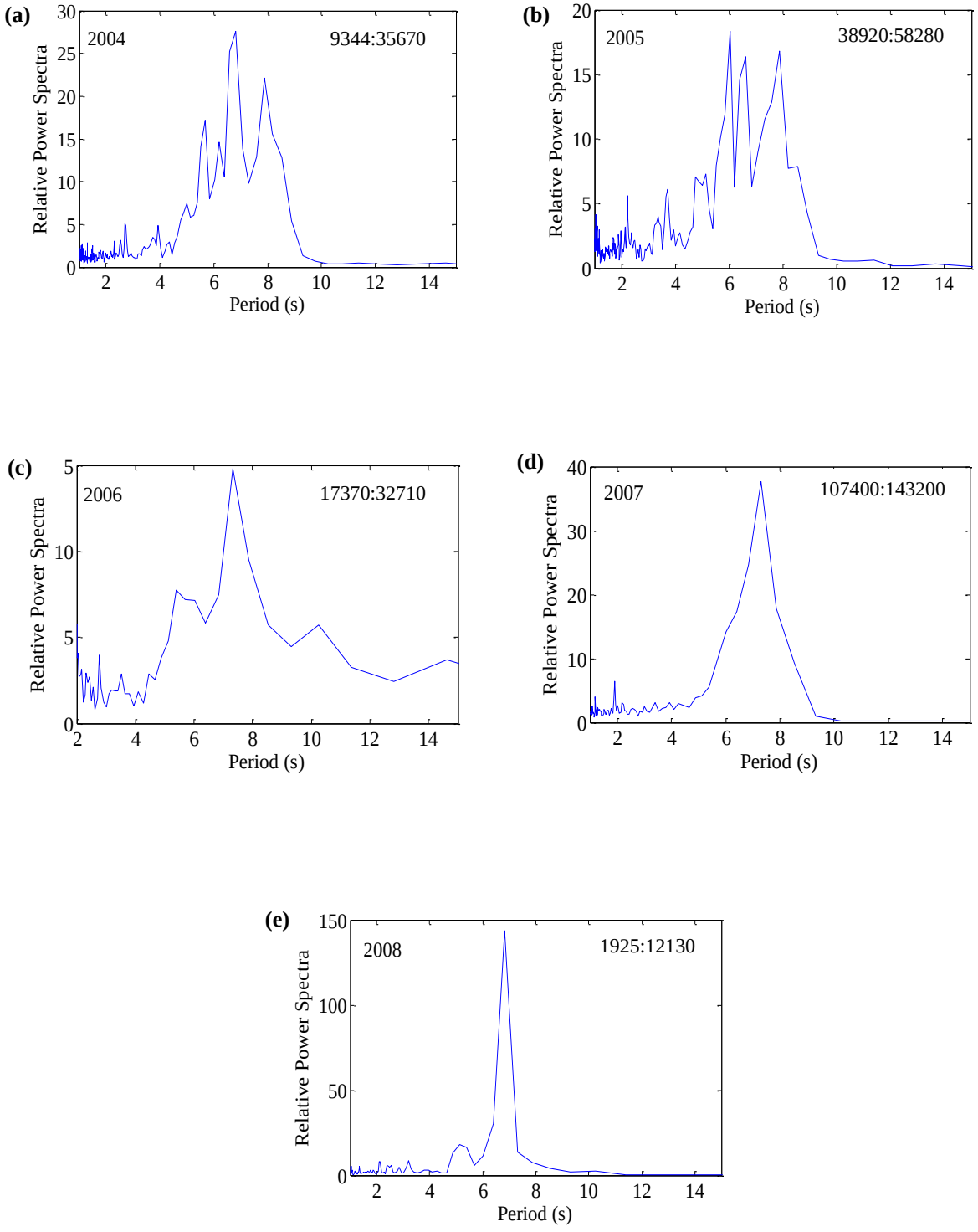

Figure 29 (a – e). HVSRs from year 2004 through 2008 for STS station (depth < 4.5 km). Upper right corner of spectra shows length of extracted data segment in samples, analyzed using Hanning window 4096. Dominant peak ranges from 6.06 to 7.87 s and is stable over time.

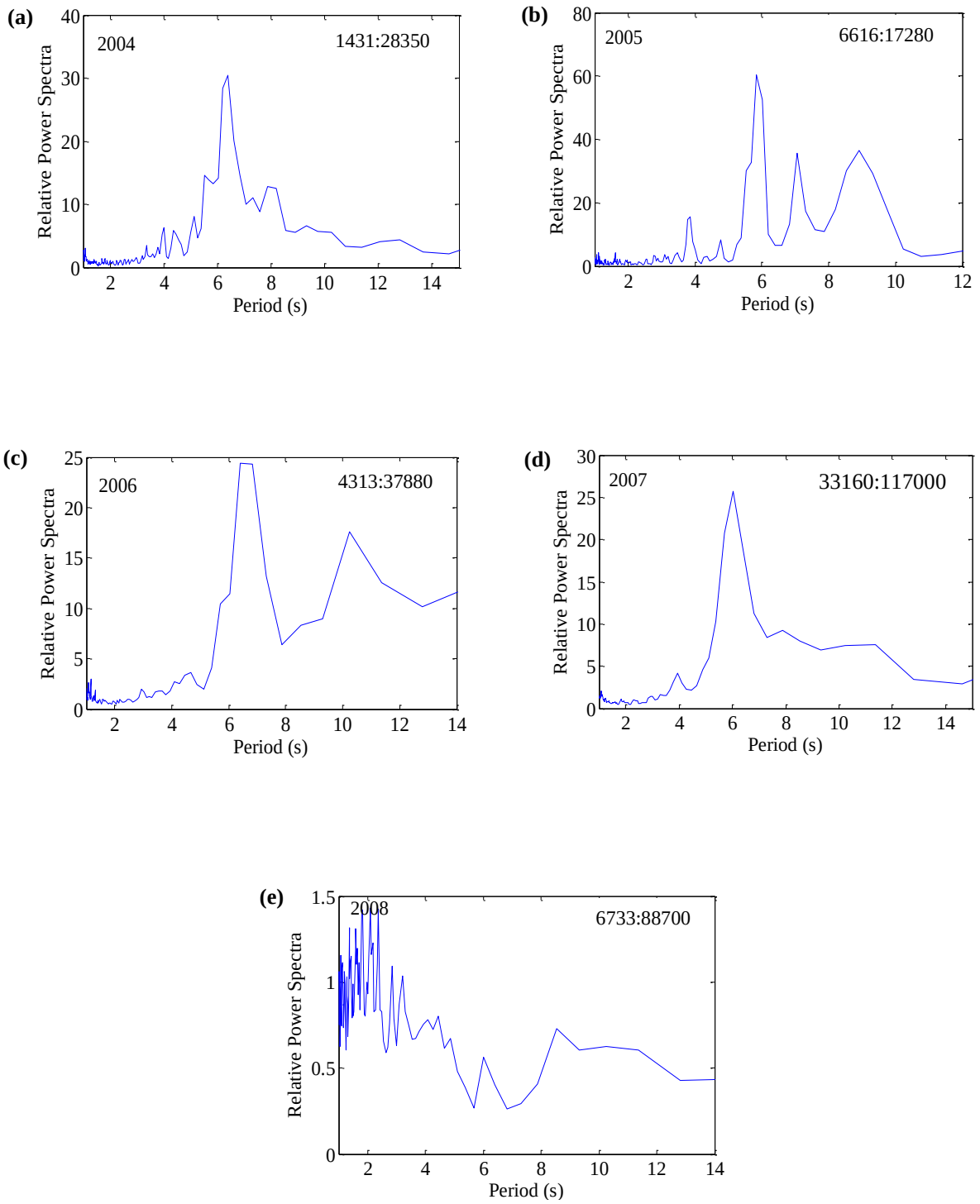

Figure 30 (a – e). HVSRs from year 2004 through 2008 for USC station (~ 7 km). Upper right corner of spectra shows length of extracted data segment in samples, analyzed using Hanning window 4096. Dominant peak ranges from 5.85 to 6.82 s and is consistent over time. Peaks in the range 1 to 3 s in the 2008 spectra indicate some nearby noise source.

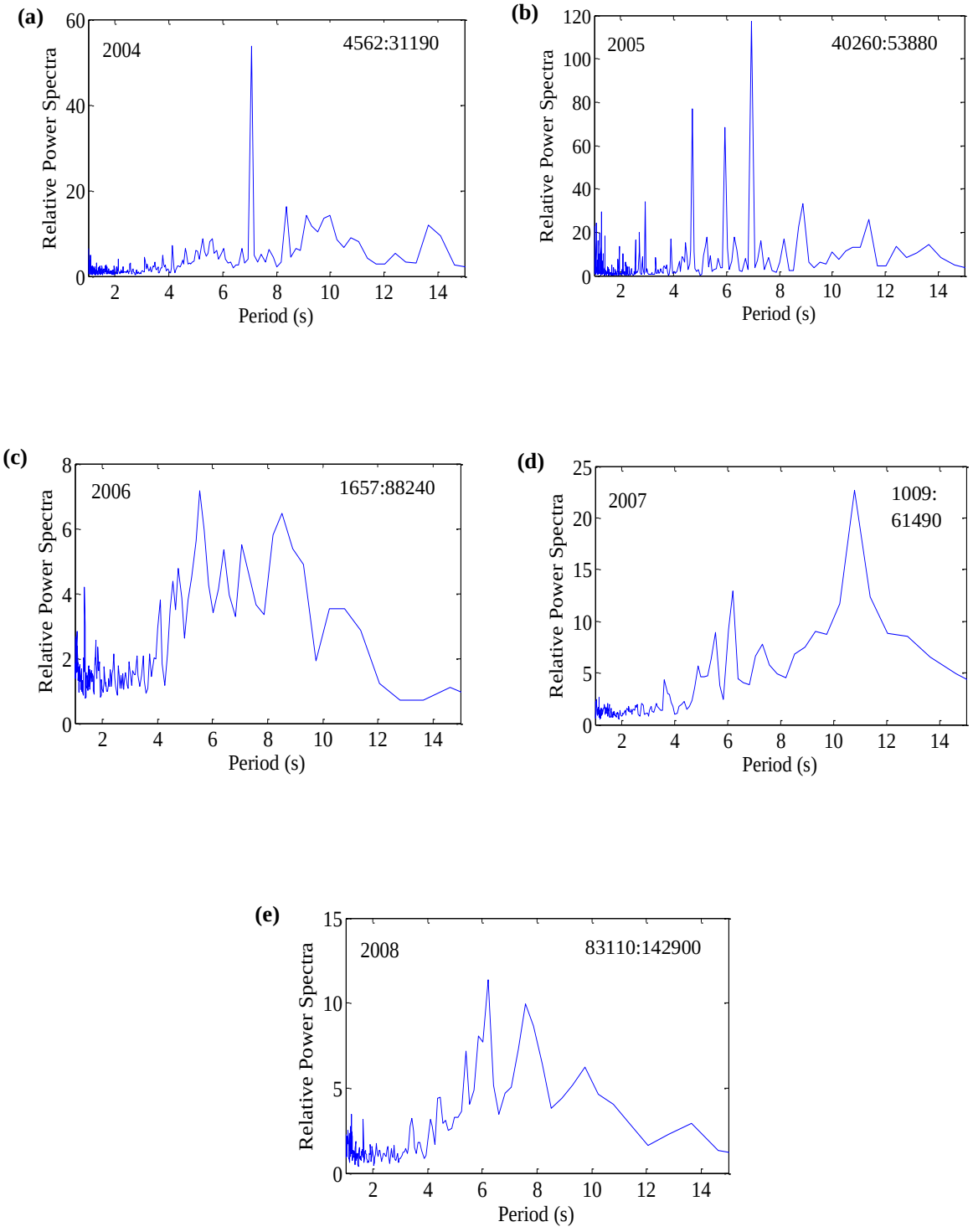

Figure 31 (a – e). HVSRs from year 2004 through 2008 for LGB station (depth ~ 8 km). Upper right corner of spectra shows length of extracted data segment in samples, analyzed using Hanning window 8192. Spectra show variable and inconsistent peaks over time, except there is always a peak in range 6 to 7.5 s.

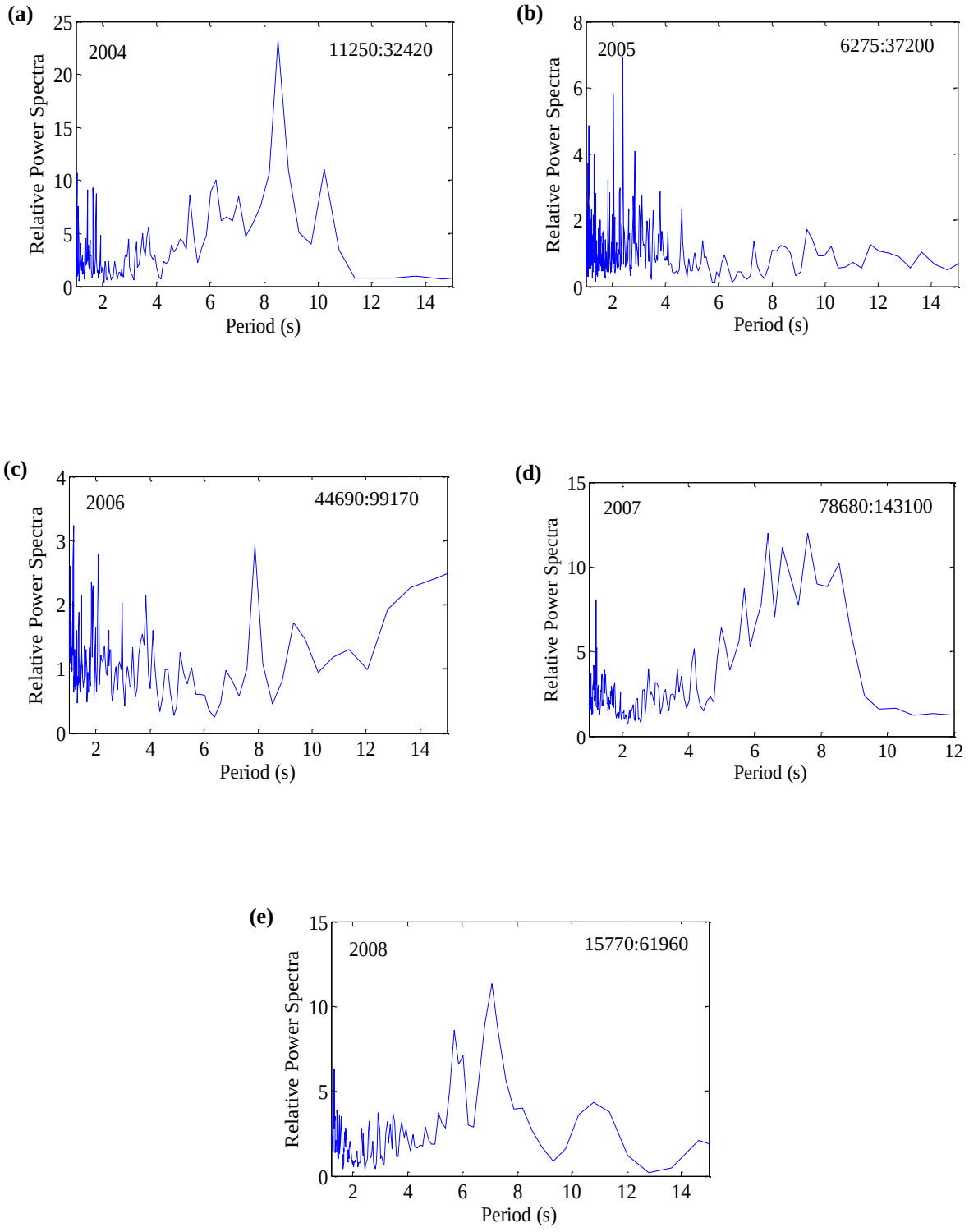

Figure 32 (a – e). HVSRs from year 2004 through 2008 for WTT station (depth ~ 7 km). Upper right corner of spectra shows length of extracted data segment in samples, analyzed using Hanning window 8192. Spectra show variable and inconsistent peaks over time, however, peak around ~ 8.0 s is usually present.

CHAPTER V

DISCUSSION

5.1. Implication of peaks obtained from microtremor HVSR

Based on the predicted periods calculated from the California 3D shear-wave velocity model, many peaks observed in the microtremor HVSR correspond to impedance contrasts in the subsurface formations. Three peak ranges, namely, short (< 4.0 s), intermediate (4 to 6 s), and long (> 6.0 s) represent site resonance within the Los Angeles basin. These period ranges correspond to different stratigraphic interfaces, located at varying basement depths. Therefore, stations are classified according to their basement depth as shallow (< 3 km), intermediate (3 to 6 km), and deep (> 6 km).

Table 5 lists four stations, FMP, LAF, RPV, and STG, with basement depths less than 3 km. These four stations exhibit short to intermediate periods corresponding to the sediment-basement interface. Two of the stations, FMP and RPV, are located over shallow basement and their HVSRs correspondingly show very low amplification except at high frequencies (Fig. 13a and Fig. 20a). Long periods (10 to 12 s) observed at these stations could not be related to any stratigraphic interface. Both FMP and RPV are located near the shoreline, and the longer periods observed in the spectra may be related to some effects of ocean waves. The cause of longer periods at LAF and STG may be related to structural complexity of basement rocks.

Table 5. Periods observed in microtremor HVSRs of stations with basement depth < 3 km. Periods are related to major stratigraphic units. A period range not observed in indicated by (–). Station locations shown in Fig. 6.

Station	Short Period (s)	Stratigraphic Unit	Intermediate Period (s)	Stratigraphic Units	Long Period (s)	Stratigraphic Units
FMP	3 to 4	Monterey shale - Catalina schist	–	–	10 to 12	Unknown
LAF	–	–	5.53 to 6.02	Monterey shale - Catalina schist	6.60 to 7.31	Unknown
RPV	3 to 4	Monterey shale - Catalina schist	–	–	10 to 12	Unknown
STG	1 to 3	Pico - Repetto Formation	4.87 to 5.85	Topanga Formation - Granitic batholith	6.40 to 7.87	Unknown

Table 6 shows list of six stations, LCG, LLS, OLI, SRN, STS, and WLT, with basement depths ranging from 3 to 6 km. This group of station exhibits short, intermediate, and long periods. The short and intermediate periods correspond to Pleistocene-Pliocene and middle to late Miocene stratigraphic contacts, respectively (Fig. 2). Although most of the long-period spectral peaks are related to the sediment-basement contact, peaks from station SRN and STS could not be related to any lithologic interface.

Table 6. Periods observed in microtremor HVSRs of stations with basement depth 3 to 6 km. Periods are related to major stratigraphic units. A period range not observed in indicated by (–). Station locations shown in Fig. 6.

Station	Short Period (s)	Stratigraphic Unit	Intermediate Period (s)	Stratigraphic Units	Long Period (s)	Stratigraphic Units
LCG	–	–	4.0 to 5.12	Members of Puente Formation	6.40 to 6.60	Topanga Formation - Granitic batholith
LLS	–	–	~ 4.0	Monterey shale - Upper Topanga Formation	6.60 to 7.31	Topanga Formation - Catalina schist
OLI	2 to 3	Pico - Repetto Formation	3.4 to 5.0	Members of Puente Formation	6.02 to 8.2	Topanga Formation - Granitic batholith
SRN	–	–	~ 4.0	Topanga Formation - Granitic batholith	~ 6.0	Unknown
STS	–	–	4.0 to 5.68	Monterey shale - Catalina schist	6.60 to 7.87	Unknown
WLT	2.02 to 2.66	Pico - Repetto Formation	4.0 to 5.25	Members of Puente Formation	6.40 to 7.58	Topanga Formation - Granitic batholith

Table 7 shows group of six stations, BRE, DLA, LGB, LTP, USC, and WTT, with basement depth greater than 6 km. These stations are located at the center of the Los Angeles basin; some are situated in areas of structural complexities, such as on flanks of the syncline or close to fault systems (Fig. 6). Stations mainly show intermediate and long periods that correspond to the impedance contrasts between members of the Puente Formation and sediment-basement interface, respectively (Fig. 2). Spectra from some of the stations, such as LGB and WTT, exhibit inconsistent HVSR peaks over time (Fig. 31 and Fig. 32). The inconsistency of spectral peaks is not only due to the impedance contrasts in stratigraphic units, but is also related to the basin structure (Lachet and Bard, 1994).

Table 7. Periods observed in microtremor HVSRs of stations with basement depth greater than 6 km. Periods are related to major stratigraphic units. Station locations shown in Fig. 6.

Station	Intermediate Period (s)	Stratigraphic Units	Long Period (s)	Stratigraphic Units
BRE	6.10 to 6.50	Members of Puente Formation	8.20 to 9.50	Topanga Formation - Granitic batholith
DLA	5.25 to 6.0		8.20 to 10.24	
LGB	4.0 to 6.0		7.06 to 8.60	
LTP	5.8 to 7.0		7.45 to 9.0	
USC	4.0 to 4.45		6.40 to 6.82	
WTT	5.25 to 6.20		8.53 to 10.24	

5.2. Comparison of microtremor and earthquake spectra

Site response characteristics inferred from microtremors and earthquake shear waves have been compared in past studies. Two important aspects, predominant period and amplification factor, are measured for use in microzonation and amplification studies.

Lermo and Chavez-Garcia (1993, 1994) applied Nakamura's (1989) H/V technique to measure shear-wave earthquake records in three cities of Mexico, all having varied geologic and tectonic setting and different epicentral distances from the source. Their results conclude that H/V ratio can give a robust estimate of frequency. The study showed comparable dominant periods of both microtremor and earthquake spectral ratios at a site. However, only a rough estimate of amplification factor was possible if geologic conditions were simple. Bonilla et al. (1997) performed a detail study of 38 aftershocks of the 1994 Northridge earthquake. They observed that predominant frequencies from microtremors corresponded well with the earthquake shear-wave, but did not capture amplifications. Results of this study were supported and carried forward by Huang and Teng (1999), who conducted several analyses using both the 1994 Northridge earthquake and microtremor data. One of the analyses compared HVSR results from microtremors at the USC site, with spectral ratios from the earthquake at the same site. The results indicated a good agreement between these two methods in terms of fundamental frequency within a specific range, together with a crude approximation to the amplification factor. Huang (2002) also observed the spectral relationship between microtremors and earthquake ground motions using the 1999 Chi Chi earthquake in

central Taiwan. In the study, HVSR could predict the predominant frequency, but the amplification at resonant frequencies seemed to be unreliable.

Predominant periods and amplitudes of spectral peaks from the HVSR of microtremors and standard spectral ratios of the Diamond Bar earthquake are compared in this study. Figure 33a shows a relative study of resonant periods from the two sources. In general, the microtremor period increases with the increase in basement depth. For example, short periods are observed for sites, such as FMP and RPV (basement depth < 2 km), whereas longer periods correspond to sites, such as BRE and DLA (basement depth > 6 km). However, the predominant periods in the earthquake recordings are between 6 to 8 s. It is only in this range that the predominant periods from microtremor and earthquake data show good harmony.

Figure 33b illustrates a comparative study of amplitudes at resonant periods from microtremor and earthquake data for the broadband stations. The plot exhibits poor correlation between microtremor and earthquake amplification factors; however, the amplification factors obtained from the microtremors have systematically lower values. Lachet and Bard (1994) investigated the variations of spectral amplitudes. They concluded that HVSR's amplitudes decreased with decreasing Poisson's ratio in sedimentary layers. The study also revealed the influence of basin structure on the H/V peak amplitudes. They obtained random variations in amplitude for stations located in structurally complex areas.

Earthquake amplification is determined by several factors. Figure 34 is a California Integrated Seismic Network (CISN) shake map representing ground shaking

produced by the Diamond Bar earthquake. The map shows the various intensity levels and peak ground acceleration (% g) ranges experienced at sites throughout the region. These ground-shaking levels at a particular site are dependent on distance from the earthquake epicenter, near-surface geologic material, and the variation in propagation of seismic waves from the source due to structural complexities in the earth's crust. Since wave energy is attenuated with increasing distance, areas close to the epicenter experience strong to very strong ground shaking (instrumental intensity VI – VII) compared to those far from the epicenter that record light to moderate shaking effect (instrumental intensity IV – V) (Fig. 34). The shake map shows variations in amplification values from a single earthquake source at different station locations.

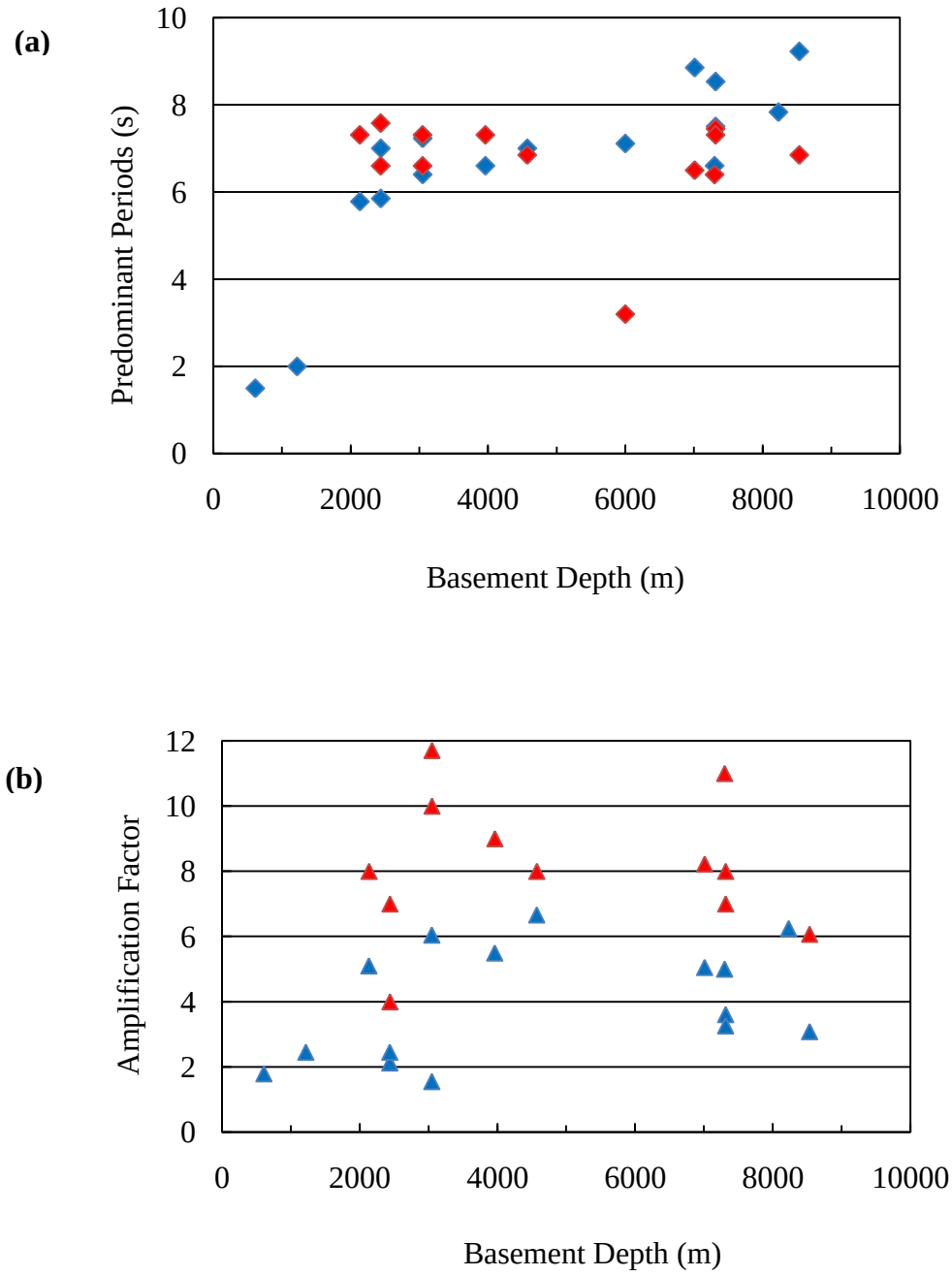

Figure 33. (a) Comparison of predominant periods obtained from microtremor (blue) and earthquake (red) recordings. Resonance periods obtained from microtremor H/V peaks (Nakamura, 1989) show good agreement with earthquake peaks. Peaks are concentrated within 6 to 8 s. (b) Comparison of relative amplification factor at predominant periods from microtremor (blue) and earthquake (red) records. In general, amplifications from microtremor show lower values.

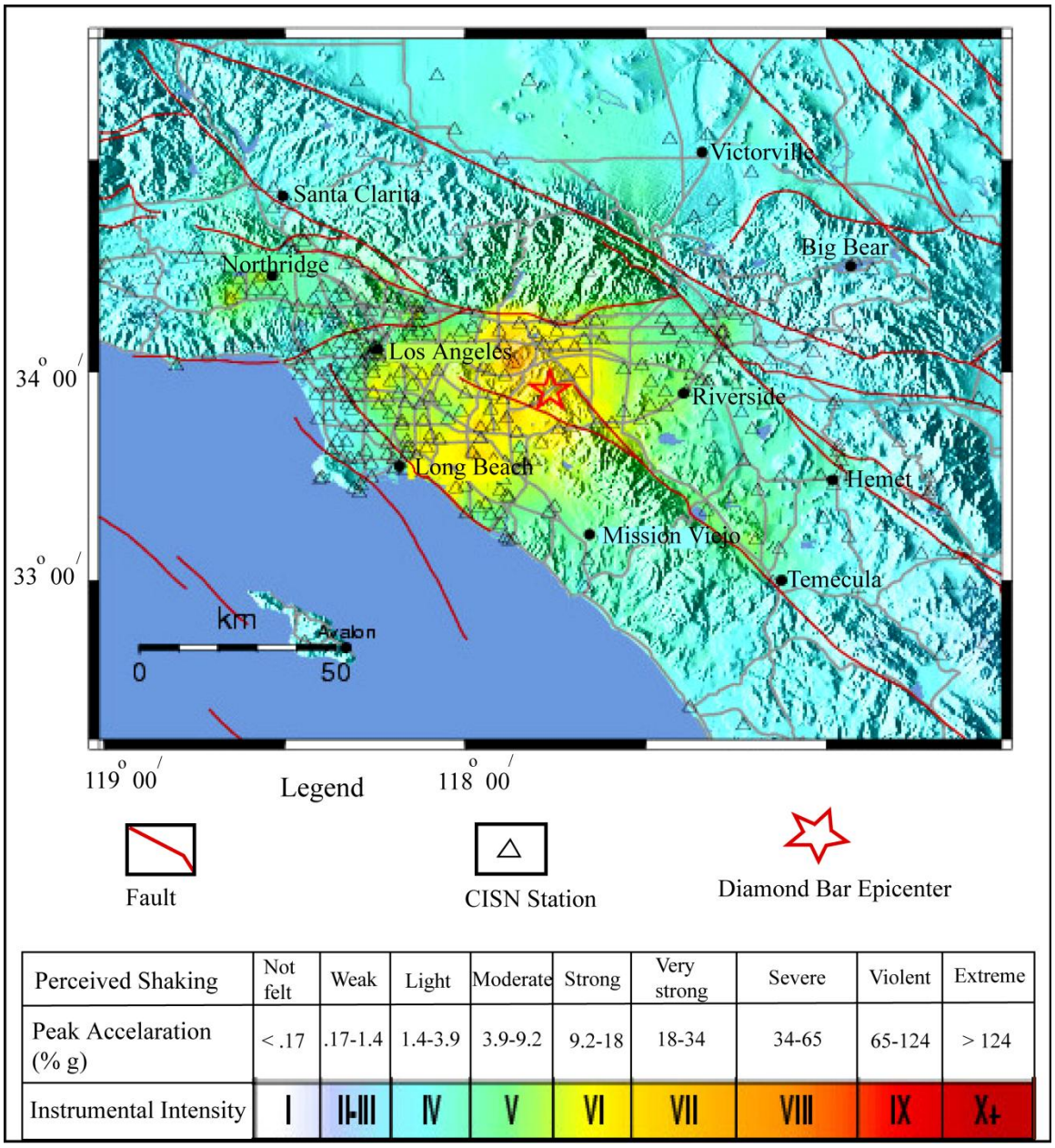

Perceived Shaking	Not felt	Weak	Light	Moderate	Strong	Very strong	Severe	Violent	Extreme
Peak Accelaration (% g)	< .17	.17-1.4	1.4-3.9	3.9-9.2	9.2-18	18-34	34-65	65-124	> 124
Instrumental Intensity	I	II-III	IV	V	VI	VII	VIII	IX	X+

Figure 34. CISN shake map showing epicenter of 2008 Diamond Bar earthquake and corresponding peak acceleration and instrumental intensity values. The southern and southeastern parts of Los Angeles basin being close to the epicenter receive strong to very strong ground shaking (instrumental intensity VI – VII). However, the northern, southwestern, and central part, experiences light to moderate shaking effect (instrumental intensity IV – V) (modified from http://www.cisn.org/shakemap/sc/shake/archive/).

5.3. Liquefaction Vulnerability (K_g index)

Earthquake waves passing through sediments increase pore pressure, distort sediment structure, and cause loosely packed particles to collapse. In this process, sediment can lose strength and behave as a viscous liquid rather than a solid, leading to "soil liquefaction" (Huang and Tseng, 2002). In the liquefied condition, soil may deform with little shear resistance. The typical effects of soil liquefaction include lateral spreading, sand boils, flow failures, ground oscillation, and settlement. Nakamura (1996, 1997, and 2000) proposed the use of a vulnerability index (K_g) to identify areas susceptible to soil liquefaction. K_g is derived from peak periods (T) observed in HVSRs and their associated amplitudes (A_p), where

$$K_g = T * A_p^2 \quad (7)$$

In their microtremor study after the 1999 Chi Chi, Taiwan earthquake, Huang and Tseng (2002) applied Nakamura's K_g technique to map the vulnerable areas. They measured microtremor and earthquake data from 42 sites located in the Yuan-Lin area and vicinity, and compared predominant frequency, amplification factor, and K_g values for these sites. They obtained higher K_g values and amplification factors for sites that have thick sediment cover and that experienced severe liquefaction during the earthquake. In their microtremor study in the Mississippi embayment, Hardesty et al. (2010) obtained very high vulnerability indices for sites located in areas of loose stream deposits and for sites that experienced liquefaction in past earthquakes.

In this study, predominant period (T), relative power or amplitude squared (A_p^2), and K_g values are calculated for each broadband station (Fig. 35). Stations are arranged from shallow to deep basement depths, from the southwest to central part of the basin. The predominant periods observed are correspondingly longer for deeper parts of the basin; however, some shallow basement stations yield intermediate to long periods (Fig. 33a). There is a correlation between amplitudes and depths of sediment. Most of the stations show higher values of amplification and K_g with increase in basement depth, except for five stations, BRE, USC, LTP, WTT, and WTT, which are situated between depths 7000 to 8500 m and on the steep flanks of the central Los Angeles syncline (Fig. 35b-c) (Fig. 6).

Results from this study compete with Nakamura's (1989) theory, which assume simply geology and flat basement for HVSR calculations. Hence, as in previous studies, this study suggests that Nakamura's (1989) method is effective for measuring resonance periods for sedimentary basins, but its potential to derive amplification characteristics is not well established. Further investigation is required to utilize the results for amplification studies.

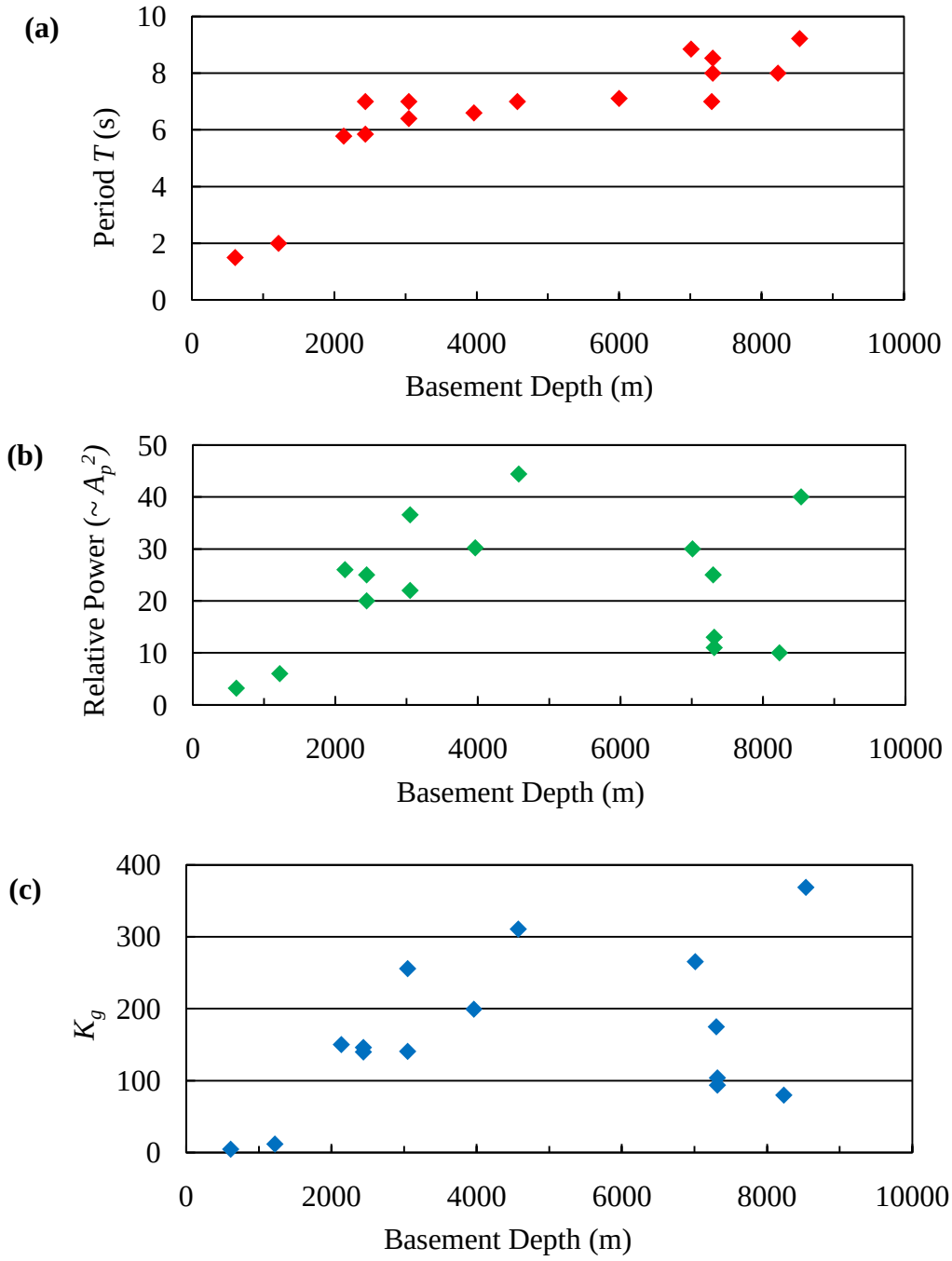

Figure 35. (a) Predominant periods (T) at study sites with increasing basin thickness from left to right. (b) Observed values of power (A_p^2) for each site determined from predominant periods in HVSRs. (c) Calculated ground vulnerability (K_g) values using equation 7 for each sites (Nakamura (1996, 1997, 2000)). T value shows linear increase with depth, whereas, A_p^2 and K_g values show variability.

5.4. Suggestions for Future Work

Results of this study reveal some interesting outcomes, which need further investigation.

(1) H/V peaks for some of the stations could not be correlated to any of the stratigraphic boundaries (for example, SRN and STS). The origin for those peaks is still unknown. A microtremor study in a regional scale centered in the Los Angeles basin may provide an answer to this question, if combined with more detailed information on the subsurface structure and geology.

(2) Stations located in areas of structural complexities, such as LGB and WTT, exhibit inconsistent spectral peaks over time. This irregularity could not be explained from lithology alone. The influence of basin structure and other physical properties of sediments, such as Poisson's ratio, should be emphasized in future work.

(3) The amplification values obtained from microtremor record do not correlate with those derived from local earthquake records. Hence, the extent to which microtremor study can produce reliable estimates of amplification and K_g values during earthquake-generated ground motion remains debatable. Microtremor measurements from other sedimentary basins with different geology and tectonic settings may yield better results.

(4) Calculating amplification factor from local earthquakes from different azimuthal directions could be interesting. This would test whether amplification is independent of path effect.

CHAPTER VI

CONCLUSIONS

The study reviews the applicability and limitations of the microtremor method (Nakamura, 1989) to estimate site characteristics for earthquake hazard analysis. H/V spectral ratio from a single station is an attractive technique to access the effects of thick sedimentary layers on ground motions in large basins where bedrock outcrops are lacking. This study applies Nakamura's (1989) H/V technique to analyze microtremor records obtained from sixteen broadband seismic stations located in the Los Angeles basin. The spectral peaks observed in the microtremor HVSRs were related to the impedance contrasts of the stratigraphic interfaces within the basin using predicted periods from the 3D California velocity model. The H/V microtremor results were also compared with the standard spectral ratios using recordings of the 2008 Diamond Bar earthquake. Despite some similarity of spectral peak frequencies, results from the two techniques showed important differences, especially in terms of amplification factors.

Stations used in the study were divided into three groups based on their basement depth. Those located in deep areas of the basin (> 6 km) showed spectral peaks with longer periods of 6.0 to 10.0 s. Intermediate periods of 4.0 to 7.0 s correspond to basin thicknesses of 3 to 6 km. The periods less than 3.0 s relate to areas with

shallow basement. These peaks correlate with sediment-basement contact and are associated with large impedance contrasts. Although many peaks in the spectra could be correlated with specific stratigraphic units or velocity discontinuities, not all of them could be explained, particularly for stations located in structurally complex areas. Interestingly, the predominant peak was not always correlated to the sediment-basement interface. The temporal stability of observed spectra was tested by comparing time segments from six stations for five consecutive years. Although many stations exhibited stable peaks through time, spectra from some stations appeared quite variable. Most stable were spectra from station locations where the basement topography was subdued. High gradients of basement topography typically yielded unstable spectral peaks due to structural complexities.

Predominant peaks and spectral amplitudes from microtremor and earthquake sources were compared. The predominant periods showed good agreement between microtremor and earthquake results. On the other hand, amplitudes of microtremor peaks have poor correlation with amplification derived from earthquake shear-waves at resonant periods. Amplification factors from microtremors were systematically lower than those from the Diamond Bar earthquake. In addition to impedance contrasts, basin structure, Poisson's ratio in sedimentary layers, and source-receiver distance may contribute to the amplitude of spectral peaks.

The microtremor study allows a better understanding of site effects and may be useful in microzonation studies, when used in combination with other geological and geophysical data. This method can effectively be used to ascertain resonance period of

sites within basins at relatively low cost and ease. However, its application to determine amplification and vulnerability needs further investigation.

REFERENCES

Bilodeau, W. L., S.W. Bilodeau, E. M. Gath, M. Oborne, and R. J. Proctor, 2007, Geology of Los Angeles, California, United States of America: Environmental and Engineering Geoscience, **13**, 99-160.

Blake, G. H., 1991, Review of the Neogene biostratigraphy and stratigraphy of the Los Angeles basin and implications for basin evolution, in Active margin basins: edited by Kevin T. Biddle, American Association of Petroleum Geology Memoir, **52**, 135-184.

Bodin, P. and S. Horton, 1999, Broadband microtremor observation of basin resonance in the Mississippi embayment, Central United States: Geophysical Research Letters, **26**, 903-906.

Bonilla, L. F., J. H. Steidl, G. T. Lindley, A. G. Tumarkin, and R. J. Archuleta, 1997, Site amplification in the San Fernando Valley, California: Variability of site-effect estimation using the S-wave, Coda, and H/V methods: Bulletin of the Seismological Society of America, **87**, 710-730.

Campbell, R. H., and R. F. Yerkes, 1976, Cenozoic evolution of the Los Angeles basin area-Relation to plate tectonics: American Association of Petroleum Geology Pacific Section Miscellaneous Publication, **24**, 541-560.

Delgado, J., 2000, Microtremor as a geophysical exploration tool: Applications and limitations: Pure and Applied Geophysics, **157,** 1445-1462.

Field, E. H., S. E. Hough, and K. H. Jacob, 1990, Using microtremors to assess potential earthquake site response: A case study in Flushing Meadows, New York City: Bulletin of the Seismological Society of America, **80**, 1456-1480.

Field, E. H., and K. H. Jacob, 1993, The theoretical response of sedimentary layers to ambient seismic noise: Geophysical Research Letters, **20**, 2925-2928.

Field, E. H., and K. H. Jacob, 1995, A comparison and test of various site response estimation techniques, including three that are non reference-site dependent: Bulletin of the Seismological Society of America, **85**, 1127-1143.

Fuis, G. S., and T. Ryberg, 2001, Crustal structure and tectonics from the Los Angeles basin to the Mojave Desert, Southern California: Geology, **29**, 1, 15-18.

Gutenberg, B., 1957, Effect of ground on earthquake motion: Bulletin of the Seismological Society of America, **47**, 221-250.

Hardesty, K., L.W. Wolf, and P. Bodin, 2010, Noise to signal: A microtremor study at liquefaction sites in the New Madrid Seismic Zone: Geophysics, **75**, 3, B83-B90.

Hartzell**,** S., S. Harmsen**,** A. Frankel, D. Carver, E. Cranswick, M. Meremonte, and J. Michael, 1998, First-generation site-response maps for the Los Angeles region based on earthquake ground motions: Bulletin of the Seismological Society of America, **88,** 463-472.

Hauksson, E., 1990, Earthquakes, faulting, and stress in the Los Angeles basin: Journal of Geophysical Research, **95**, 15, 365-15,394.

Horike, M., B. Zhao, and H. Kawase, 2001, Comparison of site response characteristics inferred from microtremors and earthquake shear waves: Bulletin of the Seismological Society of America, **91**, 6, 1526-1536.

Huang, H. C. and T. L. Teng, 1999, An evaluation on H/V ratio for site response estimation using the 1994 Northridge earthquake sequence: Pure and applied geophysics, **156**, 631-649.

Huang, H. C., 2002, Characteristics of earthquake ground motions and the H/V of microtremors in the southwestern part of Taiwan: Earthquake Engineering and Structural Dynamics, **31**, 1815-1829.

Huang, H. C. and Y. S. Teng, 2002, Charactersitics of soil liquefaction using H/V of microtremors in Yan-Lin area, Taiwan: Terrestial, Atmospheric, and Oceanic Sciences, **13**, 325-338.

Ibs-von Seht, M. and J. Wohlenberg, 1999, Microtremor measurements used to map thickness of soft sediments: Bulletin of the Seismological Society of America, **89**, 250-259.

Kagami, H., C. M. Duke, G. C. Liang, and Y. Ohta, 1982, Observation of 1-to-5 second microtremors and their application to earthquake engineering. Part II. Evaluation of site effect upon seismic wave amplification due to extremely deep soil deposits: Bulletin of the Seismological Society of America, **72**, 987-998.

Kanai, K. and T. Tanaka, 1961, On microtremors: Bulletin of Earthquake Research Institute, Tokyo University, **39**, 97-114.

Katz, L. J., 1976, Microtremor analysis of local geological conditions: Bulletin of the Seismological Society of America, **66**, 45-60.

Lachet, C. D. and P. Y. Bard, 1994, Numerical and theoretical investigations on the possibilities and limitations of the "Nakamura's" technique: Journal of Physics of the Earth, **42**, 5, 377-397.

Lermo, J. and F. J. Chavez-Garcia, 1993, Site effect evaluation using spectral ratios with only one station: Bulletin of the Seismological Society of America, **83**, 1574-1594.

Lermo, J. and F. J. Chavez-Garcia, 1994, Are microtremor useful in site response evaluation?: Bulletin of the Seismological Society of America, **84**, 1350-1364.

Nakamura, Y., 1989, A method for dynamic characteristics estimation of subsurface using microtremors on the ground surface: Quarterly Report of Railway Technical Research Institute, **30**, 1, 25-33.

Nakamura, Y., 1996, Real time information systems for seismic hazard mitigation: UrEDAS, HERAS and Quarterly Report of Railway Technical Research Institute, **37**, 112-127.

Nakamura, Y., 1997, Seismic vulnerability indices for ground and structures using microtremor: World Congress on Railway Research in Florence, Italy.

Nakamura, Y., 2000, Clear identification of fundamental idea of Nakamura's technique and its applications: Proceedings of the 12th World Conference on Earthquake and Engineering, 2656-2664.

Ohmachi, T., Y. Nakamura, and T. Toshinawa, 1991, Ground motion characteristics in the San Francisco bay area detected by microtremor measurement: Proceedings of the 2nd International Conference on Recent Advances in Geotechnical Earthquake Engineering and Soil Dynamics, Saint Louis, Missouri, 1643-1648.

Schneider, C. L., C. Hummon, R. S. Yeats, and G. L. Huftile, 1996, Structural evolution of the northern Los Angeles basin, California, based on growth strata: Tectonics, **15**, 2, 341-355.

Smith, K., 2000, Using microtremors to illuminate subsurface geology of Memphis, Tennessee: M. S. Thesis, University of Memphis.

Somerville, P. G., R. W. Graves, S. M. Day, and K. B. Olsen, 2006, Ground motion environment of the Los Angeles region: Structural Design of Tall and Special Building, **15**, 483-494.

Suss, M. P., and J. H. Shaw, 2003, P wave seismic velocity structure derived from sonic logs and industry reflection data in the Los Angeles basin, California: Journal of Geophysical Research, **108** (B3), 2170.

Suzuki, T., Y. Adachi, and M. Tanaka, 1995, Application of microtremor measurements to the estimation of earthquake ground motions in Kushiro City during the Kushiro-Oki earthquake of 15 January 1993: Earthquake Engneering Structural Dynamics, **24**, 595-613.

Wills, C. J., M. D. Petersen, W. A. Bryant, S. Reichle, G. J. Saucedo, S. S. Tan, G. C. Taylor, and J. A. Treiman, 2000, A site conditions map for California based on

geology and shear wave velocity: Bulletin of the Seismological Society of America, **90**, 6b, S187-S208.

Wills, C. J., and K. B. Chalan, 2006, Developing a map of geologically defined site-condition categories for California: Bulletin of the Seismological Society of America, **96**, 4A, 1483-1501.

Wright, T. L., 1991, Structural geology and tectonic evolution of the Los Angeles Basin, California, in K. T. Biddle, edition, Active margin basins: American Association of Petroleum Geology Memoir, **52**, 35-134.

Yamanaka, H., M. Dravinski, and H. Kagami, 1993, Continuous measurement of microtremors on sediments and basement in Los Angeles, California: Bulletin of the Seismological Society of America, **83**, 5, 1595-1609.

Yerkes, R. F., T. H. McCulloh, J. E. Schoellhamer, and J. G. Vedder, 1965, Geology of the Los Angeles basin, California- An introduction: U. S. Geological Survey Professional Paper, **420-A**, 57 p.

APPENDIX A - RAW MICROTREMOR DATA

Raw microtremor data collected from 16 stations (Fig. 6) for 2004-10-13-07:00:00 to 2004-10-13-08:00:00 are given below. The length of data sample used in the analysis for each station is shown in Table 2. Microtremor data from six selected stations for 5 years that were used to test the temporal stability of peaks (Table 4) are also provided in this section. Data from 6-selected stations for 5 years (table 4) are displayed here. The respective data segments are bounded by a black rectangle in each figure.

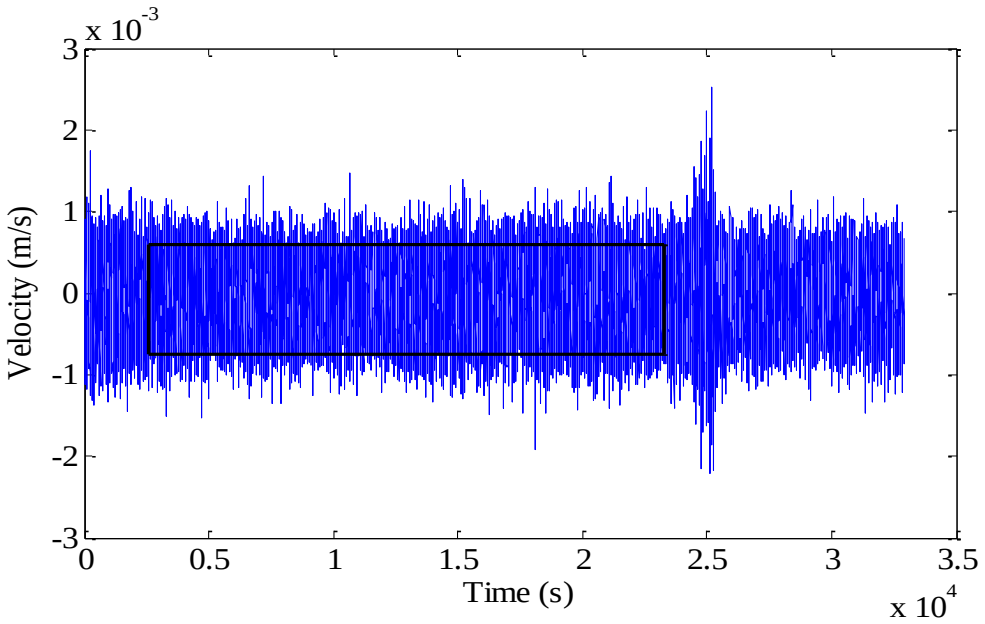

Figure A-1. Raw microtremor data and selected time segment for station BRE.

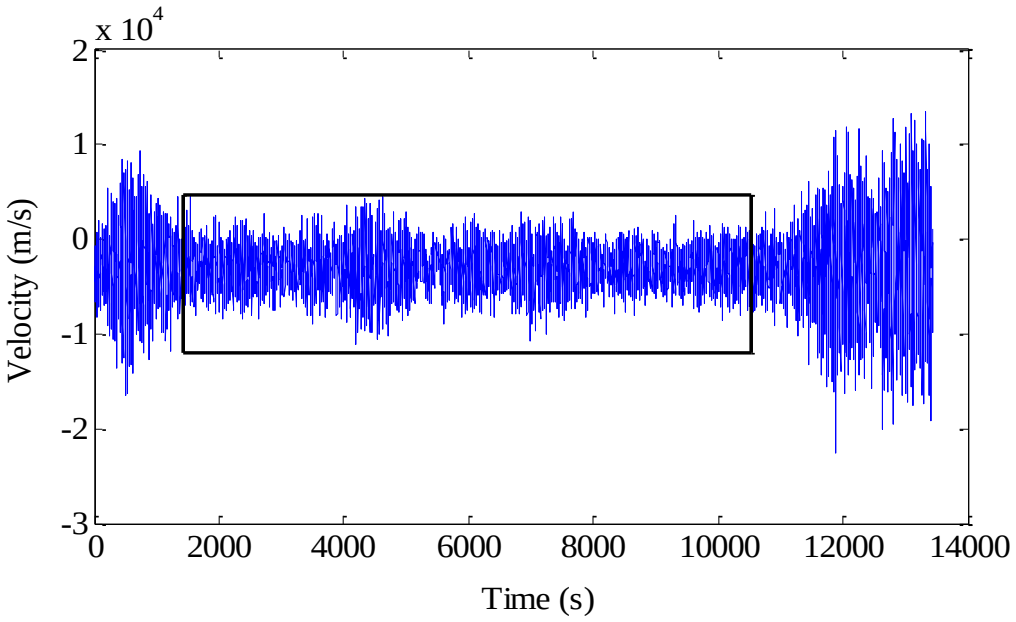

Figure A-2. Raw microtremor data and selected time segment for station DLA.

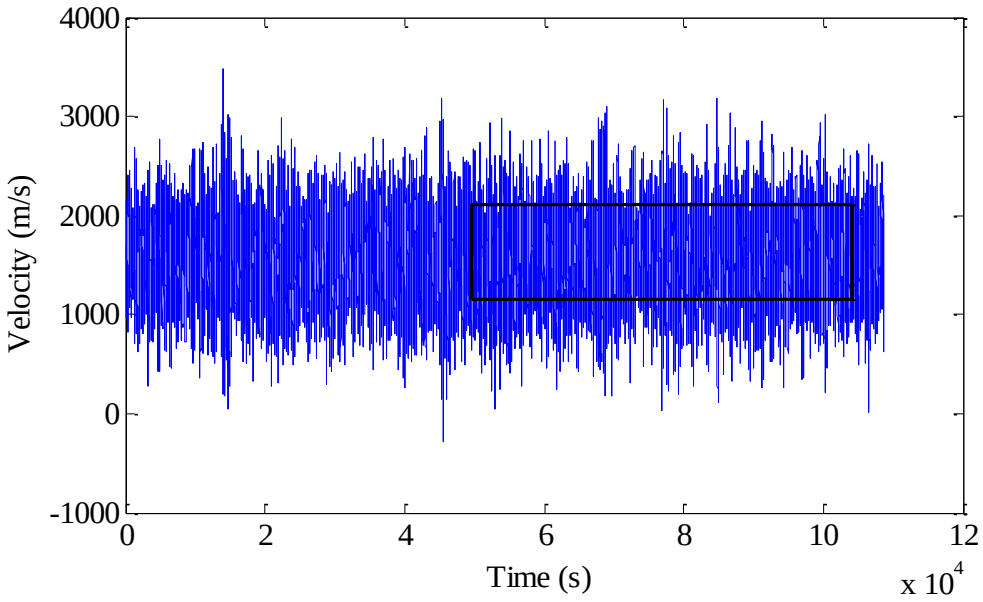

Figure A-3. Raw microtremor data and selected time segment for station FMP.

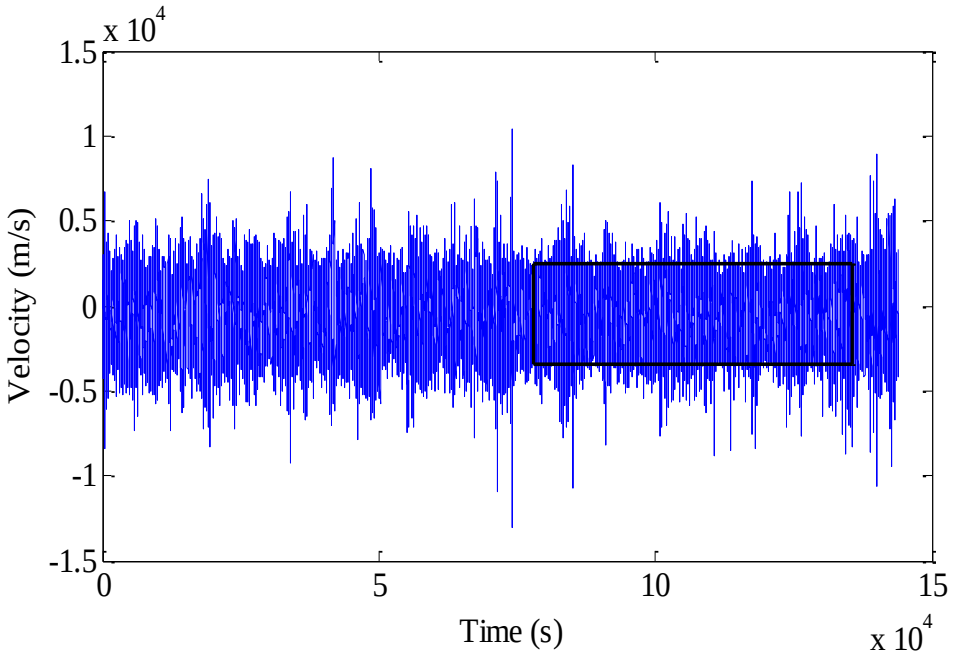

Figure A-4. Raw microtremor data and selected time segment for station LAF.

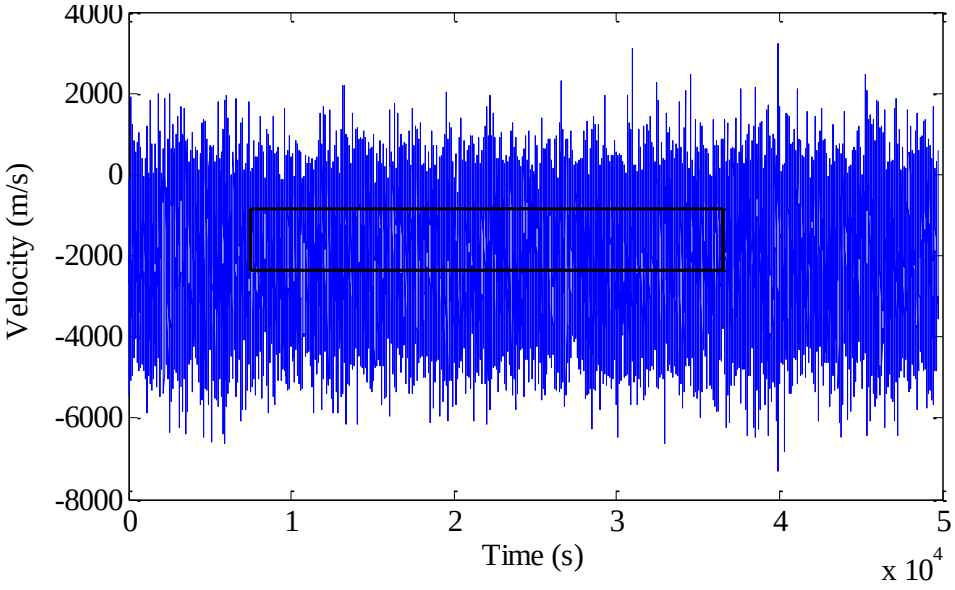

Figure A-5. Raw microtremor data and selected time segment for station LCG.

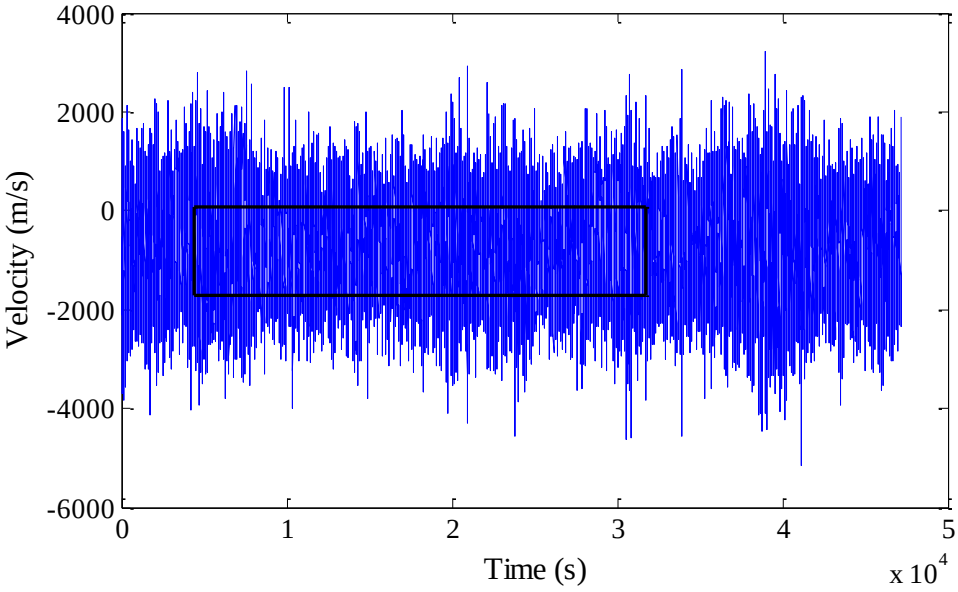

Figure A-6. Raw microtremor data and selected time segment for station LGB.

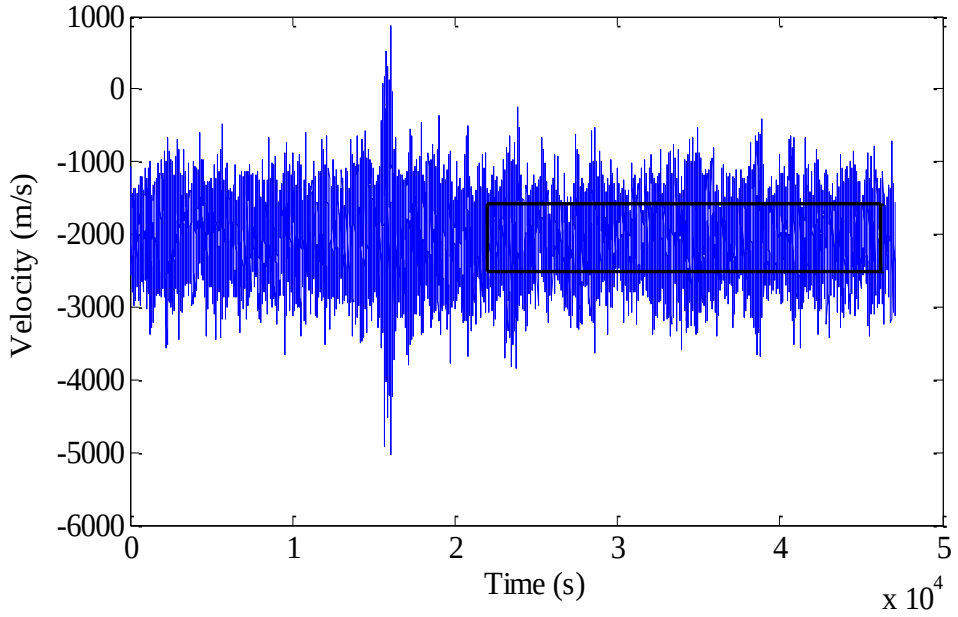

Figure A-7. Raw microtremor data and selected time segment for station LLS.

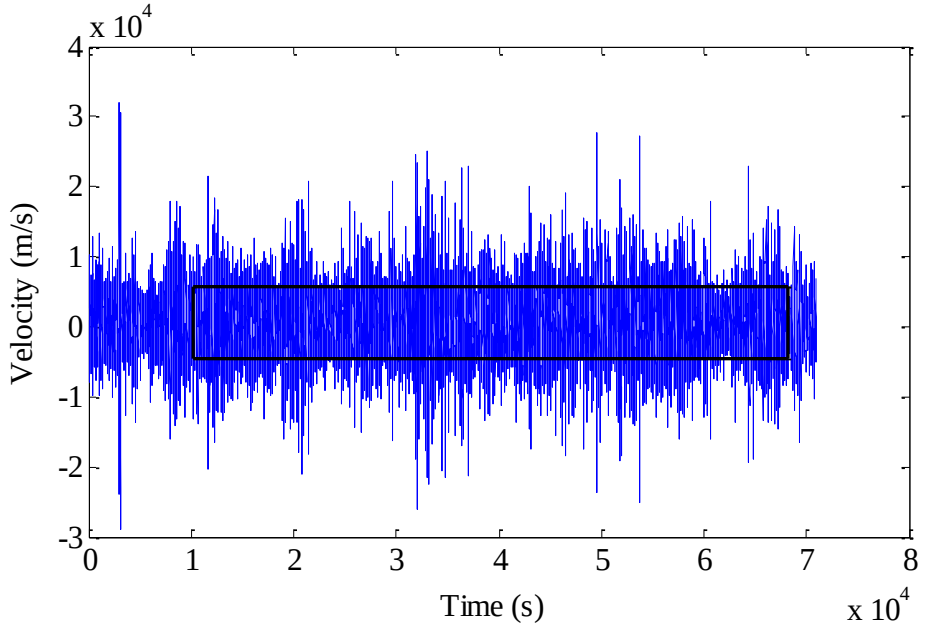

Figure A-8. Raw microtremor data and selected time segment for station LTP.

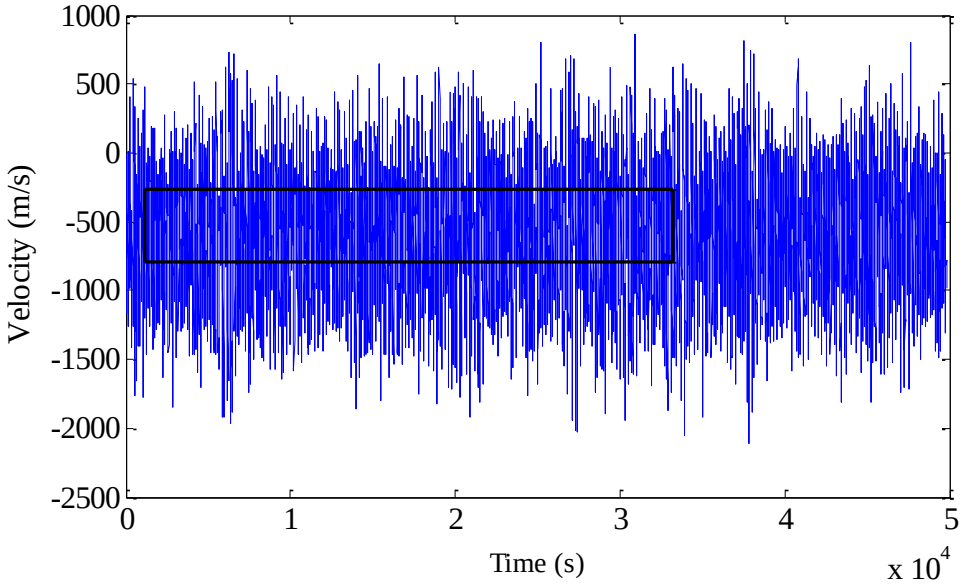

Figure A-9. Raw microtremor data and selected time segment for station OLI.

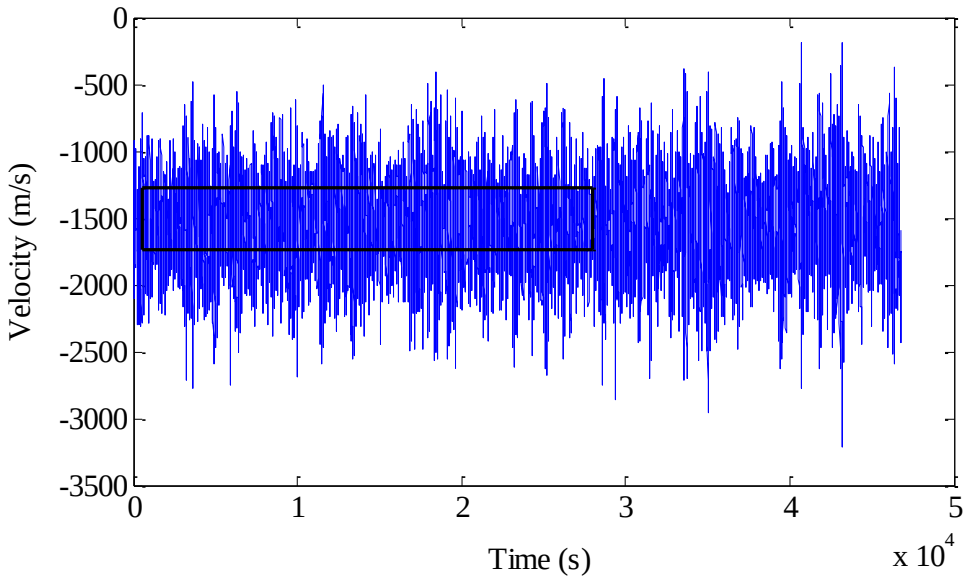

Figure A-10. Raw microtremor data and selected time segment for station RPV.

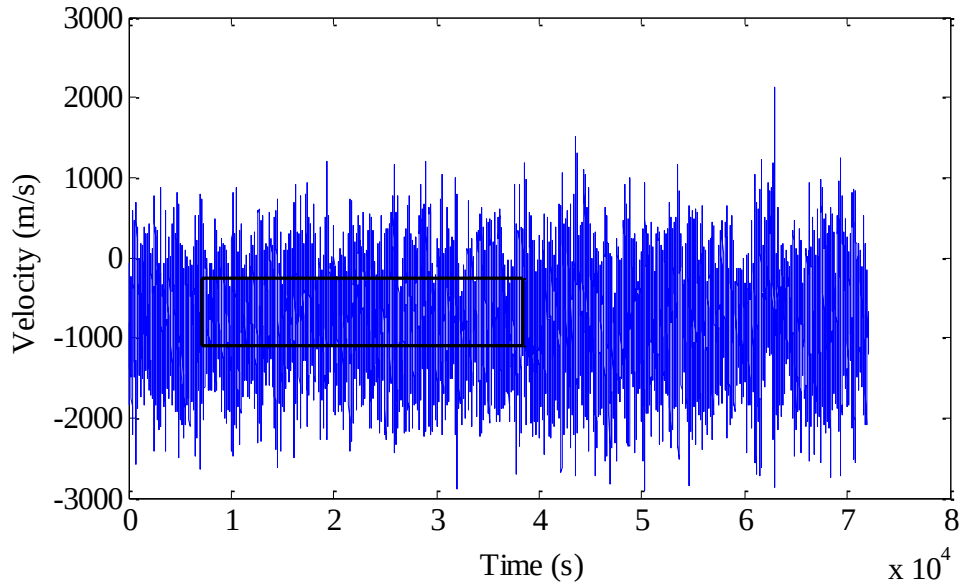

Figure A-11. Raw microtremor data and selected time segment for station SRN.

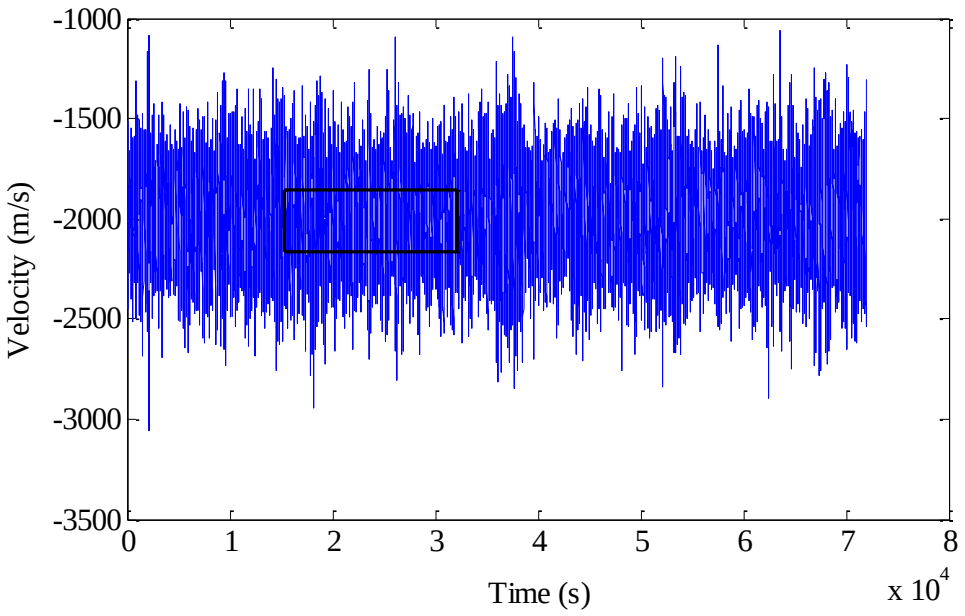

Figure A-12. Raw microtremor data and selected time segment for station STG.

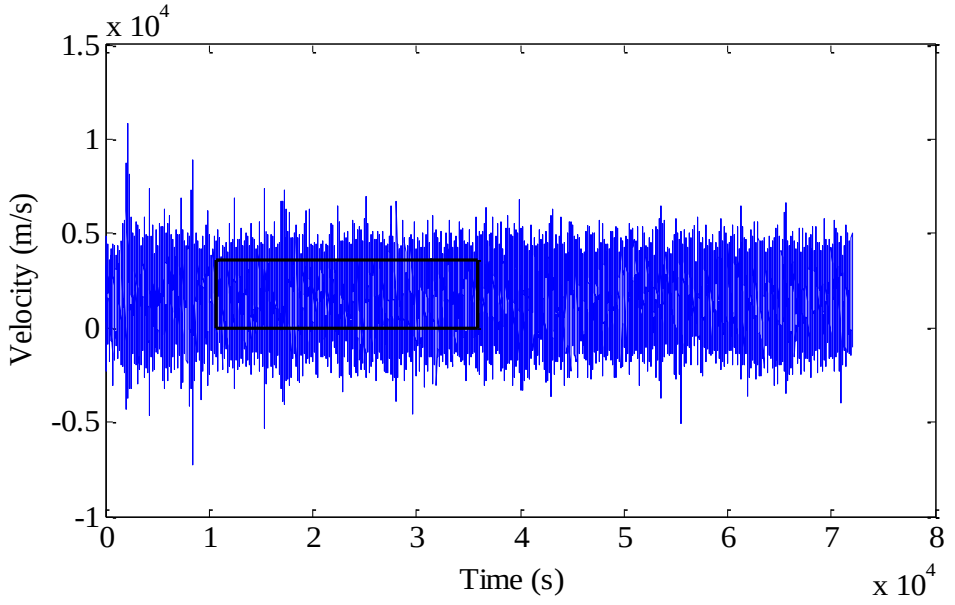

Figure A-13. Raw microtremor data and selected time segment for station STS.

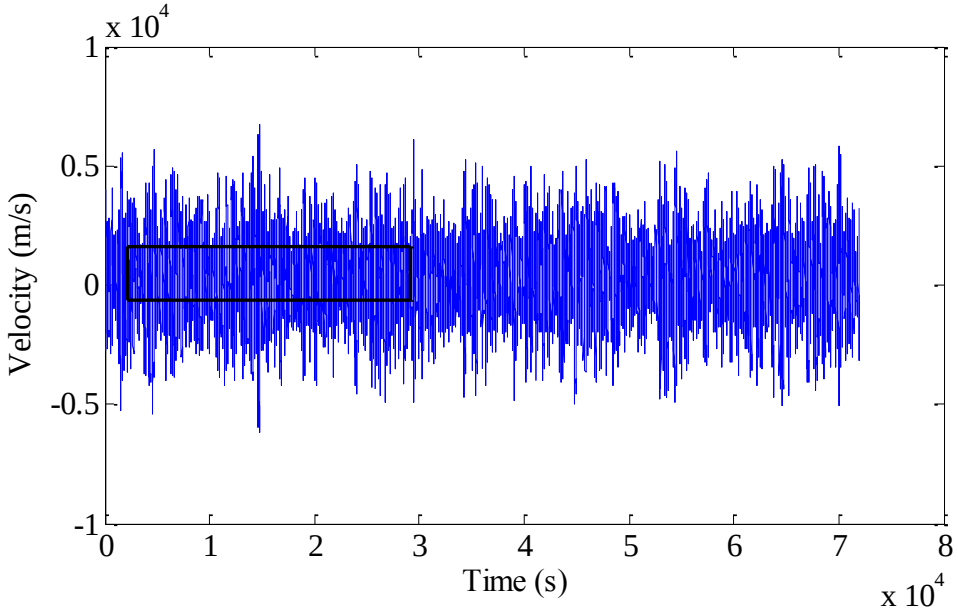

Figure A-14. Raw microtremor data and selected time segment for station USC.

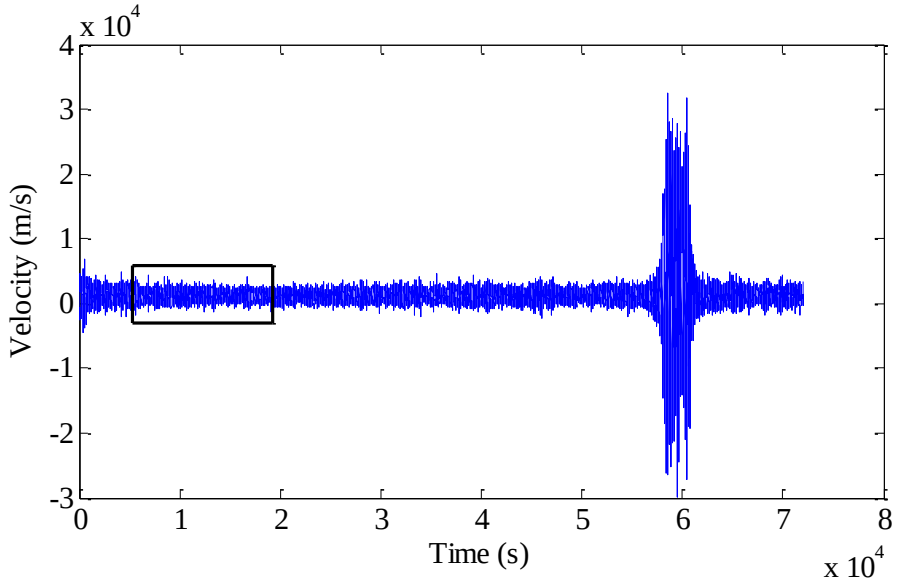

Figure A-15. Raw microtremor data and selected time segment for station WLT.

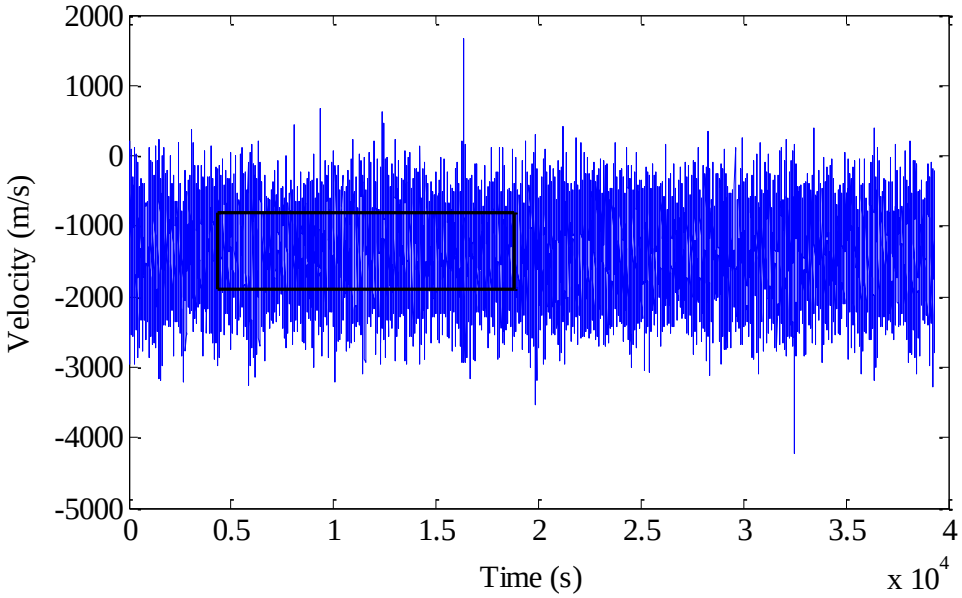

Figure A-16. Raw microtremor data and selected time segment for station WTT.

(a)

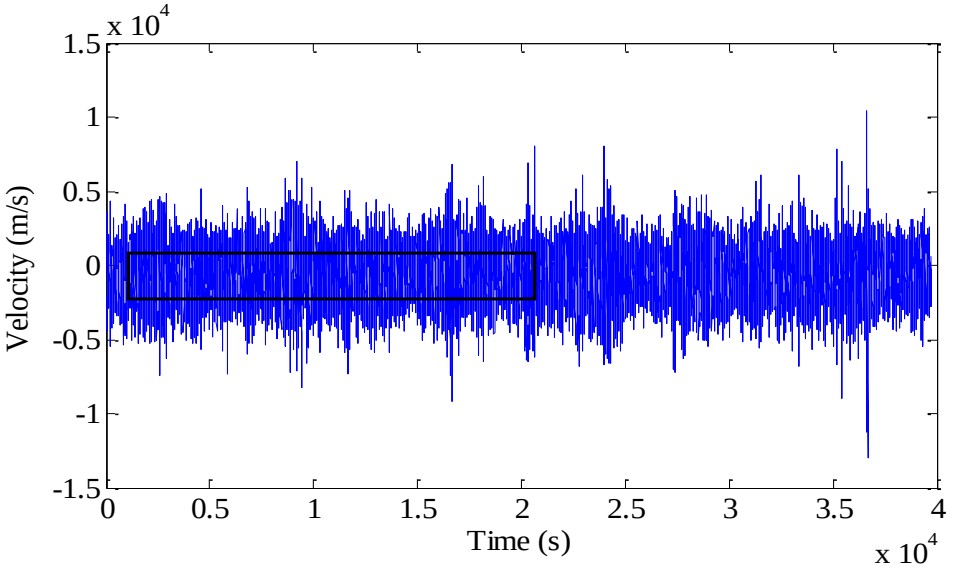

Figure A-17. Raw microtremor data and selected time segments used for testing temporal stability of peaks for station LAF: (a) 2004, (b) 2005, (c) 2006, (d) 2007, and (e) 2008.

(b)

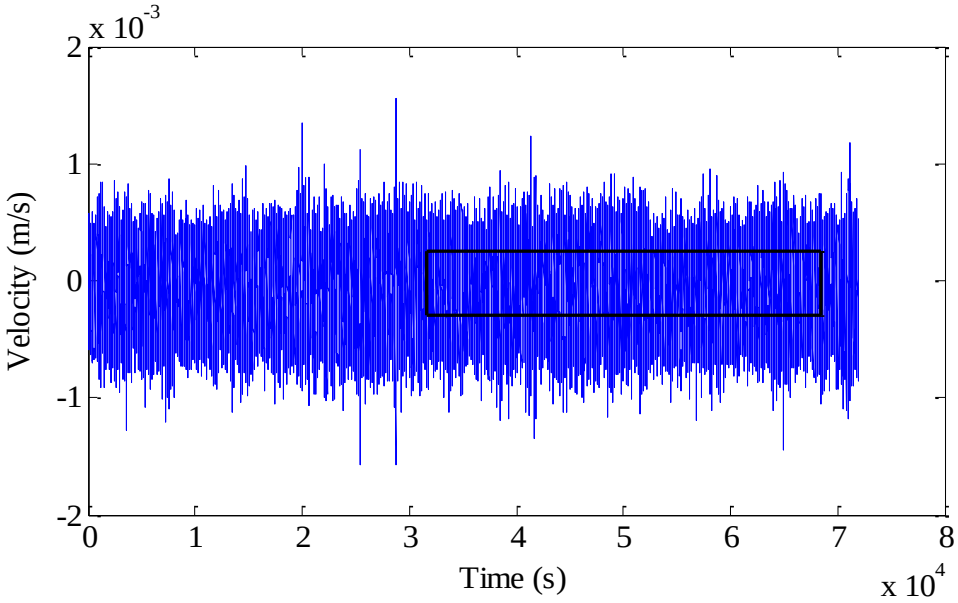
x 10^-3
2
1
0
-1
-2
Velocity (m/s)
0
1
2
3
4
5
6
7
8
Time (s)
x 10^4

(c)

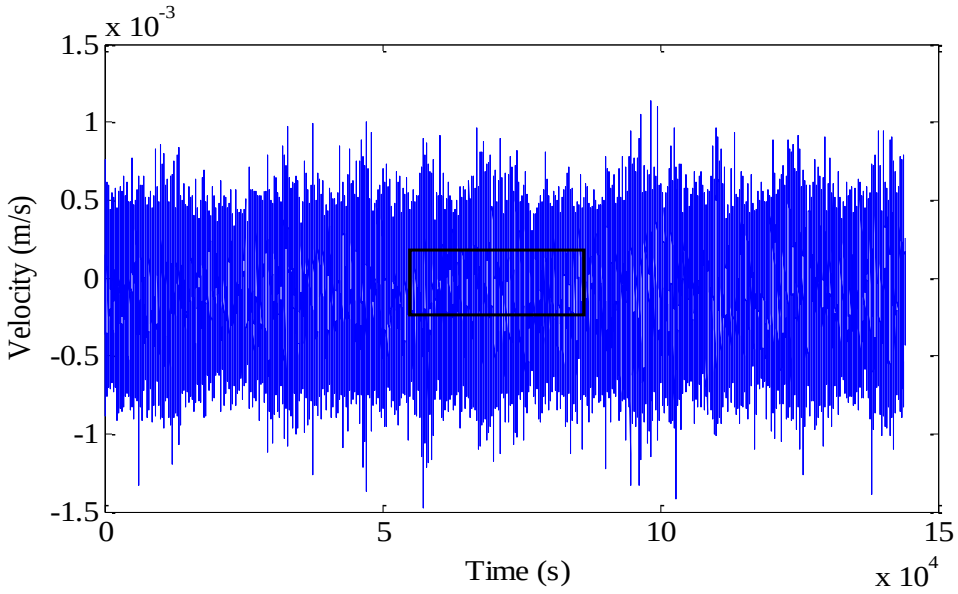
x 10^-3
1.5
1
0.5
0
-0.5
-1
-1.5
Velocity (m/s)
0
5
10
15
Time (s)
x 10^4

(d)

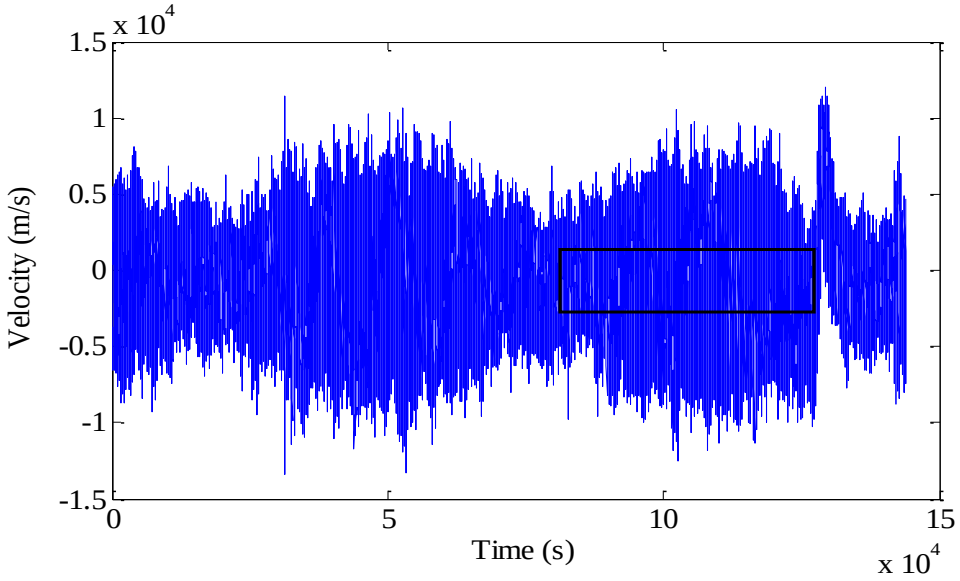
x 10^4
1.5
1
0.5
0
-0.5
-1
-1.5
Velocity (m/s)
0
5
10
15
Time (s)
x 10^4

(e)

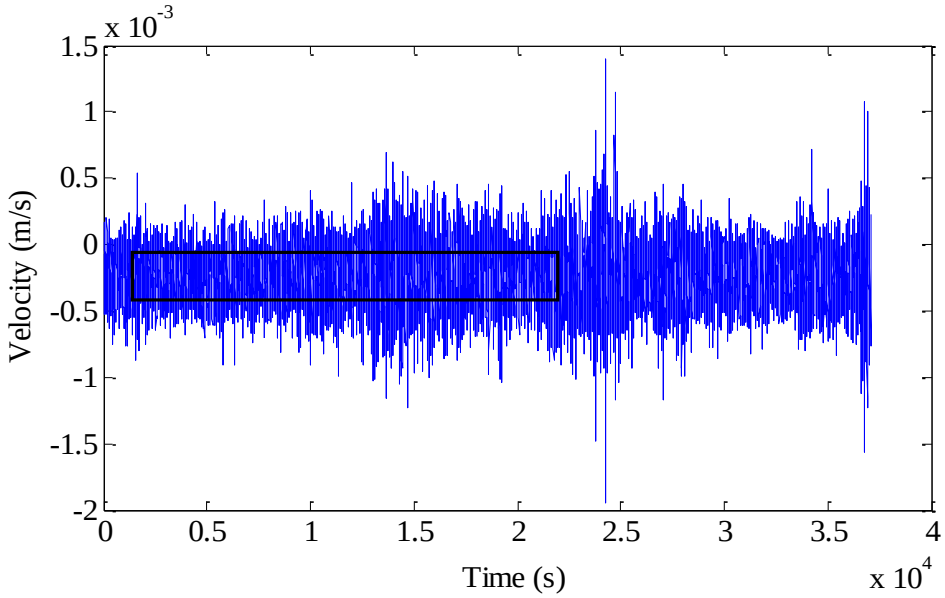
x 10^-3
1.5
1
0.5
0
-0.5
-1
-1.5
-2
Velocity (m/s)
0
0.5
1
1.5
2
2.5
3
3.5
4
Time (s)
x 10^4

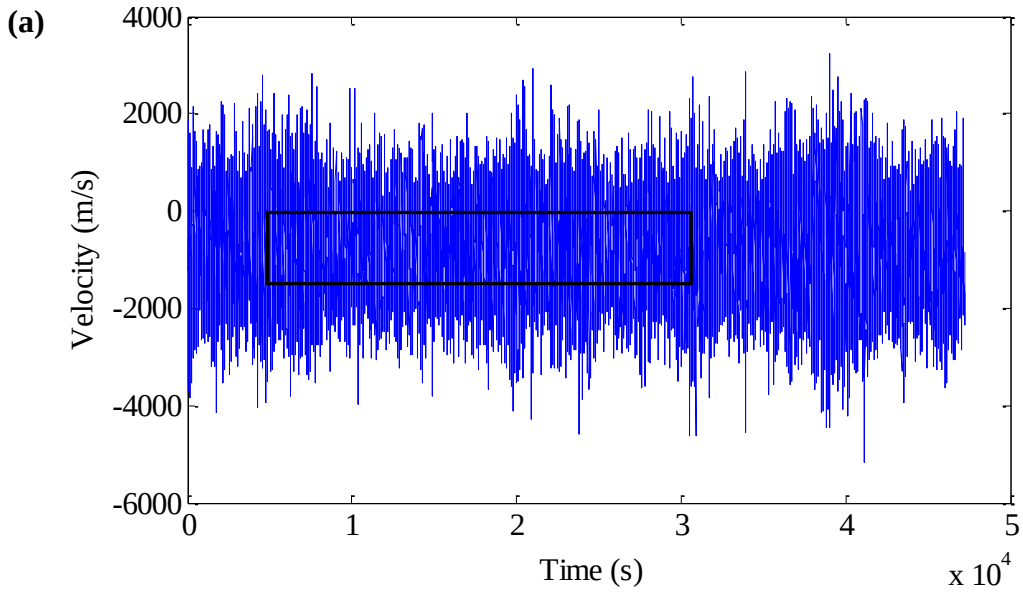

Figure A-18. Raw microtremor data and selected time segments used for testing temporal stability of peaks for station LGB: (a) 2004, (b) 2005, (c) 2006, (d) 2007, and (e) 2008.

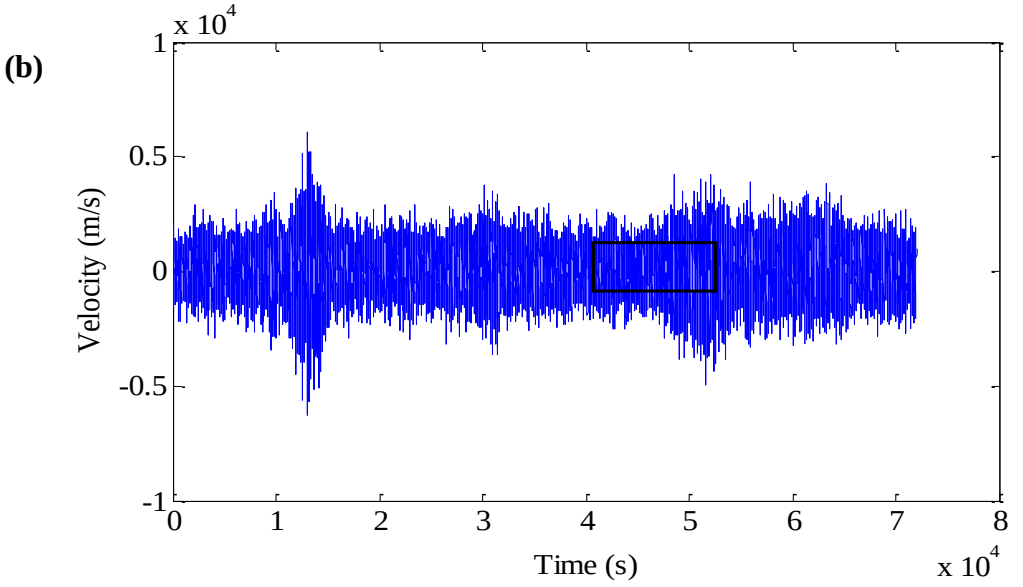

(c)

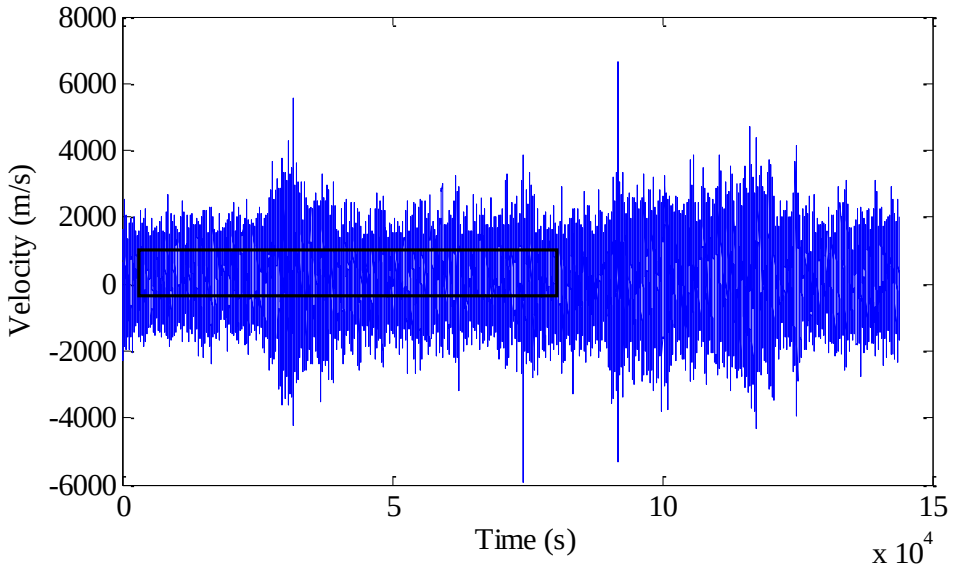
8000
6000
4000
2000
0
-2000
-4000
-6000
Velocity (m/s)
0
5
10
15
Time (s)
x 10^4

(d)

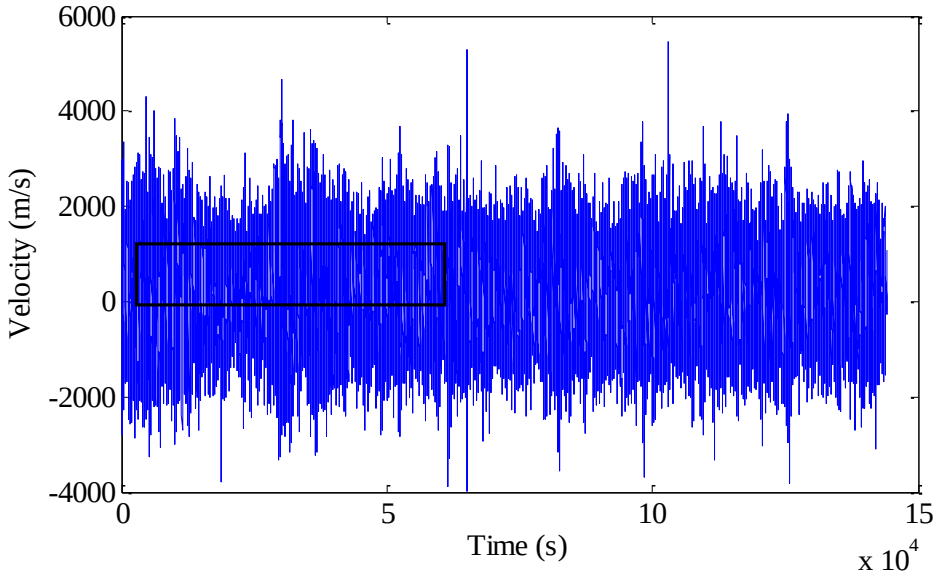
6000
4000
2000
0
-2000
-4000
Velocity (m/s)
0
5
10
15
Time (s)
x 10^4

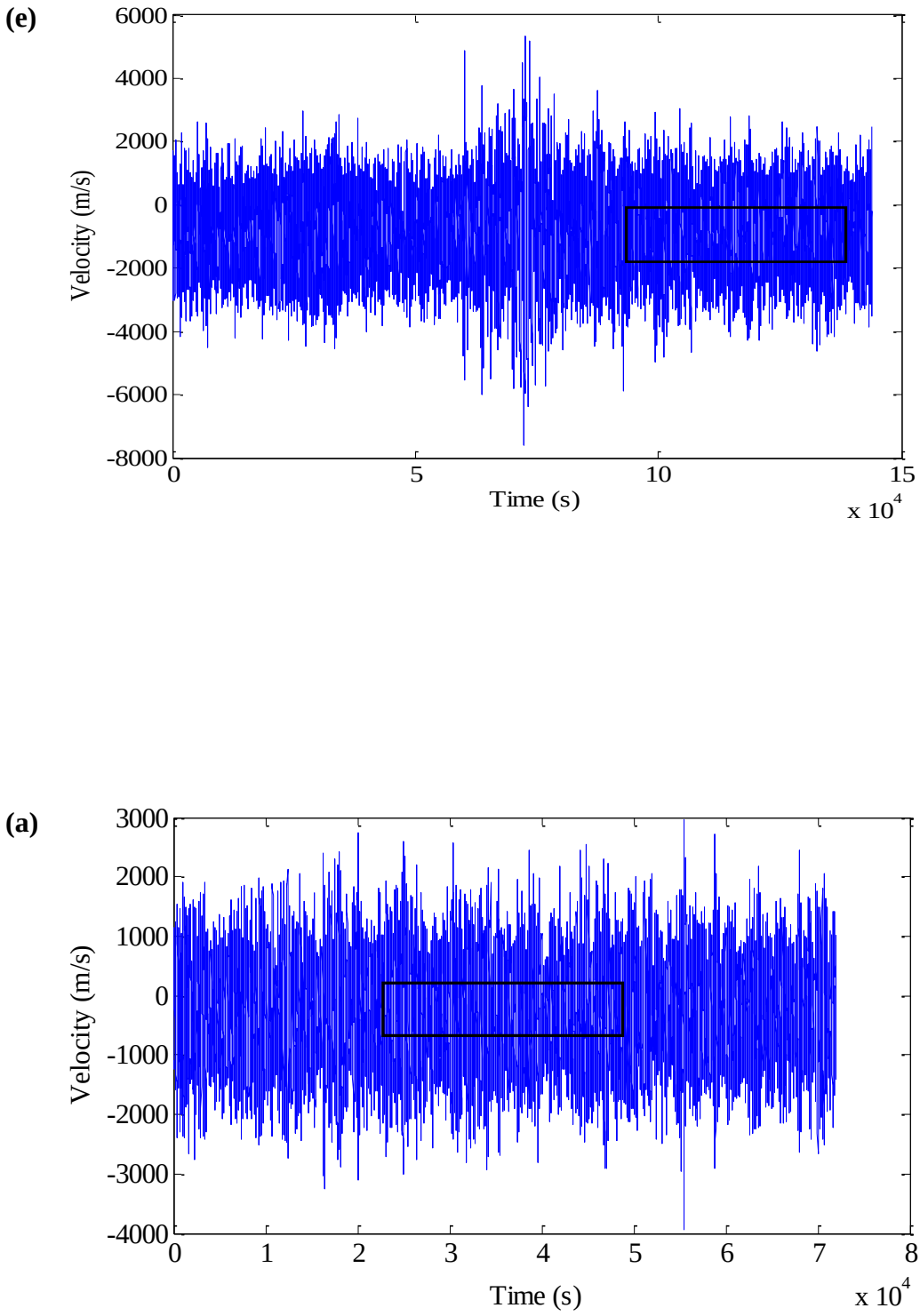

Figure A-19. Raw microtremor data and selected time segments used for testing temporal stability of peaks for station LLS: (a) 2004, (b) 2005, (c) 2006, (d) 2007, and (e) 2008.

(b)

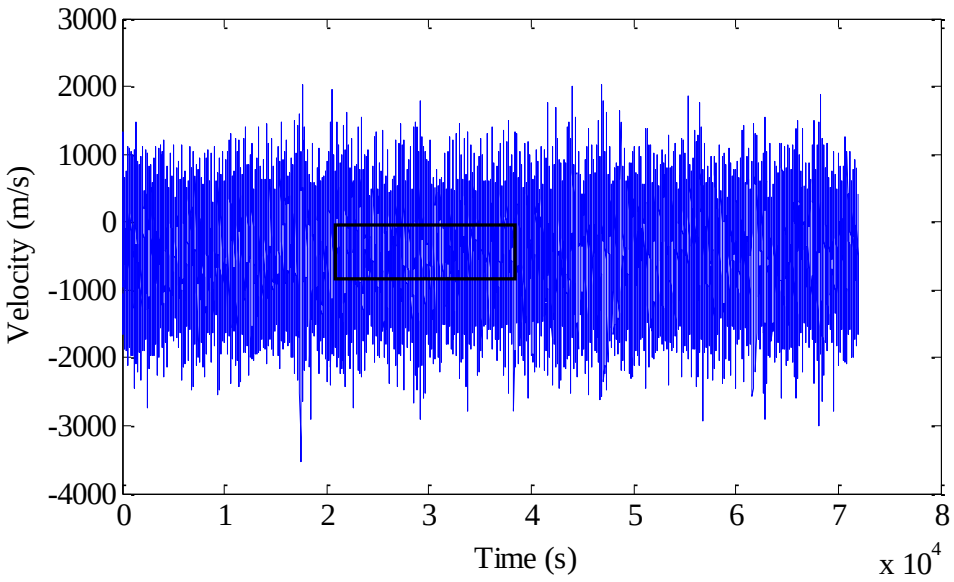
3000
2000
1000
0
-1000
-2000
-3000
-4000
Velocity (m/s)
0
1
2
3
4
5
6
7
8
Time (s)
x 10^4

(c)

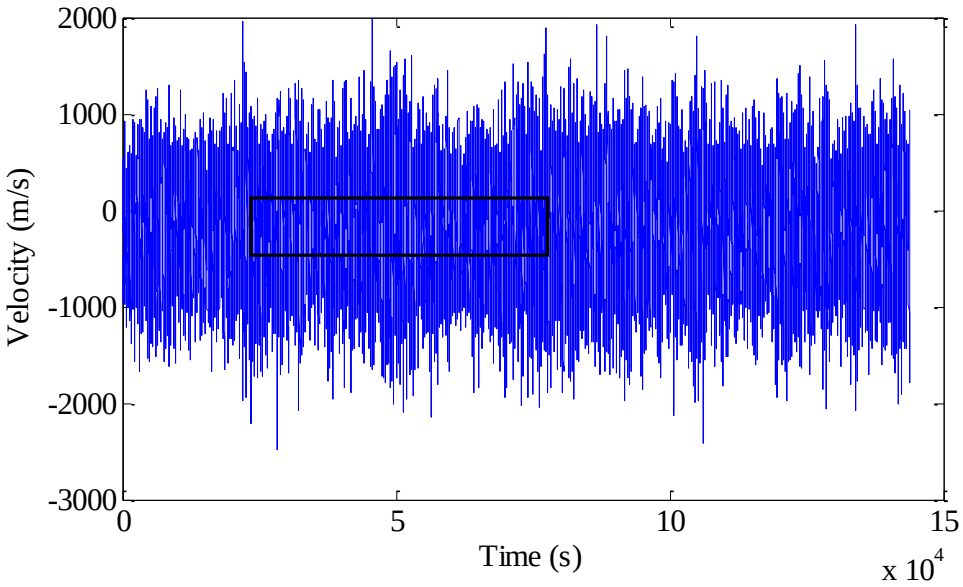
2000
1000
0
-1000
-2000
-3000
Velocity (m/s)
0
5
10
15
Time (s)
x 10^4

(d)

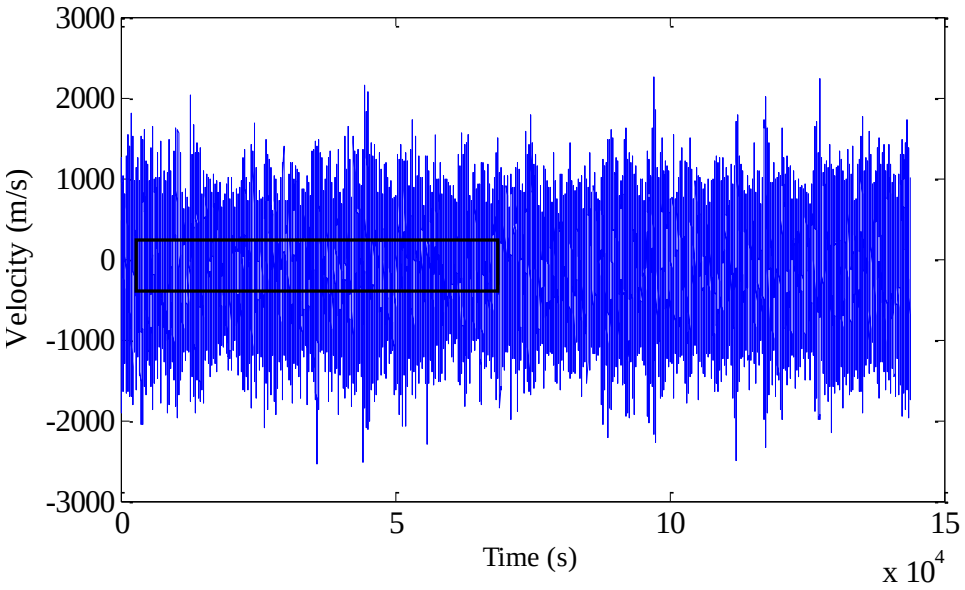
3000
2000
1000
0
-1000
-2000
-3000
Velocity (m/s)
0
5
10
15
Time (s)
x 10^4

(e)

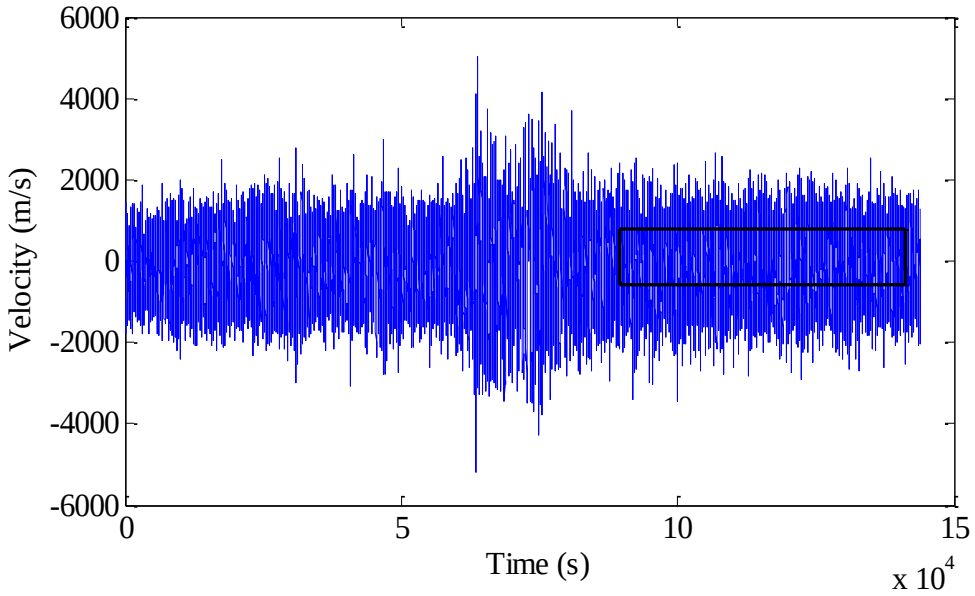
6000
4000
2000
0
-2000
-4000
-6000
Velocity (m/s)
0
5
10
15
Time (s)
x 10^4

(a)

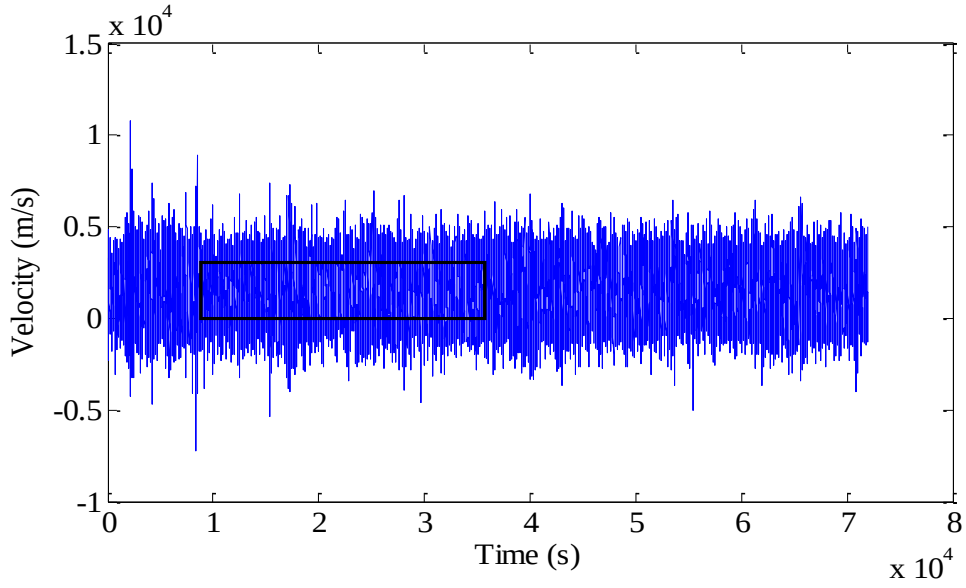

Figure A-20. Raw microtremor data and selected time segments used for testing temporal stability of peaks for station STS: (a) 2004, (b) 2005, (c) 2006, (d) 2007, and (e) 2008.

(b)

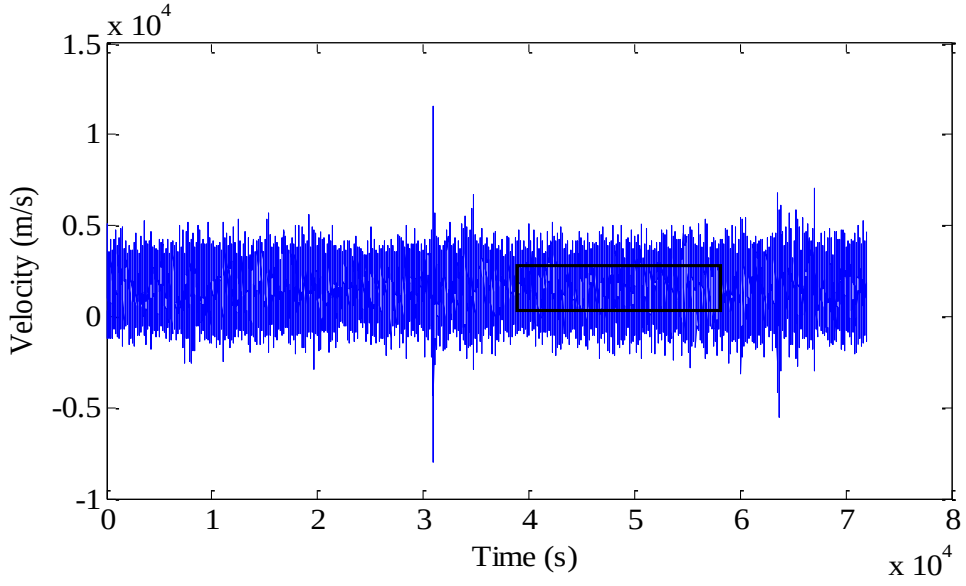

(c)

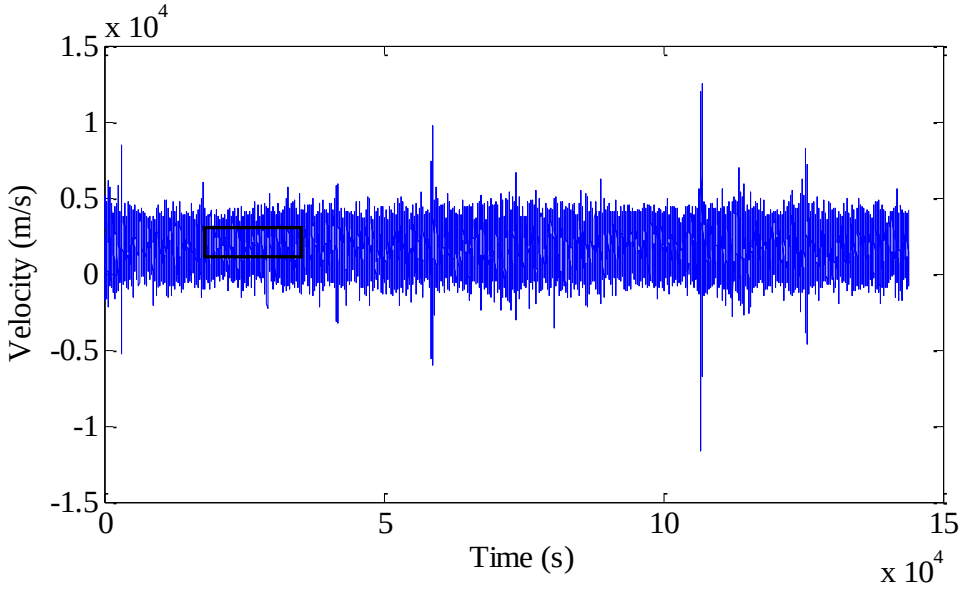
x 10^4
1.5
1
0.5
0
-0.5
-1
-1.5
Velocity (m/s)
0
5
10
15
Time (s)
x 10^4

(d)

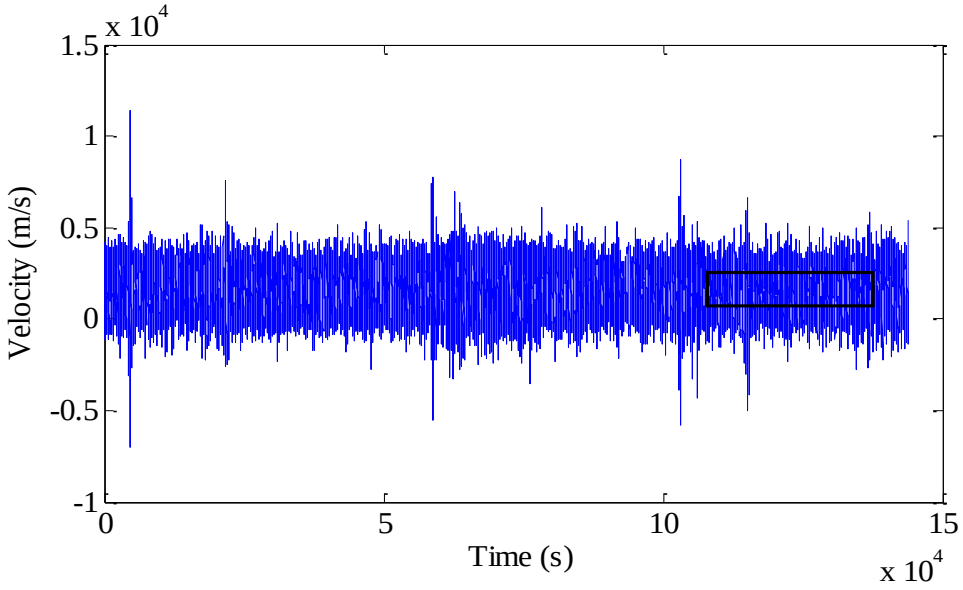
x 10^4
1.5
1
0.5
0
-0.5
-1
Velocity (m/s)
0
5
10
15
Time (s)
x 10^4

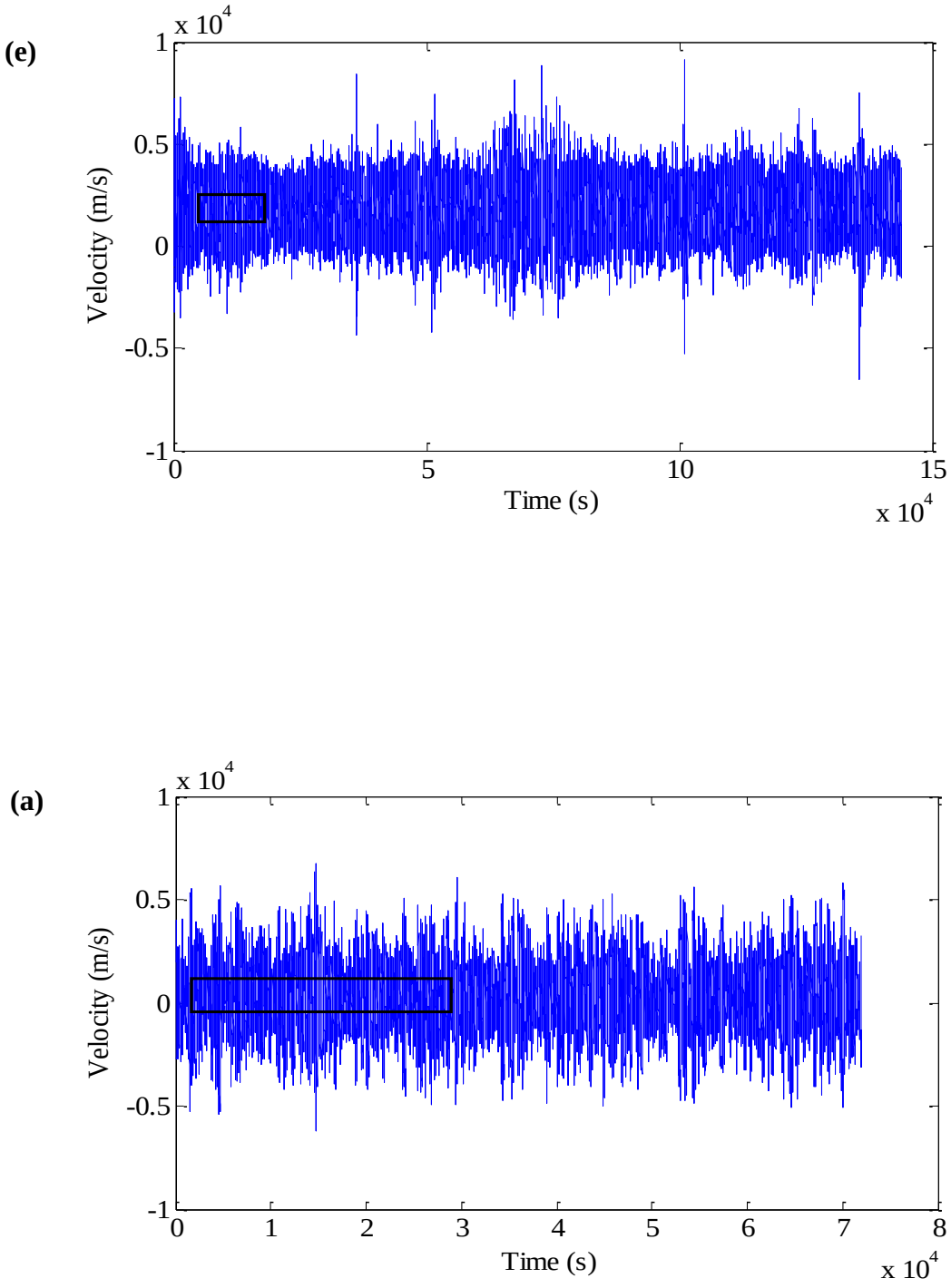

Figure A-21. Raw microtremor data and selected time segments used for testing temporal stability of peaks for station USC: (a) 2004, (b) 2005, (c) 2006, (d) 2007, and (e) 2008.

.

(b)

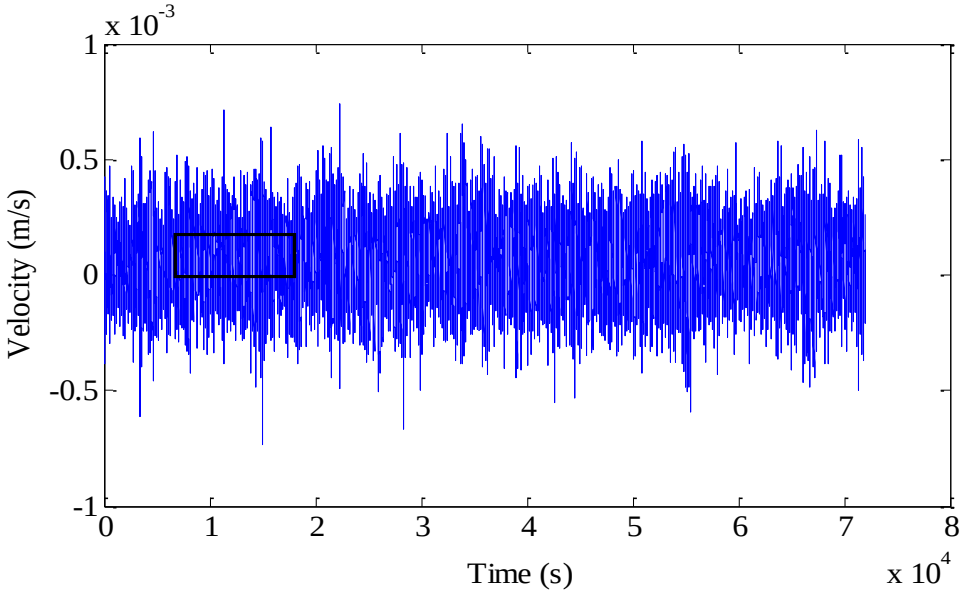
x 10^-3
1
0.5
0
-0.5
-1
Velocity (m/s)
0
1
2
3
4
5
6
7
8
Time (s)
x 10^4

(c)

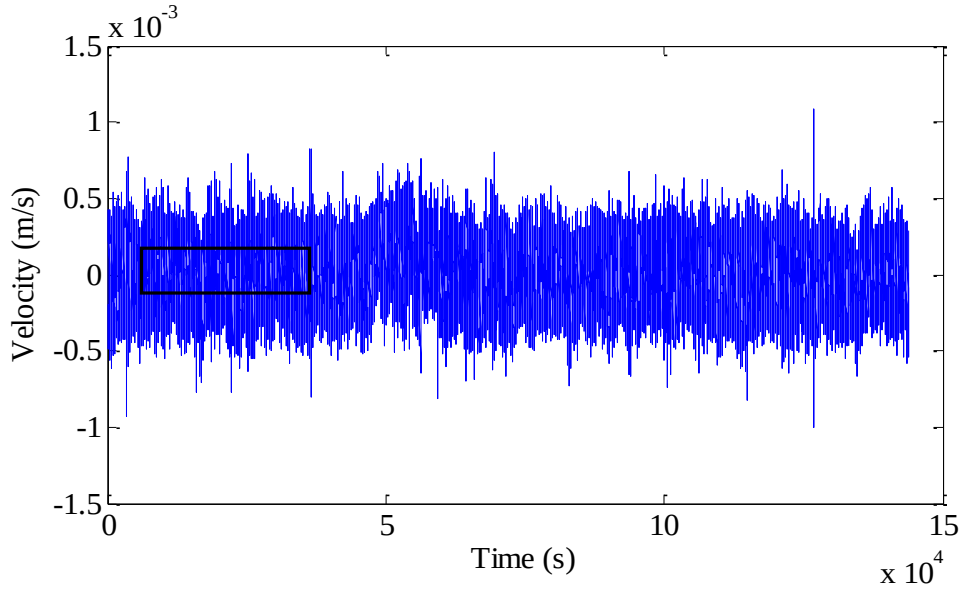
x 10^-3
1.5
1
0.5
0
-0.5
-1
-1.5
Velocity (m/s)
0
5
10
15
Time (s)
x 10^4

(d)

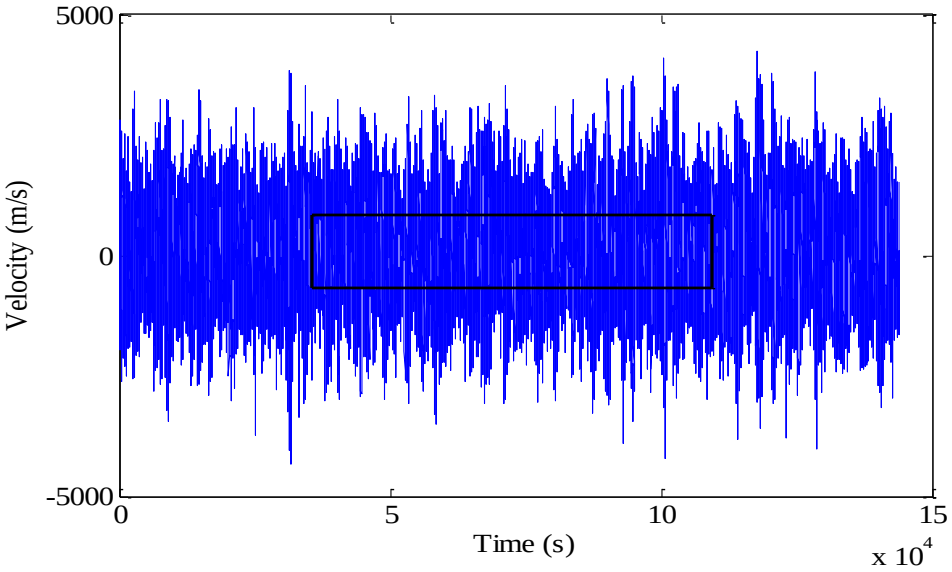
5000
0
-5000
Velocity (m/s)
0
5
10
15
Time (s)
x 10^4

(e)

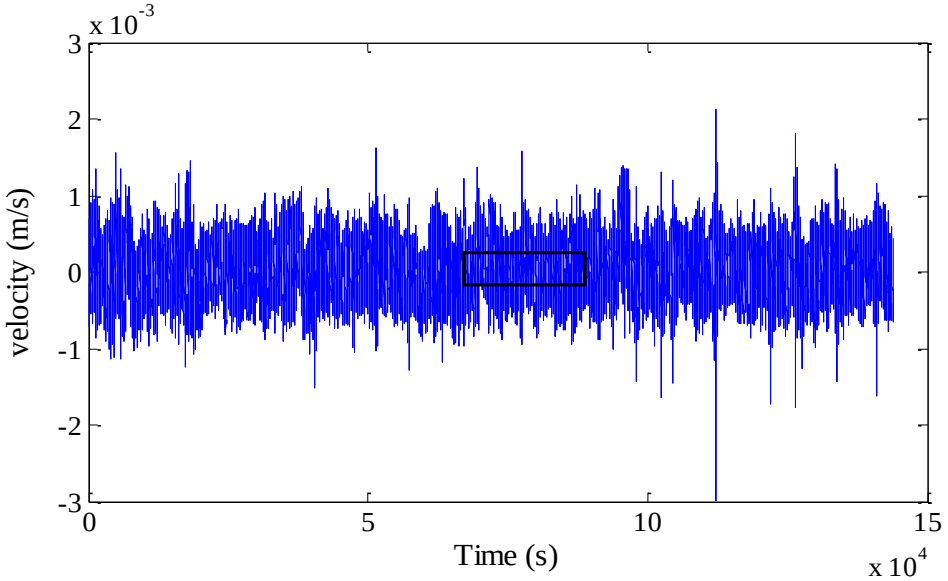
x 10^-3
3
2
1
0
-1
-2
-3
velocity (m/s)
0
5
10
15
Time (s)
x 10^4

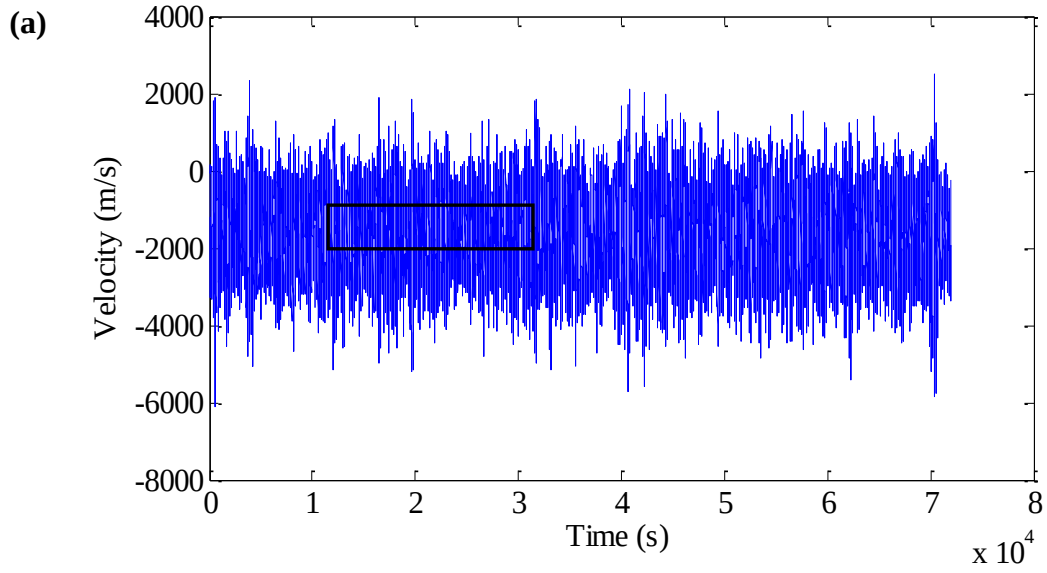

Figure A-22. Raw microtremor data and selected time segments used for testing temporal stability of peaks for station WTT: (a) 2004, (b) 2005, (c) 2006, (d) 2007, and (e) 2008.

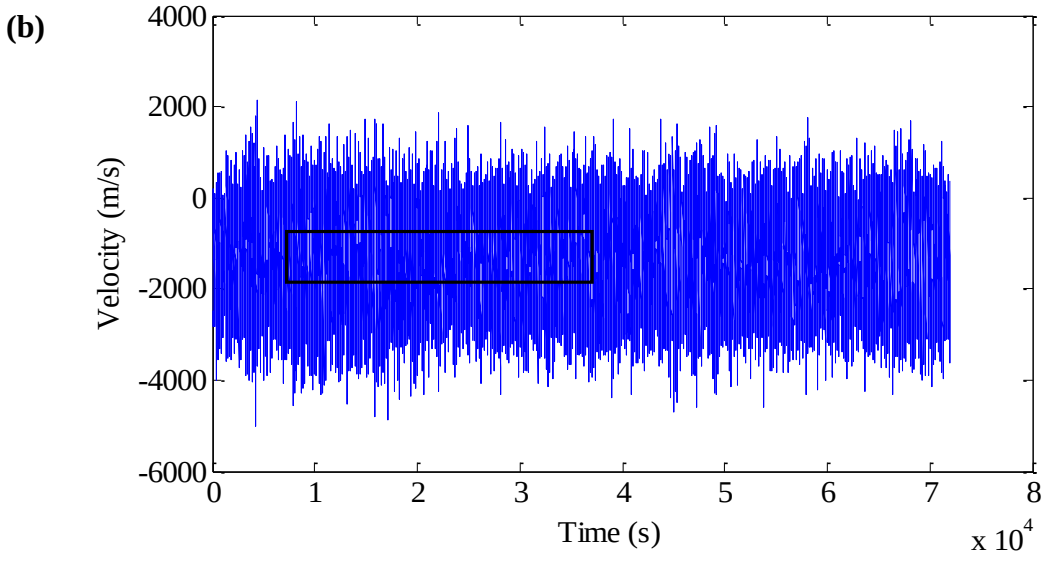

(c)

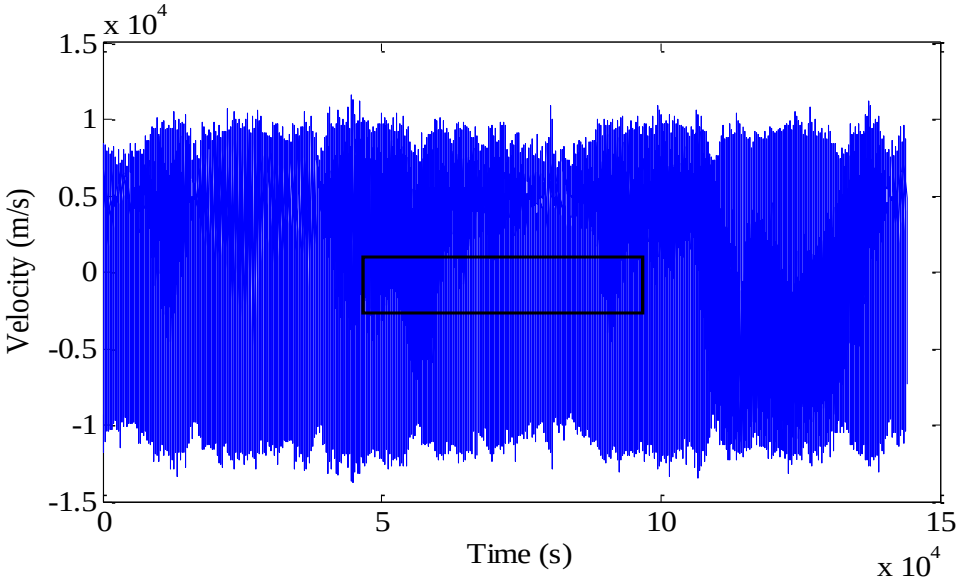
x 10^4
1.5
1
0.5
0
-0.5
-1
-1.5
Velocity (m/s)
0
5
10
15
Time (s)
x 10^4

(d)

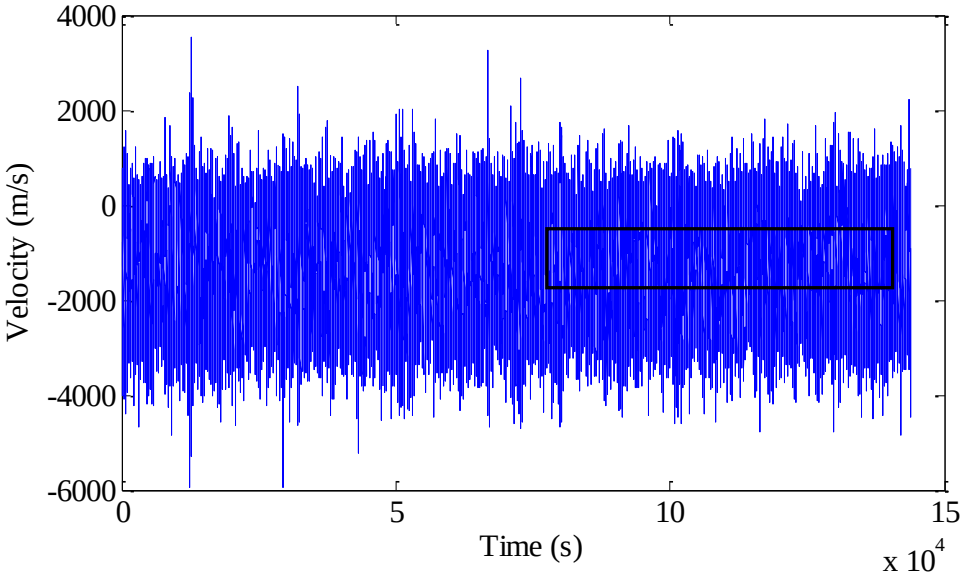
4000
2000
0
-2000
-4000
-6000
Velocity (m/s)
0
5
10
15
Time (s)
x 10^4

(e)

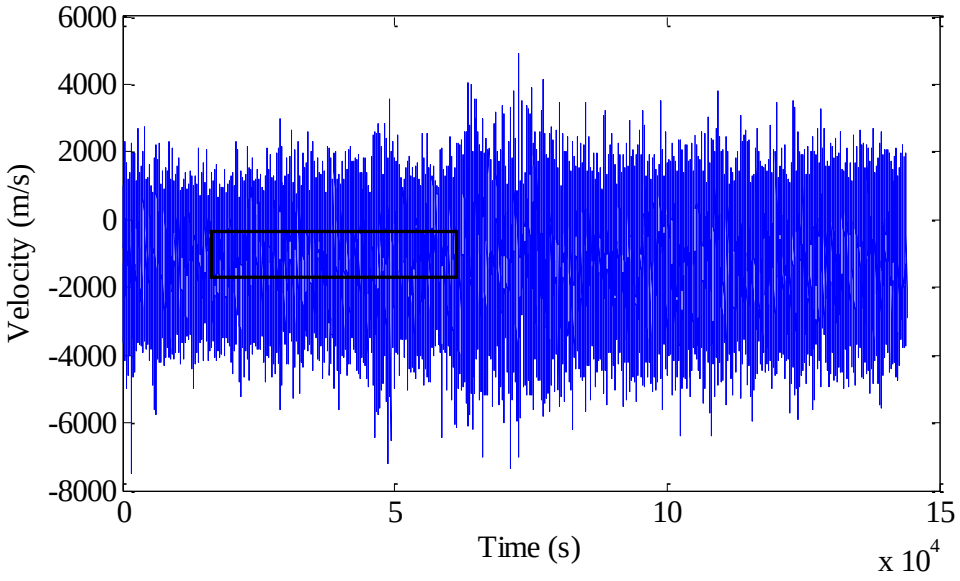
6000
4000
2000
0
-2000
-4000
-6000
-8000
Velocity (m/s)
0
5
10
15
Time (s)
x 10^4

APPENDIX B - EARTHQUAKE DATA

The 2008 Diamond Bar earthquake (Fig. 6) data collected for standard spectral ratio analysis are displayed here. Here data from 14 stations are given, as data for LGB was not available. There are two reference stations in the study area, FMP and RPV; only FMP is used for the spectral analysis. The lengths of data sample used in the analysis for each station are shown in Table 3 and the respective data segments in the two horizontal directions are bounded by black rectangle in each figure below.

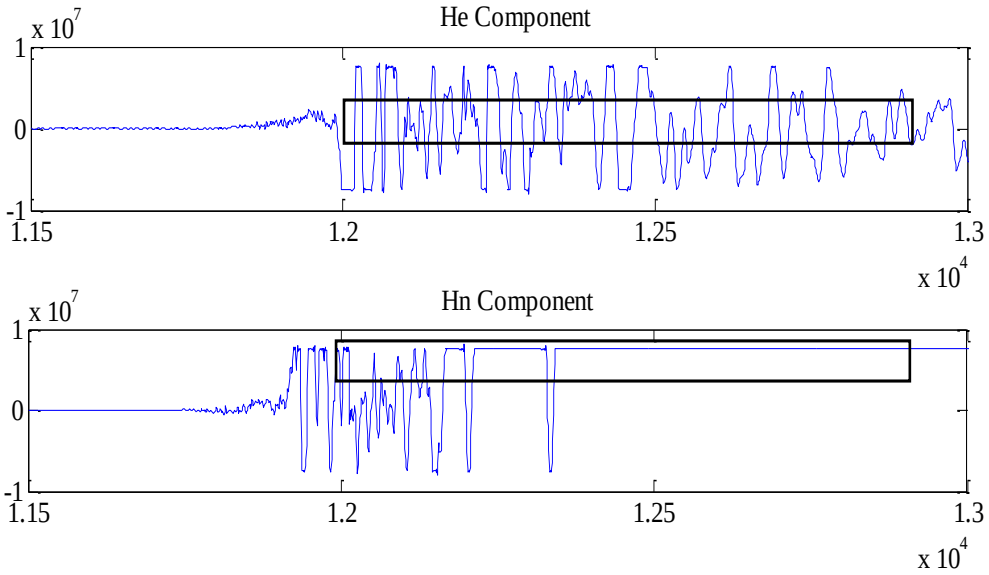

Figure B-1. Earthquake data segment showing two horizontal components for station BRE.

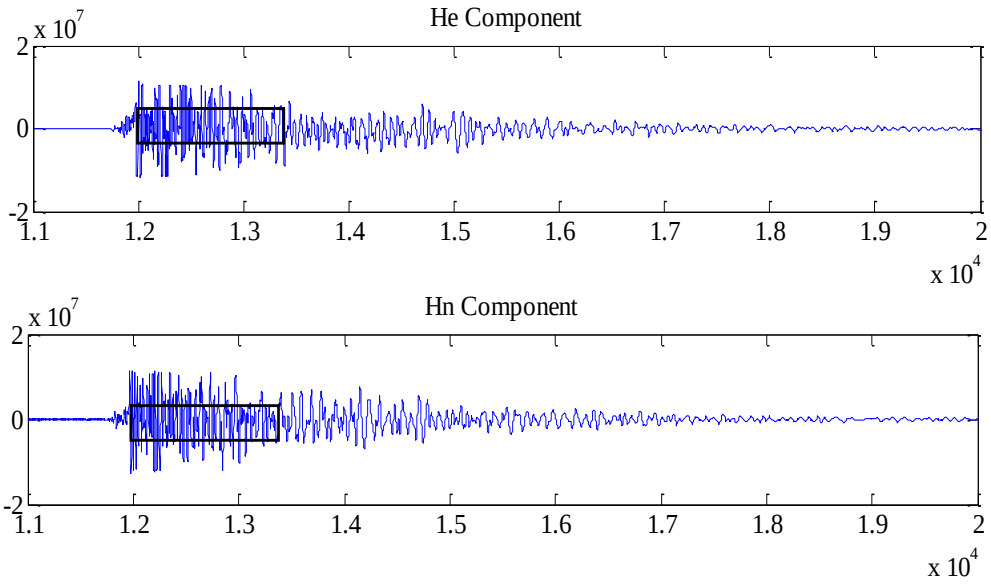

Figure B-2. Earthquake data segment showing two horizontal components for station DLA.

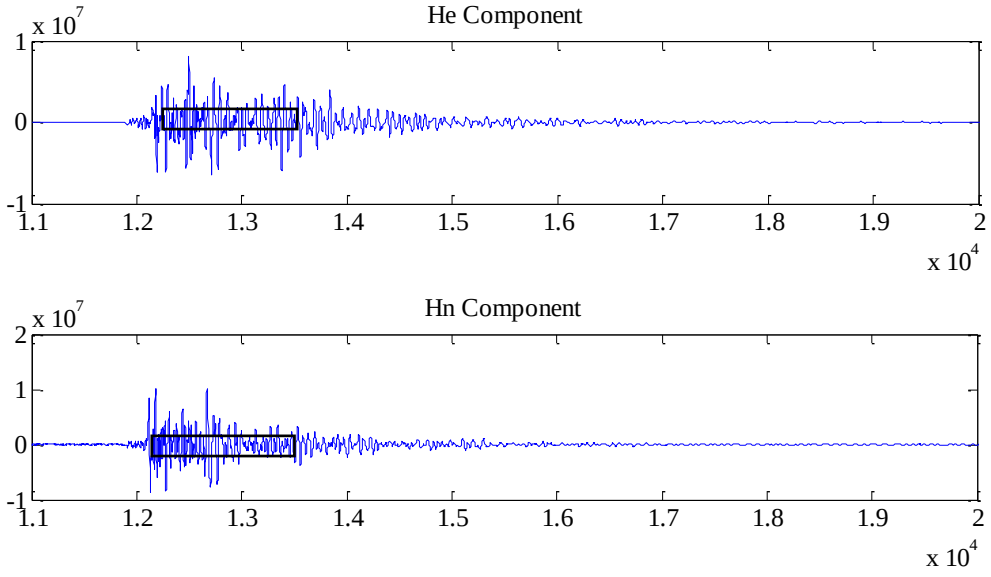

Figure B-3. Earthquake data segment showing two horizontal components for station FMP.

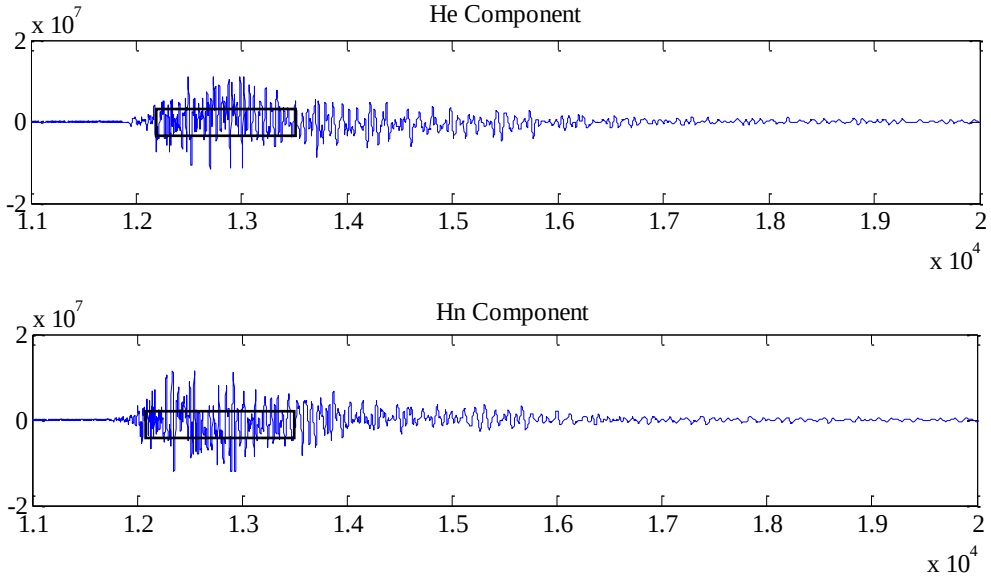

Figure B-4. Earthquake data segment showing two horizontal components for station LAF.

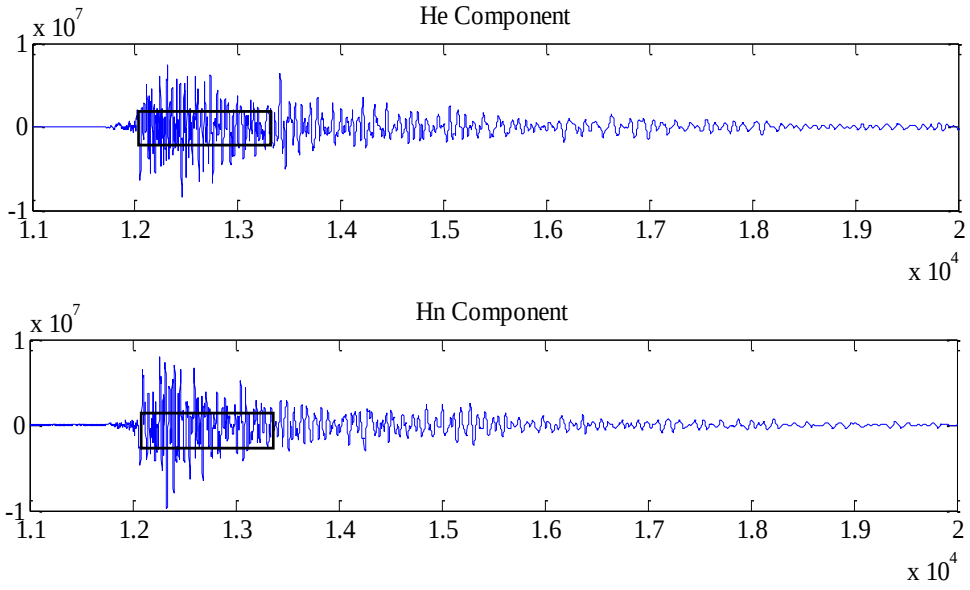

Figure B-5. Earthquake data segment showing two horizontal components for station LCG.

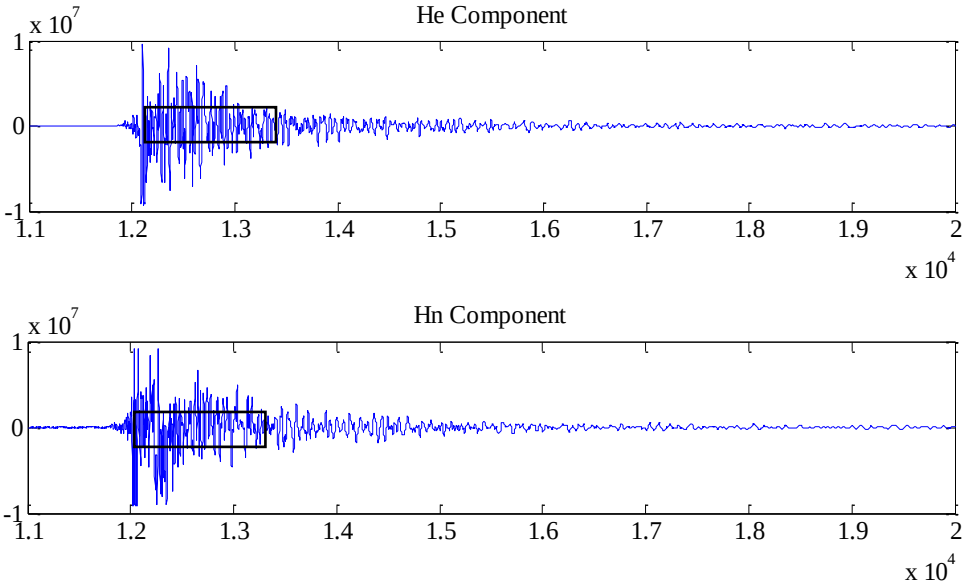

Figure B-6. Earthquake data segment showing two horizontal components for station LLS.

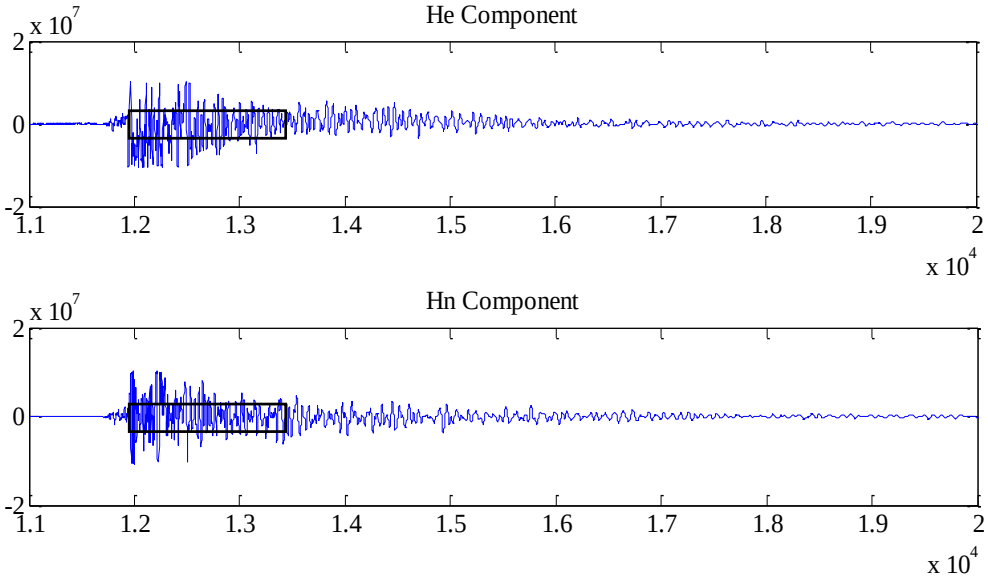

Figure B-7. Earthquake data segment showing two horizontal components for station LTP.

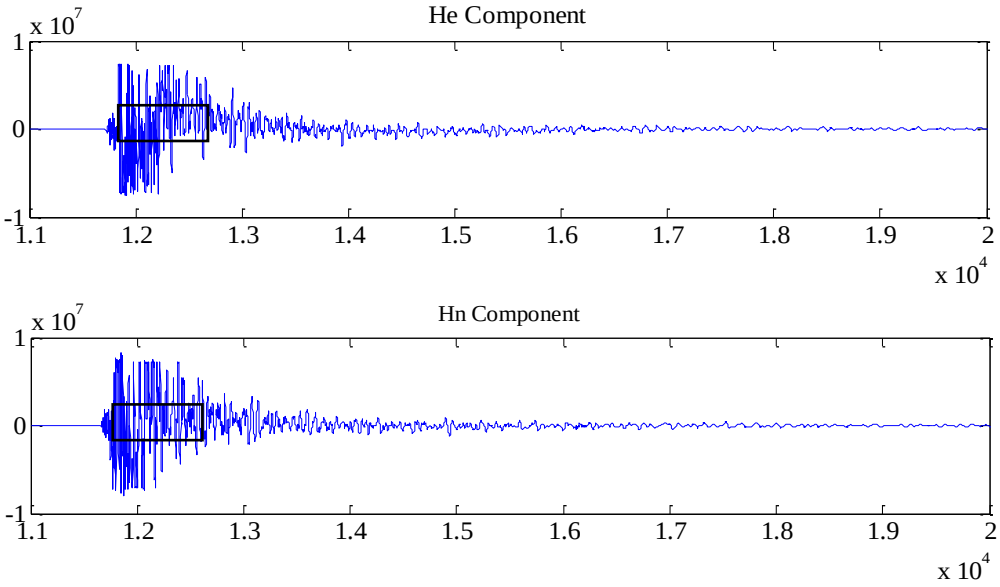

Figure B-8. Earthquake data segment showing two horizontal components for station OLI.

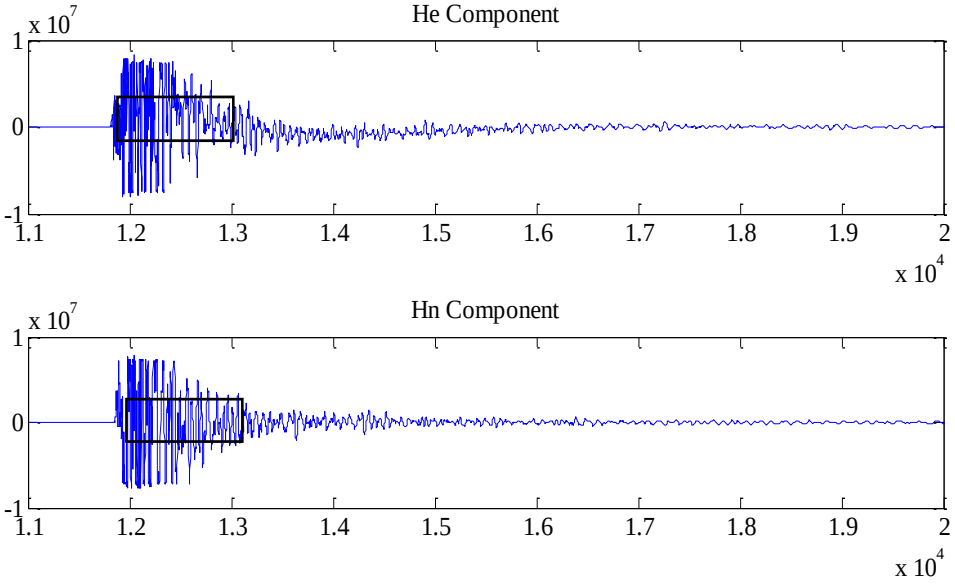

Figure B-9. Earthquake data segment showing two horizontal components for station SRN.

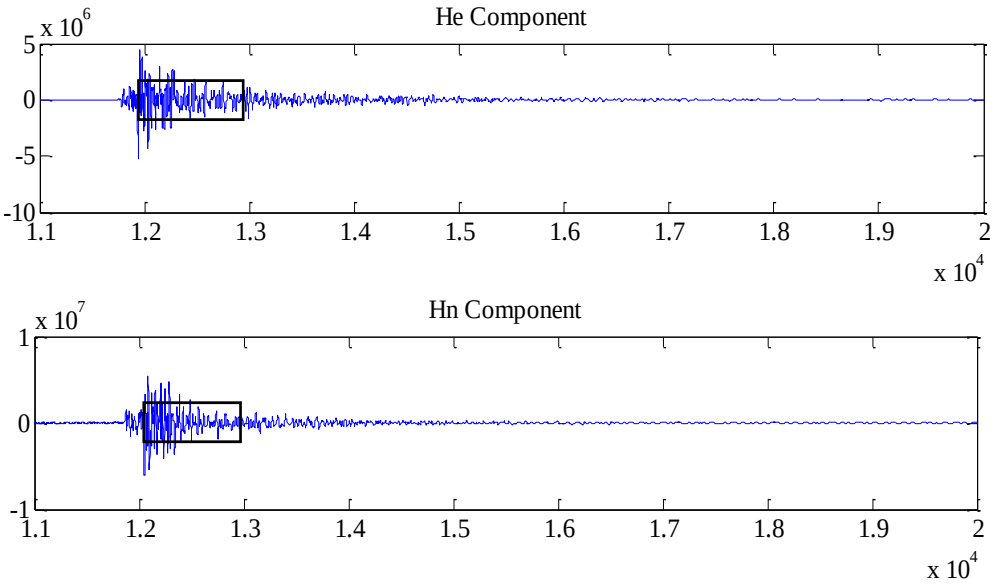

Figure B-10. Earthquake data segment showing two horizontal components for station STG.

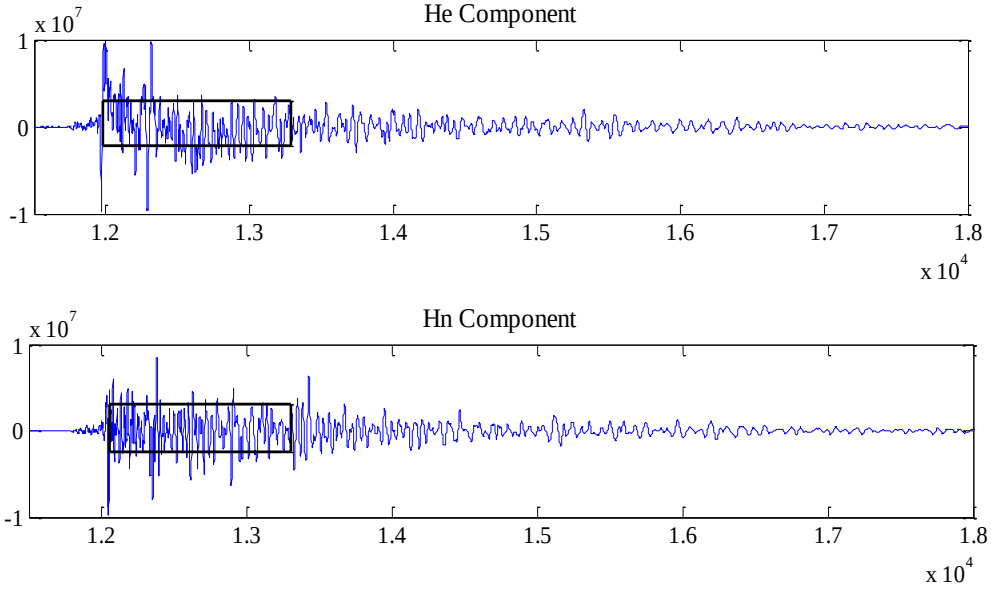

Figure B-11. Earthquake data segment showing two horizontal components for station STS.

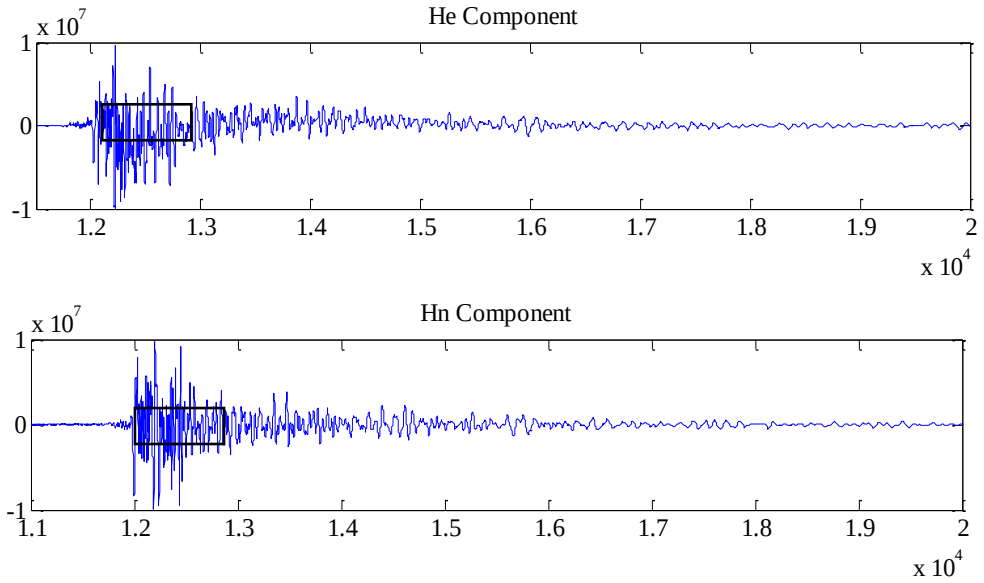

Figure B-12. Earthquake data segment showing two horizontal components for station USC.

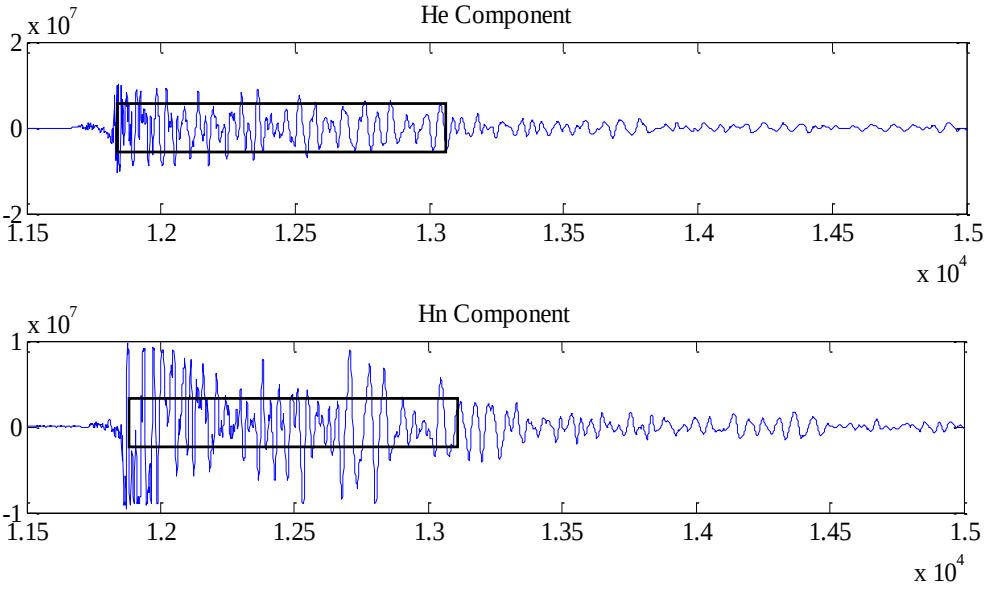

Figure B-13. Earthquake data segment showing two horizontal components for station WLT.

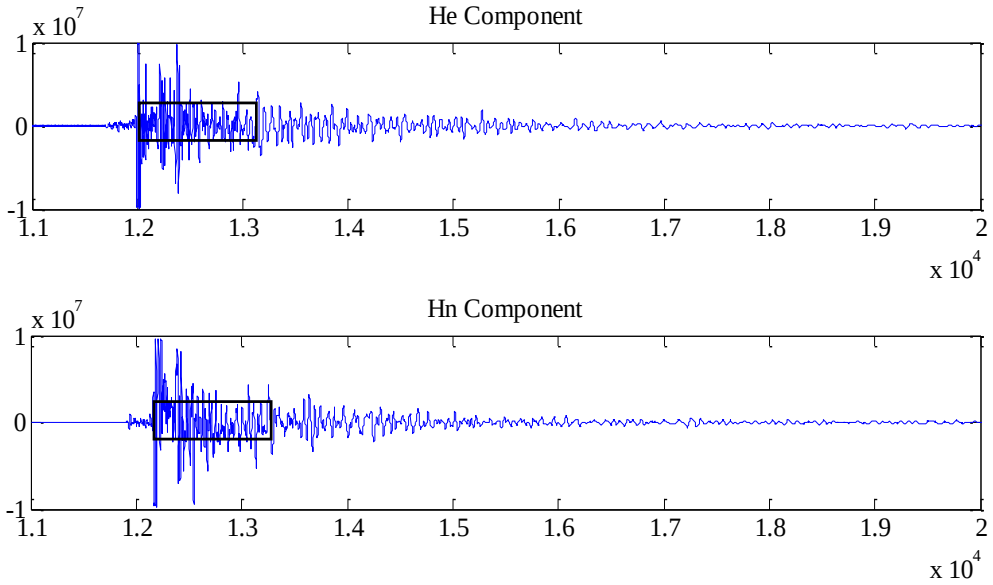

Figure B-14. Earthquake data segment showing two horizontal components for station WTT.

APPENDIX C - DATA AND MATLAB™ PROGRAMS

The CD insert in the back sleeve contains microtremor and earthquake data used in the study and the MATLAB™ program used to analyze the data. The CD is labeled "Appendix C" and contains 3 folders, with subfolders. The HVSRs calculated using the data set are shown in chapter IV. The MATLAB™ program used to view raw data and calculate spectral ratios are the 'load_sac' and 'ibs_M-files' respectively. The folders are organized as below.

FOLDER: Microtremor data

This folder contains 16 subfolders with the data for each station. The time series data are gain corrected and in SAC format. Each subfolder has the 'ibs_M-files' and 'load_sac' files required to compute the HVSRs.

FOLDER: Microtremor Stability Test

This folder contains 6 subfolders used to test microtremor peak stability. Each station subfolder contains 5 additional subfolders labeled with year 2004 through 2008.

The time series data are gain corrected and in SAC format. Each subfolder has the 'ibs_M-files' and 'load_sac' files required to compute the HVSRs.

FOLDER: Earthquake Data

This folder contains 14 subfolders, with the earthquake data for each station. The earthquake event data are gain corrected and in SAC format. Each subfolder has the 'ibs_M-files' and 'load_sac' files required to compute the standard spectral ratios.